ISTANBUL TECHNICAL UNIVERSITY ★ GRADUATE SCHOOL OF SCIENCE ENGINEERING AND TECHNOLOGY

TORSIONAL BUCKLING ANALYSIS OF COMPOSITE THIN-WALLED CYLINDRICAL SHELLS BY ANALYTICAL AND FINITE ELEMENT METHODS

M.Sc. THESIS

Güneş AYDIN

Department of Mechanical Engineering

Solid Mechanics Master Program

DECEMBER 2014

ISTANBUL TECHNICAL UNIVERSITY ★ GRADUATE SCHOOL OF SCIENCE ENGINEERING AND TECHNOLOGY

TORSIONAL BUCKLING ANALYSIS OF COMPOSITE THIN-WALLED CYLINDRICAL SHELLS BY ANALYTICAL AND FINITE ELEMENT METHODS

M.Sc. THESIS

Güneş AYDIN
503111505

Department of Mechanical Engineering

Solid Mechanics Master Program

Thesis Advisor: Prof. Dr. Ekrem TÜFEKÇİ

DECEMBER 2014

İSTANBUL TEKNİK ÜNİVERSİTESİ ★ FEN BİLİMLERİ ENSTİTÜSÜ

İNCE CİDARLI SİLİNDİRİK KOMPOZİT KABUKLARIN BURULMA BURKULMASININ ANALİTİK VE SONLU ELEMANLAR METODU İLE İNCELENMESİ

YÜKSEK LİSANS TEZİ

Güneş AYDIN
503111505

Makina Mühendisliği Anabilim Dalı

Katı Cisimlerin Mekaniği Programı

Tez Danışmanı: Prof. Dr. Ekrem Tüfekçi

ARALIK 2014

Güneş-Aydın, an **M.Sc.** student of ITU **Graduate School of Science Engineering and Technology** student ID 503111505, successfully defended the **thesis** entitled **"TORSIONAL BUCKLING ANALYSIS OF COMPOSITE THIN-WALLED CYLINDRICAL SHELLS BY ANALYTICAL AND FINITE ELEMENT METHODS"**, which he prepared after fulfilling the requirements specified in the associated legislations, before the jury whose signatures are below.

Thesis Advisor :	**Prof. Dr. Ekrem TÜFEKÇİ** İstanbul Technical University	.....
Jury Members :	**Prof. Dr. Ekrem TÜFEKÇİ** İstanbul Technical University	.....
	Yrd. Doç. Dr. Oğuz ALTAY İstanbul Technical University	.....
	Prof. Dr. Uğur GÜVEN Yıldız Technical University	.....

Date of Submission : 11 December 2014
Date of Defense : 22 January 2015

To my family and friends,

FOREWORD

I would like to thank to my thesis advisor Prof. Dr. Ekrem TÜFEKÇİ and his teaching assistant Dr. Ahmad Partovi MERAN, for their relevancy, guidance, support and helps for every step of my thesis study.

I would like to thank to thank to my family, firstly my mum and dad, and my friends for their mental support to me and all for their helps on my thesis study.

Moreover, I would like to acknowledge to the Technical Director of the Repkon Machine and Tool Industry and Trade Inc. Mr. İbrahim Külekçi for the helps on MATLAB for introducing me the helpful functions and the usage of 4-D arrays.

I would also like to thank to Turkish Technic, Design Development engineers for support and guidance to my thesis study.

December 2014

Güneş AYDIN
(Mechanical Engineer)

TABLE OF CONTENTS

ABBREVIATIONS

ASME **:** American Society of Mechanical Engineers
CFRP **:** Carbon Fiber Reinforced Plastic (or Plymer)
SI **:** System International
GFRP **:** Glass Fiber Reinforced Plastic (or Polymer)
FEM **:** Finite Element Method
WASET **:** World Academy of Science Engineering and Technology

LIST OF TABLES

LIST OF FIGURES

TORSIONAL BUCKLING ANALYSIS OF COMPOSITE THIN-WALLED CYLINDRICAL SHELLS BY ANALYTICAL AND FINITE ELEMENT METHOD

SUMMARY

Nowadays, carbon fiber materials are increasingly important. These materials are used not only for strength applications but also for low density, which means that low mass applications.

Carbon fiber materials have some advantages and some disadvantages. The advantages can be listed as; low mass, high strength, which means that high strength/weight ratio, high stiffness, good surface finish and so on. The disadvantages can be listed as; high cost, difficult to manufacture, the dimensional tolerances are dependent to the manufacturing method.

Buckling strength of a material is different when compared with other kinds of strength properties such as axial loading, bending and torsion. As known, every material has a stress strain curve.

For axial loading, bending and torsion strength, the applied force is known and the problem is to find whether or not the material resist that force. To do that, the yield strength of the material is known from the stress strain curve of that specific material. First of all, the stress occurred because of the force exerted on the material, is calculated from the strength equations. Then, the calculated stress value is compared with the yield strength of the material to see if the material is strong enough.

The buckling strength of the material is independent from the stress occurred on the material. The yield strength of the material is compared with the stress occurred on the material whereas in buckling point of view the critical buckling load is different from one geometry to the other geometry and it cannot be generalized.

The important thing in buckling is the limit value (the critical buckling load) is calculated by using the buckling equations but for axial loading, bending and torsion; the limit value (yield strength) is known and it is a material property.

Another difficult and critical thing for buckling is the buckling failure is seen in the elastic region of the material's stress strain curve.

As it is known, for the axial loading, bending and torsional strength problems, the material fractures after the permanent deformation occurs. For that reason, the material gives signals for fracture. In the first stage, by increasing the applied force, the material elongates elastically which means that if the force is reduced, the material saves its original shape.

After that, again by increasing the force, the material reaches its yield point. Beyond that point, the original dimensions of the material has changed permanently even if the applied force is reduced to zero.

By increasing the force after the yield point, the material deforms more and the necking situation is seen. This situation gives a brief signal for the fracture region because the necking situations occurs where the fracture occurs. If the force is increased more the material fractures from the necking point.

For the compression, bending and torsional strength problems, as it is seen the fracture region is seen before the fracture.

However; for buckling problems, since the buckling occurs in the elastic region, there is no sign when or where the fracture occurs. This makes the buckling problem is very important.

There are also some types of buckling such as, buckling under compression load, buckling due to the hydrostatic pressure, buckling due to bending and buckling due to torsion. This means that buckling not only occurs because of compression but also occurs because of torsion or bending.

Fracture due to buckling is an immediate fracture that is because it occurs in the elastic region. This shows the importance of buckling problem.

The other thing that this thesis studies is shell theories. Many structures are made of shells. Therefore, the strength analysis of shells is important.

The shell theories are much more complex when they are compared to the beam theories. The differential equations become more complex.

This study is about the buckling of composite shells. The purpose of this study is to find the optimum fiber angles that carry the maximum buckling load in different loading conditions for the same geometrical properties by analytically and Finite Element Method.

The fiber angle orientation plays a very crucial role for strength of the carbon fiber structures in every loading condition.

If the loading direction and sequence is known, the fiber angle orientation can be calculated for plies.

For buckling point of view, the loading conditions are important because, the fiber angle orientation differs from the load direction. This also makes the buckling modes different. The shape that occurs from buckling deformation differs due to loading condition and the fiber angle orientation.

Another crucial thing in this study is to see if the part is fractured due to yield or buckling.

To see that first, the optimum fiber angles that carries the maximum load is calculated iteratively. Then, Tsai – Hill failure theory is applied to the structure to see if the structure is yielded or buckled. If the structure is yielded, the maximum load that makes the structure was not to yield but buckled is found out.

In this study, MATLAB is used for the analytical solution procedure. The buckling equations for composite shell structures are used for calculating the critical buckling load.

As mentioned before, the shell theories are harder than other strength equations. In addition, the composite equations are complex because the carbon fiber material is not isotropic material.

A carbon fiber lamina is an orthotropic material, which means that, it must have 9 independent material constants and the stiffness matrix is 6x6. A simplification can be performed by using plane stress assumption. This reduces the material's stiffness matrix from 6x6 to 3x3. This assumption can be performed because the stress distribution along the layer thickness axis is negligible when compared the longitudinal and lateral axes. Since a shell type of material is very thin this assumption does not make a big change.

Moreover, as mentioned before, the crucial thing in this thesis is to make angle optimization. This is also performed by MATLAB.

To do that, an angle matrix is created randomly depending on the precision of the program, and the layer amount. The precision of the MATLAB program can be defined in the MATLAB code. This is the angle increments from 0° to 90° such as, 0-30-60-90 or 0-15-30-45-..-90 or 0-1-2-3-…-90.

This angle matrix consists of all angle configurations. The column number of this matrix gives the angle configurations. The stiffness matrix must be computed for all angle configurations and at the end of the program, the buckling load must be calculated for all angle configurations. The angle configuration that gives the maximum buckling load for the specified geometry (diameter, length, and layer thicknesses) is the optimum angle configuration for that geometry.

In addition, one more thing must be checked. That is the yielding or buckling. To check that Tsai – Hill failure theory is used. If the structure is yielded before it is buckled, the load that makes the structure is buckled but not yielded is found.

After all, a finite element analysis is performed to verify the analytical solution. To do that, ABAQUS CAE is used. The structure is defined as shell and all of the properties are written from the results of MATLAB analytical solution. At the end, the results are compared for MATLAB analytical solution and ABAQUS finite element solution.

İNCE CİDARLI SİLİNDİRİK KOMPOZİT KABUKLARIN BURULMA BURKULMASININ ANALİTİK VE SONLU ELEMANLAR METODU İLE İNCELENMESİ

ÖZET

Günümüzde karbon fiber malzemelerin önemi giderek artmaktadır. Bu malzemeler yüksek mukavemet gereken veya düşük yoğunlukları sayesinde hafiflik istenilen uygulamalarda tercih edilmektedirler.

Karbon fiber malzemelerin bazı avantaj ve dezavantajları bulunmaktadır. Hafiflik, yüksek mukavemet ve rijitlik, yüzey pürüzlülüğünün az olması avantajları arasında sayılabilir. Dezavantajları ise yüksek maliyet, üretim zorluğu ve boyut toleranslarının üretim metoduna bağlı olmasıdır.

Mühendislik tasarımlarında burkulma üzerinde dikkatle durulması gereken konulardan biridir. Malzemelerin burkulma mukavemetleri; çekme, basma, eğilme veya burulma gibi diğer mukavemetlerinden farklıdır. Çekme, basma, eğilme ve burulma mukavemetleri için malzemenin uygulanan kuvvete dayanıp dayanamayacağına bakılır. Bunun için malzemenin gerilme şekil değiştirme eğrisindeki akma mukavemetinin bilinmesi gerekmektedir. Malzemeye etkiyen kuvvete bağlı olarak mukavemet denklemlerinden oluşan gerilme değeri bulunmaktadır. Bu değer akma mukavemetiyle karşılaştırılıp malzemenin hasar alıp almadığı bulunur.

Malzemenin burkulma mukavemeti ise üzerinde oluşan gerilmeden bağımsızdır. Kritik burkulma kuvveti, malzeme geometrisine bağlı olarak değişmektedir. Çekme, basma, eğilme ve burulma mukavemetleri için limit değeri olan akma mukavemeti bir malzeme özelliğidir fakat burkulma mukavemeti için limit değeri olan kritik burkulma yükü, burkulma denklemleriyle hesaplanabilmektedir.

Ayrıca burkulma için önemli olan bir diğer durum ise burkulma hasarının malzemenin gerilme şekil değiştirme eğrisinde belirtilen elastik bölge içerisinde gerçekleşmesidir.

Çekme, basma, eğilme ve burulma mukavemeti problemlerinde malzeme kırılması, şekil değiştirme aşaması tamamlandıktan sonra gerçekleşmektedir. Bu nedenle malzeme kırılma belirtileri görülebilmektedir. İlk aşamada, uygulanan kuvvet arttıkça malzeme elastik olarak şekil değiştirmektedir, yani uygulanan kuvvetin kaldırılması sonucu malzeme ilk haline dönebilmektedir.

Eğer uygulanan kuvvet yeteri arttırılmaya devam edilirse, malzeme akma sınırına ulaşacaktır. Bu noktadan sonra malzemenin üzerindeki kuvvet kaldırılsa bile ilk boyutuna geri dönemeyecektir.

Akma sınırından sonra kuvvet arttırılmaya devam edilirse malzeme şekil değiştirmesi de artar ve çekme durumu için boyun verme durumu gözlenebilir. Bu durum malzeme kırılmasının da boyun veren bölgede oluşacağı göstermektedir. Eğer uygulanan kuvvet arttırılmaya devam edilirse malzeme boyun veren bölgeden kırılıp hasar görecektir.

Çekme, basma, eğilme ve burulma durumları için kırılma belirtileri görülebilmesine rağmen burkulma problemlerinde hasar elastik bölgede oluştuğu için bu tarz belirtiler görülmemektedir ve kırılma bir anda gerçekleşmektedir. Bu yüzden burkulma problemlerine önem gösterilmesi gereklidir.

Burkulma çeşitlerine örnek olarak eksenel basma kuvveti, hidrostatik basınç, eğilme kuvveti veya burulma momenti altında burkulma verilebilir. Yani burkulma durumu sadece basma kuvveti altında gerçekleşmemektedir, diğer kuvvetler altında da gerçekleşebilmektedir.

Yapılan bu çalışma kompozit silindirik kabuk yapıların burkulmasıyla ilgilidir. Kabuk yapılar uygulamada birçok yerde kullanılmaktadırlar. Bu durum kabuk yapıların mukavemet analizlerini önemli kılmaktadır. Kabuk yapı teorileri, kiriş teorilerine kıyasla kullanılan diferansiyel denklemler ve çözümleri bakımından çok daha karmaşıklardır. Ayrıca karbon fiber gibi izotropik olmayan kompozit malzemelerin teorileri de daha karmaşık olmaktadır.

Karbon fiber lamina bir ortotropik malzemedir ve 6x6 rijitlik matrisi içerisinde 9 adet bağımsız malzeme sabiti bulunmaktadır. Yüzey gerilme yaklaşımı yapılarak bu durum basitleştirilebilir. Böylece malzeme rijitlik matrisi 3x3 boyutuna indirgenmektedir. Bu yaklaşım lamina kalınlığı çok az ve kalınlık doğrultusundaki gerilme değişimi ihmal edilebilecek düzeyde olduğu için uygulanabilmektedir.

Çalışmanın amacı aynı geometrik ve malzeme özellikleri için maksimum burkulma kuvvetini taşıyabilecek en uygun fiber açılarını analitik ve sonlu eleman yöntemleri yardımıyla bulmaktır.

Fiberlerin açı düzeni, bütün kuvvet koşullarında karbon fiber yapıların mukavemeti için önemli bir rol oynamaktadır. Eğer kuvvet doğrultusu ve lamina sayısı biliniyorsa, fiberlerin açı düzeni her lamina için bulunabilmektedir.

Burkulma durumunda, kuvvet koşulları önem kazanmaktadır. Çünkü fiber açıları kuvvet doğrultusu ile değişmektedirler. Bu durum burkulma modunun ve burkulma deformasyon şeklinin de değişmesine yol açmaktadır.

Bu çalışmada önemli bir diğer nokta ise yapının burkulmaya bağlı ya da akmaya bağlı olarak hasar aldığının belirlenebilmesidir.

Bu amaçla öncelikle maksimum burkulma kuvvetini taşıyabilen fiber açı düzeni hesaplanmıştır. Daha sonra Tsai - Hill hasar teorisi kullanılarak yapının akma sınırına bağlı hasar alıp almadığı araştırılmıştır. Bu şekilde yapının akmaya bağlı hasar almadığı, sadece burkularak hasar aldığı durumlar belirlenmiştir.

Analitik çözüm süreci için MATLAB sayısal hesaplama programından yararlanılmıştır. Programda kritik burkulma kuvvetinin hesaplanması için burkulma teorisindeki denklemler kullanılmıştır.

Fiber açı optimizasyonunu sağlamak için lamina sayısına bağlı olarak ve programda tanımlanan bir hassasiyetle rastgele bir açı matrisi oluşturulmuştur. Oluşturulan bu açı matrisi hassasiyet oranına bağlı olarak 0° ile 90° arasında bütün açı kombinasyonlarını içermektedir. Açı matrisinin kolon sayısı oluşturulan açı düzenlerinin sayısı kadar olmaktadır. Bu açı düzenlerinin hepsi için ayrı olarak rijitlik matrisi ve burkulma kuvvetleri program tarafından hesaplanmıştır. Daha önce belirlenmiş olan malzeme geometrisi için maksimum burkulma kuvvetini veren açı düzeni belirlenmiştir. Bu açı düzeni malzemenin optimum açı düzeni olmaktadır.

Daha sonra malzemenin Tsai – Hill hasar teorisi kullanılarak akmaya bağlı olarak hasar alıp almadığı kontrol edilmiştir. Böylece akmaya bağlı hasar alan durumlar elenmiş ve optimum açı düzeni sadece burkulmaya bağlı olan durumlar için bulunmuştur.

Bundan sonra analitik çözümü kıyaslamak için sonlu elemanlar analizi gerçekleştirilmiştir. Bu analiz için ABAQUS sonlu elemanlar analiz programı kullanılmıştır. Malzeme kabuk yapı olarak tanımlanmış ve malzeme özellikleri MATLAB programındaki optimizasyon çalışmasından çıkan duruma göre yazılmıştır. Daha sonra ABAQUS sonlu eleman çözümü ve MATLAB analitik çözümleri kıyaslanmıştır.

Sonuç olarak ince cidarlı silindirik kompozit yapıların tasarımında kullanılabilecek bir optimizasyon yöntemi elde edilmiştir.

1. INTRODUCTION

Thin walled structural materials are commonly used in automotive, marine and aerospace industries. Especially, for weight reduction purpose, the composite materials are commonly preferred. The thicknesses of that type of materials are small in proportion to their length. If a tensional force is applied to a material, it can carry that load up to its ultimate tensile strength then it cracks. This type of failure is independent from the part geometry because the limit stress i.e. ultimate tensile strength is defined for all types of materials. Whereas if a compression force is applied to a material, the buckling failure can occur. Since the material is thin like a shell, the torsional loads and hydrostatic pressure can also cause buckling. For that reason, the structural analysis of that type of shell materials must be performed carefully. The buckling criteria must be investigated.

The buckling situations can be seen many systems. The columns that are not supported with side ribs can be fractured due to bucking. The thin walled shells that are strong due to tension are very weak due to compression because of buckling situations.

As an example, a submarine or a vacuum tank that are exposed to hydrostatic pressure can fracture due to buckling. Moreover, a drive shaft that is made of a thin-walled composite material can also fracture due to torsional buckling.

This and similar problems must be emphasized carefully in design problems. For that reason, the buckling behavior of structural materials is important and must be investigated carefully.

1.1. Purpose of Thesis

In this study, the buckling behavior of thin walled composite materials under torsional loads is investigated. According to the number of layers, layer thicknesses, part length and part diameter the layer angles are optimized. To do that the shell theories and the composite structural theories are put into together and the problem is solved by those theories. For layer angle optimization, MATLAB is used.

In addition, the problem is solved by using finite element analysis by using ABAQUS. The optimum layer angles are directly imported to the finite element analysis and the analytic and finite element solutions are compared.

1.2. Literature Review

Bisagiani and Cordisco (2003), researched the buckling and post-buckling behavior of the carbon fiber composite cylindrical structures under compression and torsional loads individually and together experimentally. They saw the effect of the layer stacking and the fiber angles.

Meyer-Piening, et al. (2001), researched buckling behavior of the thin walled cylindrical carbon fiber composite shells by analytically, finite element methods and experimentally. For this purpose, they apply axial and torsional loads together.

Bisagiani (2000), researched the buckling and post-buckling behavior of the thin walled multilayer composite cylinders under axial compression. She used finite element methods and compared the eigenvalue, nonlinear Riks and dynamic analysis methods. She also analyzed the effect of geometrical imperfections to the critical buckling load.

Semerdov (2000), researched the buckling problem and optimization of the multi-layer thin walled cylinders under axial compression. The formulations were compared for different layer amount and angles. He also added, for the most situations, the maximum number of layers should be 4 and the maximum variables in the formulations should be 2. He said that increasing the values con not provide any benefit.

Semerdov (2000), researched the optimization of the multi-layered thin walled composite cylinders under external pressure loads. For most situations if the number of layers is more than 3, this won't increase the critical buckling load more.

Moon, et al. (2009), researched the thin walled composite cylinders under external pressure. They compare 3 different specimens with 30-45-60 layer angles by using finite element and experimental methods. They understood that the angle configuration has an important effect on critical buckling load.

Lopatin and Morozov (2011), researched the buckling problem of the thin walled cylindrical structures under uniform outside pressure with one side is fixed. They used

Galerkin's method and compared their results with finite element methods. They have resulted that the analytical solution is valid and acceptable when it is compared the finite element solution and it can be used for the design of the composite structures.

Kim and Kim (2001), researched the buckling strength of the thin walled cylindrical structures under axial compression loads. The models with both ends are open and close are investigated individually for prefect and imperfect geometrical conditions.

Gal, et al. (2006), investigated that the finite element model that they were developed. They resulted that the method that they developed gives good results with the experiments and the results in the literature.

Chen, et al. (2012), researched the buckling of the thin walled composite cylinders with variable thicknesses under axial compression. They saw that if the difference between the thicknesses increased the buckling strength decreased.

Kirkpatrick and Holmes (1989), researched the buckling and post-buckling behavior of the thin walled cylindrical structures. For the finite element methods, the geometrical and force distribution imperfections are considered. These results show a very big effect in buckling and post-buckling behavior.

Goldfred, et al. (2005), worked to find an optimum fiber layup for thin walled composite structures. For this purpose, they changed the thickness and fiber angle of the structure and found out that this affects the buckling property.

Tafreshi (2004), researched the effect of delamination in the cylindrical composite shell to the buckling load. The finite element method is used for analyzing the effect of delamination and it is seen that if the delamination increases the buckling load decreases critically.

Bert and Kim (1994), investigated the torsional buckling behavior of the thin walled structures. They also researched the effect of the layer angle, boundary conditions and the geometrical conditions on the buckling load.

Shokrieh, et al. (2004), researched the torsional buckling behavior of the thin walled structures that transmits power. The finite element results are compared with the analytical and experimental results. In addition the effect of fiber angle, layer arrangement, boundary conditions are investigated.

Lennon and Das (2000), made a finite element model for a cylinder under torsional deflection and buckling behavior. The effect of ribs are investigated.

Hassani, et al. (1997), investigated the buckling behavior of the composite cylindrical thin walled structures analytically in different boundary conditions. They determined that their approach could be used for different boundary conditions by comparing with the different theoretical solutions and experiments.

Bisagiani and Cordisco (2006), investigated the buckling and post buckling behavior by experimentally for the thin walled cylindrical composite structures. They also investigated the crack initiation by using some tests for axial compression and torsion.

Messager, et al. (2002), made an optimization study for thin walled laminated cylindrical composite structures under hydrostatic pressure for maximizing the strength. They try their approach for the fiber glass and carbon fiber structures. The algorithm behind this approach is genetic algorithm.

Tafreshi (2006), investigated the buckling and post bucking behavior of the thin walled cylindrical composite shells for different material, different layer arrangement, and delamination size under axial load, lateral pressure. The finite element solution gives a very important effect on the layer arrangement for buckling load.

2. THEORETICAL BACKGROUND OF COMPOSITE MATERIALS

2.1. Composite Materials

A composite is a structural material that consists of two or more different materials. Composite materials have the properties of all materials that are reinforced. Thanks to that property of composite materials, they can carry various combinations of loads.

Such as a Carbon Fiber Reinforced Plastic (CFRP) is a composite material. It contains the properties of both carbon and epoxy resin, which is a polymer plastic. The carbon itself is a very high strength material but it is very brittle. Epoxy is an elastic material itself but it does not have high strength values. However, CFRP is an optimum material for high strength applications. Since it has reinforced with epoxy, the new material (CFRP) has a good elastic behavior, and thanks to the carbon in it can carry high amount of loads.

The following table shows some properties of composite and bulk materials to compare.

Table 2.1 : Some properties of composite and bulk materials.

Material Units	Specific gravity	Young's modulus (GPa)	Ultimate strength (MPa)	Specific modulus (GPa-m³/kg)	Specific strength (MPa-m³/kg)
System of Units: SI					
Graphite fiber	1.8	230.00	2067	0.1278	1.148
Aramid fiber	1.4	124.00	1379	0.08857	0.9850
Glass fiber	2.5	85.00	1550	0.0340	0.6200
Unidirectional graphite/epoxy	1.6	181.00	1500	0.1131	0.9377
Unidirectional glass/epoxy	1.8	38.60	1062	0.02144	0.5900
Cross-ply graphite/epoxy	1.6	95.98	373.0	0.06000	0.2331
Cross-ply glass/epoxy	1.8	23.58	88.25	0.01310	0.0490
Quasi-isotropic graphite/epoxy	1.6	69.64	276.48	0.04353	0.1728
Quasi-isotropic glass/epoxy	1.8	18.96	73.08	0.01053	0.0406
Steel	7.8	206.84	648.1	0.02652	0.08309
Aluminum	2.6	68.95	275.8	0.02652	0.1061

2.1.1. Advantages of composite materials

- Special purpose of materials.
- Lightweight design.
- High strength.
- The designer can optimize the material for different loading conditions.
- Suitable for special applications.
- Corrosion resistant
- Vibration isolation property is higher when compared to the metals.
- Fatigue life is higher when compared to the metals.
- The surface finish is good.

2.1.2. Disadvantages of composite materials

- Expensive solution when compared to bulk material.
- Not very applicable for mass production.
- Hard to manufacture when compared to bulk materials.

2.2. Mechanics of Composite Materials

2.2.1. Lamina and laminate

A lamina is a thin layer of a composite material that has a thickness on order of 0.125mm. A laminate is made of multiple laminas on and on with same or different angle orientations. Mechanical structures can be made of laminates such as car suspension parts, pipes etc. These kinds of structures can carry various combinations of loads.

A lamina contains a fiber cross-section and a matrix cross-section. The fiber cross-section is generally a high strength and brittle material whereas; the matrix cross-section is an elastic material. In other words, the fiber is reinforced with the matrix.

Since two or more materials are reinforced, the stiffness of the composite material is related with the fiber material and the matrix material.

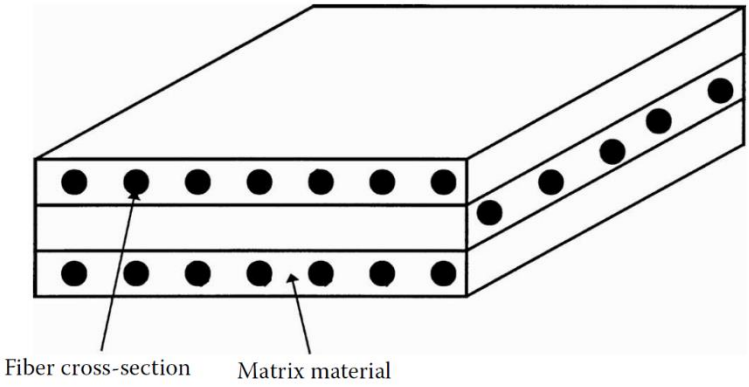

Figure 2.1 : A typical laminate made of three laminas.

The figure blow shows a typical laminate that is made of three laminas with different fiber angle orientations.

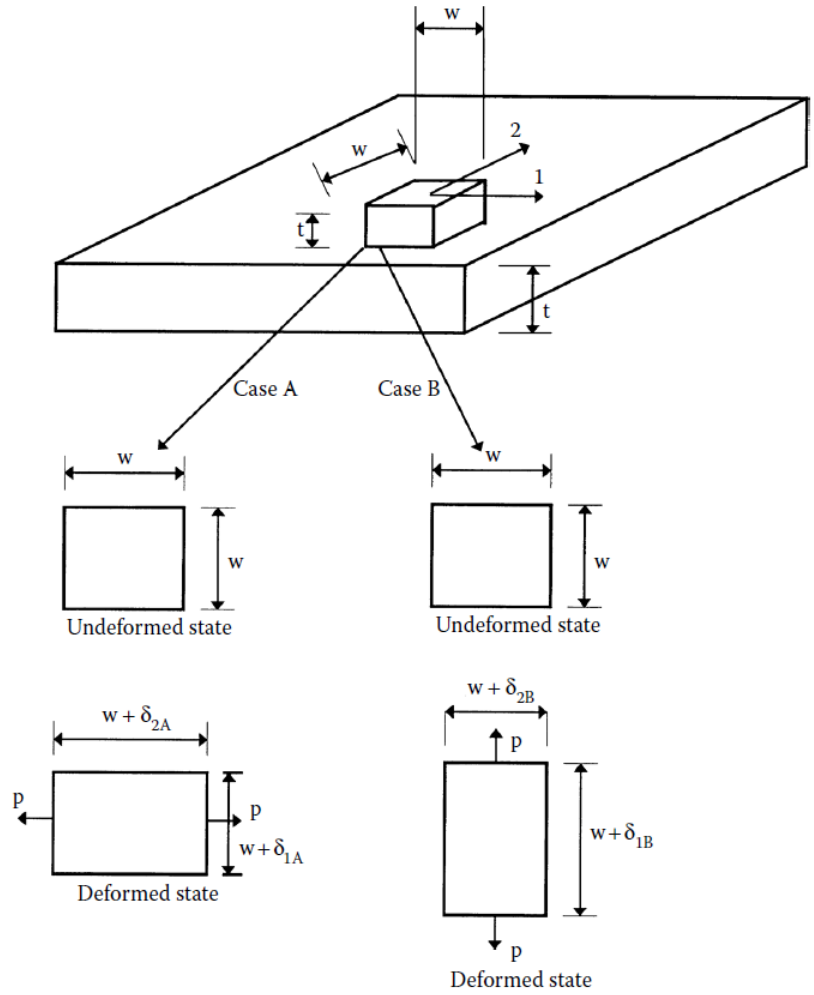

Figure 2.2 : Deformation of a square element of an isotropic material.

If we take an isotropic material and see the deformations under normal loads. The deformation on one side is proportional to the Poisson's Ratio. Moreover, the loading direction is independent from the deformation amount. See the figure below.

As it is seen from the figure when the loading direction changes the deformation does not change. In other words;

$$\delta_{1A} = \delta_{2B},$$

$$\delta_{2A} = \delta_{1B}.$$

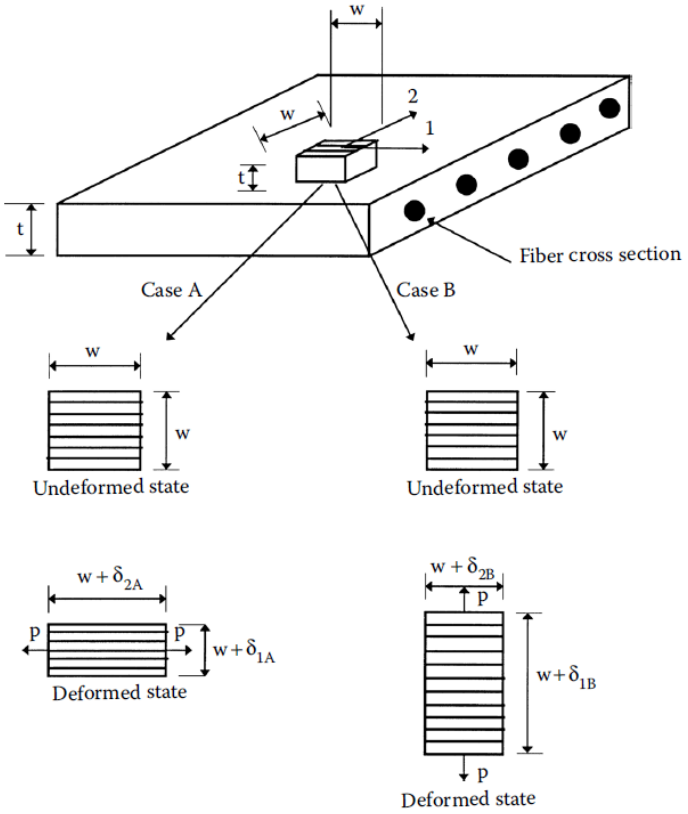

Figure 2.3 : Deformation of a square element of a composite material.

However, in composite materials the deformation is not independent form the loading direction. See the figure below.

As it is seen from the figure when the loading direction changes the deformation changes. The reason is the fiber orientation. In other words;

$$\delta_{1A} \neq \delta_{2B},$$

$$\delta_{2A} \neq \delta_{1B}.$$

2.2.2. Lamina and laminate arrangement in composite materials

In general, the composite materials are not built just one lamina; generally, the composite materials are stacked as laminates, which are made from laminas. This situation is shown in the figure 2.4.

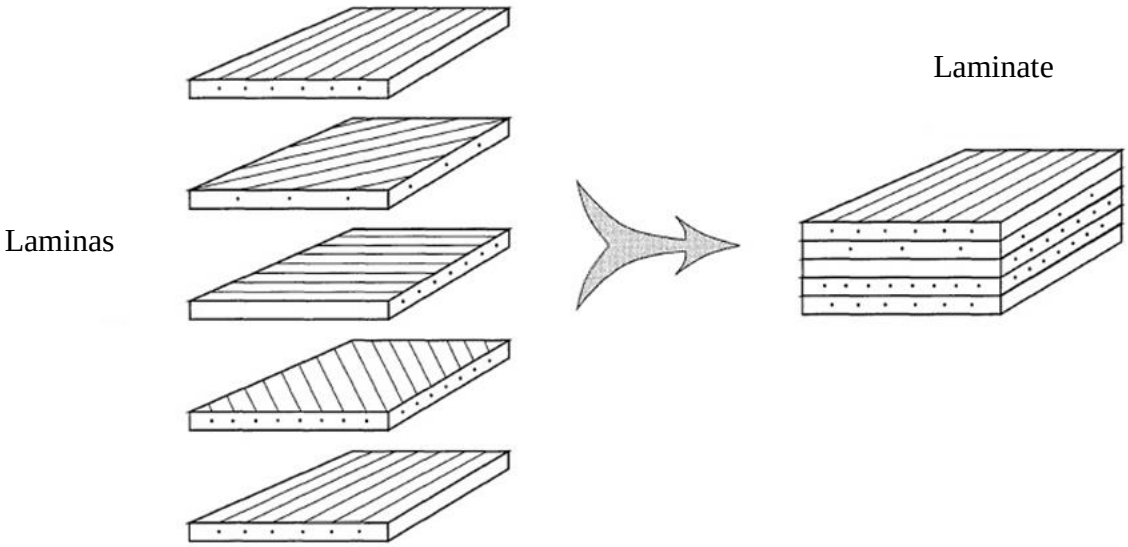

Figure 2.4 : Lamina and laminate structure.

Laminate structures are made from the laminas that,

- Are made from unidirectional laminas.
- Can be stacked as different fiber angle.
- Can include different fiber materials.
- Can include honeycomb or foam structures in the middle of plies.
- Can include cut fibers or metal powders.

In this study, the mechanical properties of laminates can change according to the stacking of the unidirectional laminas.

To represent the angle arrangement of laminates, the angle of the each lamina with respect to the x-axis must be known. After that, if the consecutive angle is different from previous one, the "/" sign is put and the other angles must be written respectively. If the consecutive angle is same with the previous one the amount of same angles are written as and indice. Whole expression is written in square brackets. This situation is

shown in the figure 2.5 and the angle designation in this stacking is $[30/90_2/45/0/45]$.

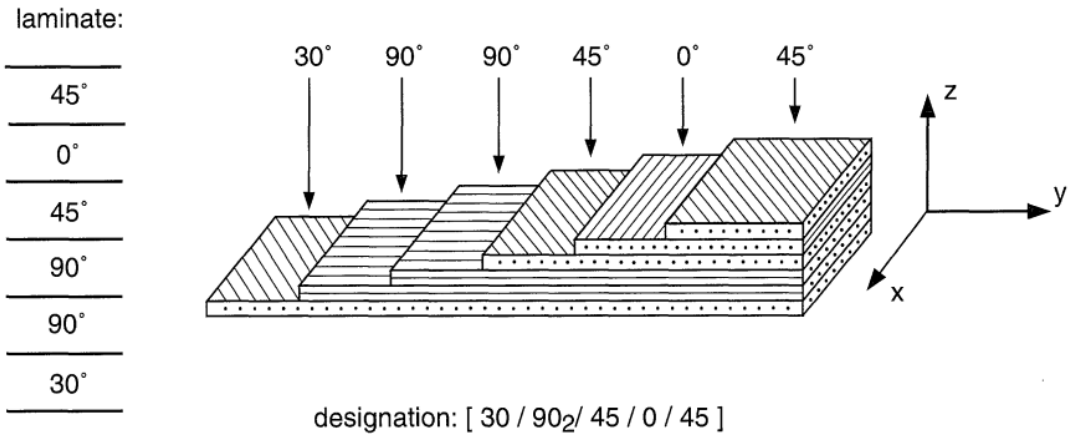

Figure 2.5 : Laminate angle designation.

If the lamina has a negative angle, the minus "-" sign is put before the angle. This situation is shown in the figure 2.6.

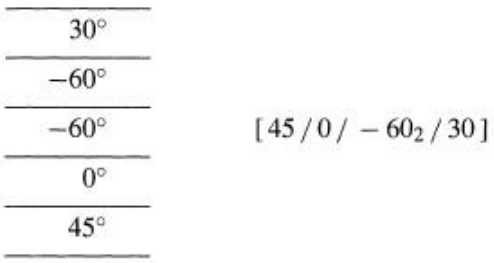

Figure 2.6 : Negative direction lamina.

If the negative and positive angled, laminas are used consequently the "±" sign is used to define the angle stacking.

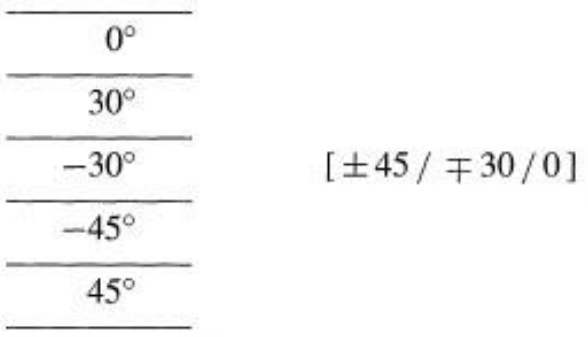

Figure 2.7 : Negative and positive direction laminas.

If there is a symmetric stacking with respect to the middle plane of the laminate, the angles are written from the first angle to the angle that lays on the middle plane and the “s” symbol is written after the square brackets.

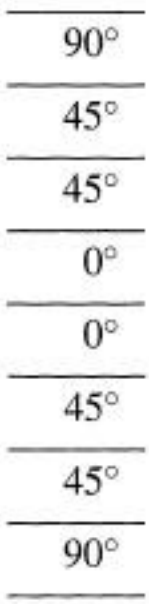

$[90/45_2/0]_S$

Figure 2.8 : Symmetric laminate.

If the number of layers is an odd number for a symmetrical laminate, and that lamina is laying on the middle plane, the “ ¯ “ sign is put on the angle of the middle plane lamina.

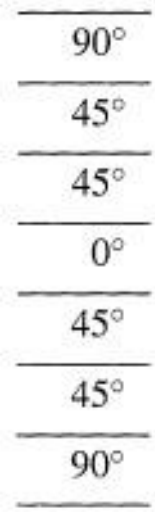

$[90/45_2/\bar{0}]_S$

Figure 2.9 : Symmetric laminate that consists of odd laminas.

If the laminate has a repeated sequence, the amount of repetition is written as an indice of that angle. This situation is shown in the following figure.

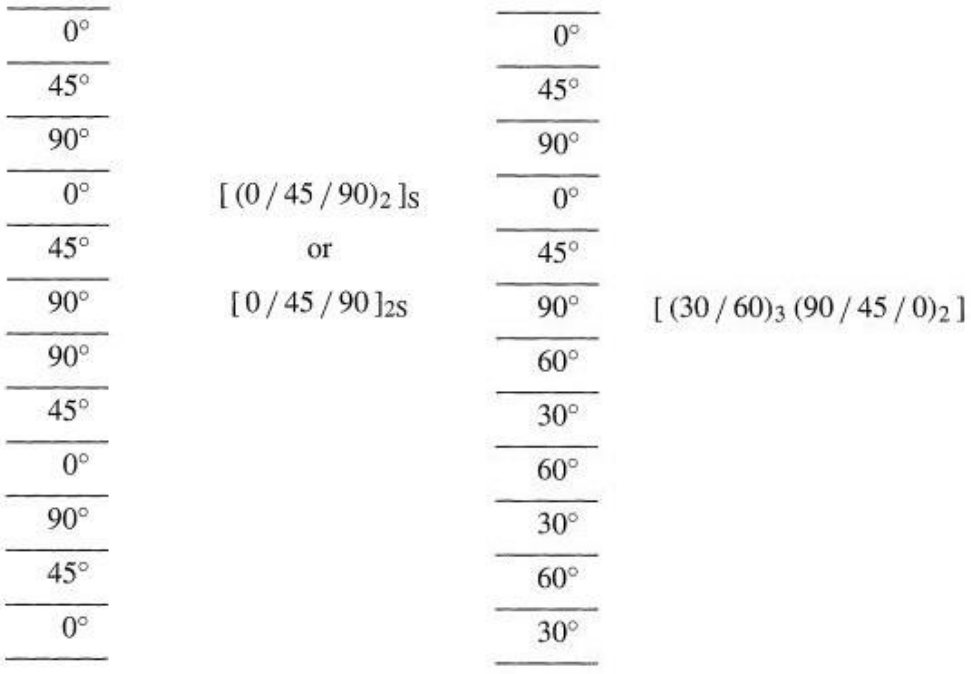

Figure 2.10 : The laminate that has a repeated sequence.

2.3. Generalized Hooke's Law

The stress-strain relationship is defined by Hooke's Law. For a general material that is not linearly elastic and isotropic is defined at the equation below which is also called as Voigt notation.

$$[\sigma] = [C][\varepsilon] \overset{OR}{\rightarrow} \begin{bmatrix} \sigma_1 \\ \sigma_2 \\ \sigma_3 \\ \tau_{23} \\ \tau_{31} \\ \tau_{12} \end{bmatrix} = \begin{bmatrix} C_{11} & C_{12} & C_{13} & C_{14} & C_{15} & C_{16} \\ C_{21} & C_{22} & C_{23} & C_{24} & C_{25} & C_{26} \\ C_{31} & C_{32} & C_{33} & C_{34} & C_{35} & C_{36} \\ C_{41} & C_{42} & C_{43} & C_{44} & C_{45} & C_{46} \\ C_{51} & C_{52} & C_{53} & C_{54} & C_{55} & C_{56} \\ C_{61} & C_{62} & C_{63} & C_{64} & C_{65} & C_{66} \end{bmatrix} \begin{bmatrix} \varepsilon_1 \\ \varepsilon_2 \\ \varepsilon_3 \\ \gamma_{23} \\ \gamma_{31} \\ \gamma_{12} \end{bmatrix} \qquad (\mathbf{2.1})$$

Where,

[σ]: Vector representation of stress tensor

[ε]: Vector representation of strain tensor

[C]: Stiffness matrix.

This matrix equation can also be written with the sum symbol.

$$\sigma_i = \sum_{i=1}^{6} C_{ij}\varepsilon_j, \quad i = 1,2,\dots,6 \qquad (\mathbf{2.2})$$

If the stiffness matrix and strain vector are known the stress vector can be calculated the above equation. If the stiffness matrix and stress vector are known the strain vector can be calculated by taking the inverse of the stiffness matrix. This matrix is called compliance matrix and shown as [S].

$$[\varepsilon] = [S][\sigma] \overset{OR}{\rightarrow} \begin{bmatrix} \varepsilon_1 \\ \varepsilon_2 \\ \varepsilon_3 \\ \gamma_{23} \\ \gamma_{31} \\ \gamma_{12} \end{bmatrix} = \begin{bmatrix} S_{11} & S_{12} & S_{13} & S_{14} & S_{15} & S_{16} \\ S_{21} & S_{22} & S_{23} & S_{24} & S_{25} & S_{26} \\ S_{31} & S_{32} & S_{33} & S_{34} & S_{35} & S_{36} \\ S_{41} & S_{42} & S_{43} & S_{44} & S_{45} & S_{46} \\ S_{51} & S_{52} & S_{53} & S_{54} & S_{55} & S_{56} \\ S_{61} & S_{62} & S_{63} & S_{64} & S_{65} & S_{66} \end{bmatrix} \begin{bmatrix} \sigma_1 \\ \sigma_2 \\ \sigma_3 \\ \tau_{23} \\ \tau_{31} \\ \tau_{12} \end{bmatrix} \quad (\mathbf{2.3})$$

$$[C]^{-1} = [S] \quad OR \quad [S]^{-1} = [C] \quad (\mathbf{2.4})$$

The stiffness and compliance matrices are 6x6 so they have 36 constants. In addition, these matrices are symmetric matrix so the number of constants reduces to 21.

$$S_{ij} = S_{ji} \quad and \quad C_{ij} = C_{ji}$$

2.4. Different Types of Materials and Hooke's Law for these materials

Some materials show different characteristics when loaded in different directions. In other words, the materials' properties change from one direction to another direction at a single point, which means that the material properties are not symmetric. This property is called anisotropy. This does not mean nonhomogeneous material. Even is the material is homogeneous, the anisotropy can be seen. The main thing is the material properties are defined at one single point. This means that the material properties can change from one point to another point in the material if the material is nonhomogeneous. This affects directly the material properties. In addition, some materials show symmetric property at a single point. This reduces the unknowns in the stiffness and compliance matrices. Material types can be listed as follows.

- Anisotropic material
- Monoclinic material
- Orthotropic material
- Transversely isotropic material
- Isotropic material

2.4.1. Anisotropic material

The material that has 21 independent elastic constants at a point is called and anisotropic material. This is the most generalized case of material. If the stress and strain relationship wanted to be developed, all of the 21 independent material constants must be known. The stiffness matrix with 21 unknowns (including matrix symmetry) can be seen at the following equation.

$$[C] = \begin{bmatrix} C_{11} & C_{12} & C_{13} & C_{14} & C_{15} & C_{16} \\ C_{12} & C_{22} & C_{23} & C_{24} & C_{25} & C_{26} \\ C_{13} & C_{23} & C_{33} & C_{34} & C_{35} & C_{36} \\ C_{14} & C_{24} & C_{34} & C_{44} & C_{45} & C_{46} \\ C_{15} & C_{25} & C_{35} & C_{45} & C_{55} & C_{56} \\ C_{16} & C_{26} & C_{36} & C_{46} & C_{56} & C_{66} \end{bmatrix} \qquad (\mathbf{2.5})$$

2.4.2. Monoclinic material

The materials that show one single plane symmetry is called that monoclinic materials. The material symmetry means that the properties of the material are identical with respect to the symmetry plane. In other words, the mirror image with respect to the symmetry plane is identical with each other. The figure below is an example for a monoclinic material behavior. As it is seen from the example, the direction 3 is normal to the plane of material symmetry.

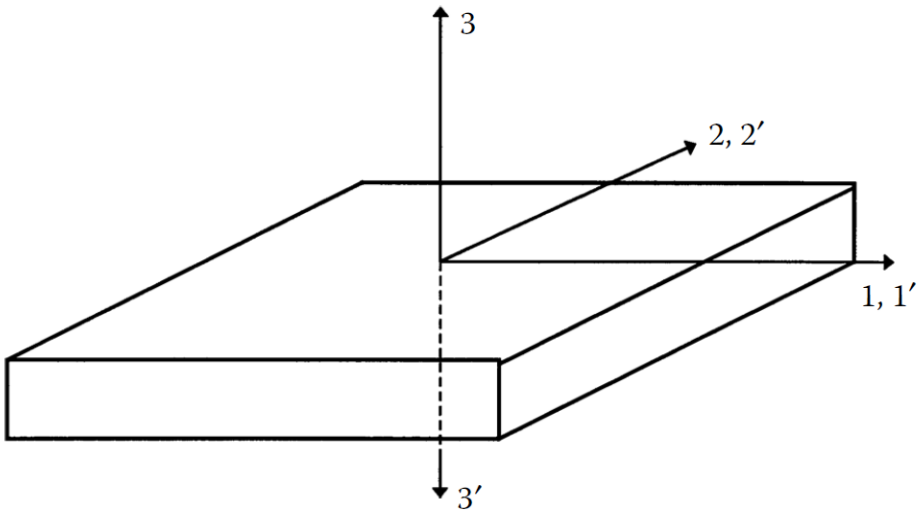

Figure 2.11 : Symmetry plane for the monoclinic material.

The perpendicular direction to the symmetry plane is called that the principal direction. The stiffness and compliance matrices have 13 independent constants. The following matrix shows the stiffness matrix for a monoclinic material.

$$[C] = \begin{bmatrix} C_{11} & C_{12} & C_{13} & 0 & 0 & C_{16} \\ C_{12} & C_{22} & C_{23} & 0 & 0 & C_{26} \\ C_{13} & C_{23} & C_{33} & 0 & 0 & C_{36} \\ 0 & 0 & 0 & C_{44} & C_{45} & 0 \\ 0 & 0 & 0 & C_{45} & C_{55} & 0 \\ C_{16} & C_{26} & C_{36} & 0 & 0 & C_{66} \end{bmatrix} \quad (\mathbf{2.6})$$

The compliance matrix is the inverse of the stiffness matrix.

Figure 2.12 : An example of a monoclinic material, orthoclase.

Orthoclase is an example of a monoclinic material. The following figure shows the orthoclase.

The following cube shows the deformation characteristics of a monoclinic material. The surfaces BEHA, CFGD are perpendicular to the direction 3 will change to parallelograms from rectangles whereas, the remaining four surfaces ABCD, BEFC, GFEH and AHGD will stay as rectangles which means that the material properties are identical with respect to the symmetry plane.

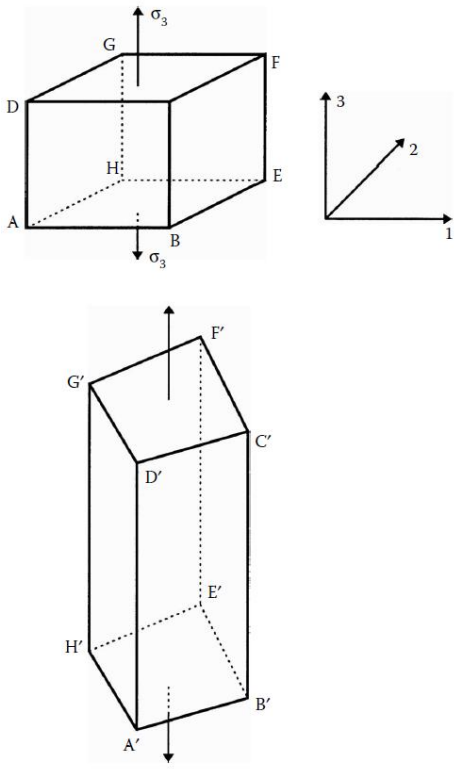

Figure 2.13 : Deformation of a monoclinic system.

2.4.3. Orthotropic material

If a material has three mutually perpendicular planes of material symmetry then the material is called orthotropic material. An aligned unidirectional fiber matrix composite is a good example for an orthotropic material. The following figure shows a unidirectional lamina as an example of orthotropic material. It has the 3 mutually plane of symmetry. A wooden bar and a rolled steel bar can be examples of an orthotropic material.

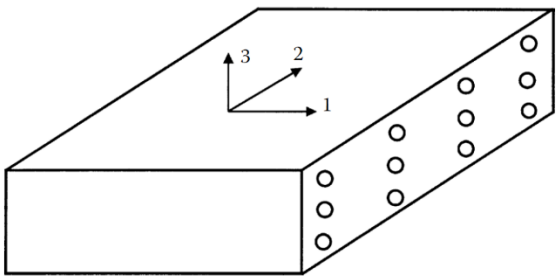

Figure 2.14 : A unidirectional lamina with fibers aligned in a rectangular array is an example of an orthotropic material.

This makes the number of stiffness and compliance matrix elements reduced. The number of independent constants reduces to 9.

$$[C] = \begin{bmatrix} C_{11} & C_{12} & C_{13} & 0 & 0 & 0 \\ C_{12} & C_{22} & C_{23} & 0 & 0 & 0 \\ C_{13} & C_{23} & C_{33} & 0 & 0 & 0 \\ 0 & 0 & 0 & C_{44} & 0 & 0 \\ 0 & 0 & 0 & 0 & C_{55} & 0 \\ 0 & 0 & 0 & 0 & 0 & C_{66} \end{bmatrix} \quad (\mathbf{2.7})$$

The following figure shows the elastic symmetry of an orthotropic material. When a normal force is applied to a cube segment. The following deformations will occur. All of the rectangle faces will remain as rectangles. The directions at the cube element 1,2 and 3 are the principle directions which means that the 1-2, 2-3 and 3-1 planes are three mutually perpendicular planes of symmetry.

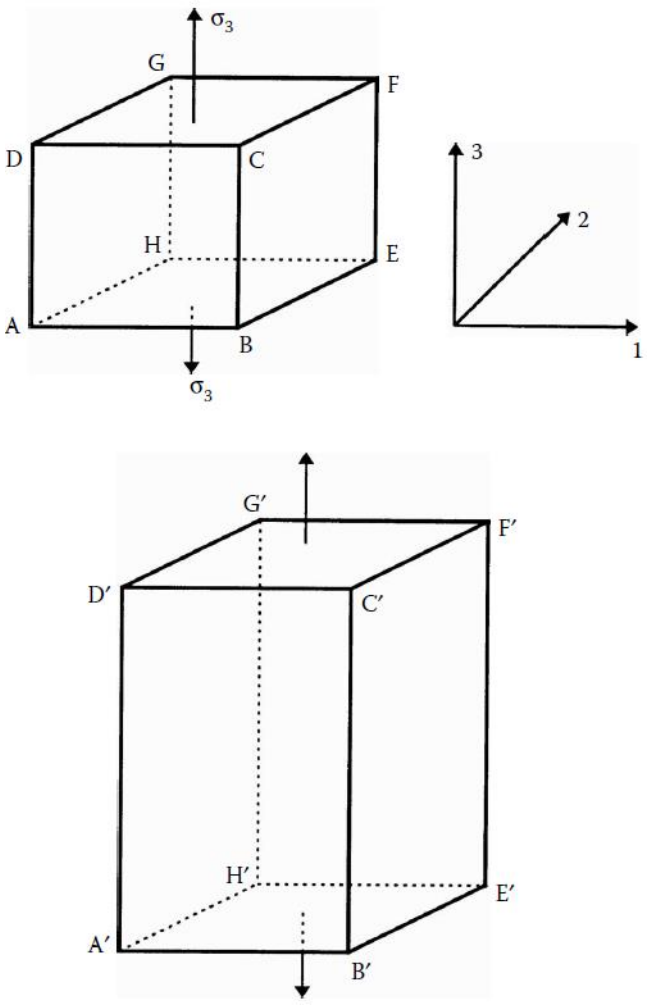

Figure 2.15 : Deformation of an orthotropic material.

2.4.4. Transversely isotropic material

Consider a plane of material symmetry in one of the planes of an orthotropic body. If the direction 1 is perpendicular to that plane (2-3) of isotropy, then the material is called transversely isotropic material.

The stiffness and compliance matrix elements will be reduced. The number of independent materials constants will be 5 for a transversely isotropic material.

$$[C] = \begin{bmatrix} C_{11} & C_{12} & C_{12} & 0 & 0 & 0 \\ C_{12} & C_{22} & C_{23} & 0 & 0 & 0 \\ C_{12} & C_{23} & C_{22} & 0 & 0 & 0 \\ 0 & 0 & 0 & \frac{C_{22} - C_{23}}{2} & 0 & 0 \\ 0 & 0 & 0 & 0 & C_{55} & 0 \\ 0 & 0 & 0 & 0 & 0 & C_{55} \end{bmatrix} \qquad (\mathbf{2.8})$$

The following relations can be resulted by transversely isotropic structure

- $C_{22} = C_{33}$
- $C_{12} = C_{13}$
- $C_{55} = C_{66}$
- $C_{44} = \frac{C_{22} - C_{23}}{2}$

A unidirectional lamina with fibers aligned in a rectangular array is an example of an orthotropic material

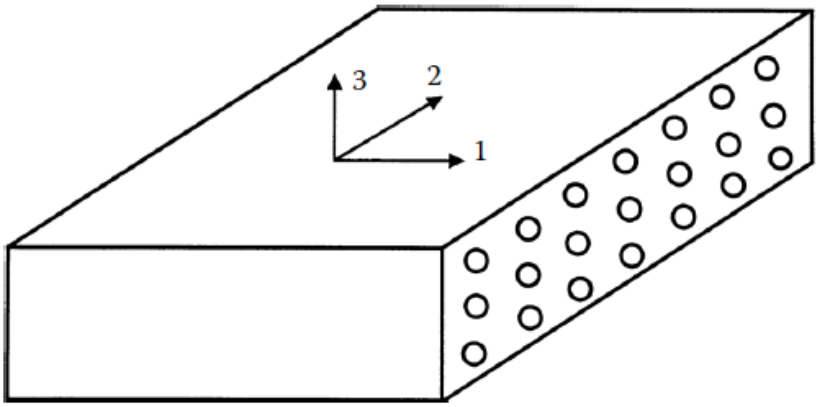

Figure 2.16 : A unidirectional lamina with fibers aligned in a rectangular array.

2.4.5. Isotropic material

If all of the planes of an orthotropic material are identical then the material is called to be an isotropic material.

The stiffness and compliance matrix elements will be reduced. The number of independent material constants will be 2 for an isotropic material.

$$[C] = \begin{bmatrix} C_{11} & C_{12} & C_{12} & 0 & 0 & 0 \\ C_{12} & C_{11} & C_{12} & 0 & 0 & 0 \\ C_{12} & C_{12} & C_{11} & 0 & 0 & 0 \\ 0 & 0 & 0 & \frac{C_{11}-C_{12}}{2} & 0 & 0 \\ 0 & 0 & 0 & 0 & \frac{C_{11}-C_{12}}{2} & 0 \\ 0 & 0 & 0 & 0 & 0 & \frac{C_{11}-C_{12}}{2} \end{bmatrix} \quad (\mathbf{2.9})$$

Moreover, the compliance matrix is the inverse of the stiffness matrix. The compliance matrix becomes as follows.

$$[S] = \begin{bmatrix} S_{11} & S_{12} & S_{12} & 0 & 0 & 0 \\ S_{12} & S_{11} & S_{13} & 0 & 0 & 0 \\ S_{12} & S_{12} & S_{11} & 0 & 0 & 0 \\ 0 & 0 & 0 & 2(S_{11}-S_{12}) & 0 & 0 \\ 0 & 0 & 0 & 0 & 2(S_{11}-S_{12}) & 0 \\ 0 & 0 & 0 & 0 & 0 & 2(S_{11}-S_{12}) \end{bmatrix} \quad (\mathbf{2.10})$$

The following relations can be resulted by transversely isotropic structure

- $C_{11} = C_{22}$
- $C_{12} = C_{23}$
- $C_{66} = \frac{C_{22}-C_{23}}{2} = \frac{C_{11}-C_{12}}{2}$

This relationship shows that there is infinite number of principle planes of symmetry. Many types of materials are isotropic materials such as iron, aluminum etc.

The C_{11} C_{12} and $(C_{11}-C_{12})/2$ constants can be converted to well-known constants that are modulus of elasticity (E) and Poisson's ratio (ν).

$$C_{11} = \frac{E(1-\nu)}{(1-2\nu)(1+\nu)} \quad (\mathbf{2.11})$$

$$C_{12} = \frac{\nu E}{(1-2\nu)(1+\nu)} \quad (\mathbf{2.12})$$

$$\frac{C_{11} - C_{12}}{2} = \frac{1}{2}\left[\frac{E(1-\nu)}{(1-2\nu)(1+\nu)} - \frac{\nu E}{(1-2\nu)(1+\nu)}\right] = \frac{E}{2(1+\nu)} = G \quad (\mathbf{2.13})$$

As a result, by using the above constants the stiffness matrix becomes,

$$[C] = \begin{bmatrix} \frac{E(1-\nu)}{(1-2\nu)(1+\nu)} & \frac{\nu E}{(1-2\nu)(1+\nu)} & \frac{\nu E}{(1-2\nu)(1+\nu)} & 0 & 0 & 0 \\ \frac{\nu E}{(1-2\nu)(1+\nu)} & \frac{E(1-\nu)}{(1-2\nu)(1+\nu)} & \frac{\nu E}{(1-2\nu)(1+\nu)} & 0 & 0 & 0 \\ \frac{\nu E}{(1-2\nu)(1+\nu)} & \frac{\nu E}{(1-2\nu)(1+\nu)} & \frac{E(1-\nu)}{(1-2\nu)(1+\nu)} & 0 & 0 & 0 \\ 0 & 0 & 0 & G & 0 & 0 \\ 0 & 0 & 0 & 0 & G & 0 \\ 0 & 0 & 0 & 0 & 0 & G \end{bmatrix} \quad (\mathbf{2.14})$$

Moreover, the compliance matrix, which is the inverse of the stiffness matrix, becomes,

$$[S] = \begin{bmatrix} \frac{1}{E} & -\frac{\nu}{E} & -\frac{\nu}{E} & 0 & 0 & 0 \\ -\frac{\nu}{E} & \frac{1}{E} & -\frac{\nu}{E} & 0 & 0 & 0 \\ -\frac{\nu}{E} & -\frac{\nu}{E} & \frac{1}{E} & 0 & 0 & 0 \\ 0 & 0 & 0 & \frac{1}{G} & 0 & 0 \\ 0 & 0 & 0 & 0 & \frac{1}{G} & 0 \\ 0 & 0 & 0 & 0 & 0 & \frac{1}{G} \end{bmatrix} \quad (\mathbf{2.15})$$

2.4.6. Summary of material types

To sum up, the number of independent variables for different types of materials can be seen as follows.

- Anisotropic: 21

- Monoclinic: 13
- Orthotropic: 9
- Transversely isotropic: 5
- Isotropic: 2

This shows that the most complex material types is anisotropic material and the simplest material is isotropic material.

To solve the stress strain relationship the Hooke's Law must be solved. For isotropic material this equation becomes very simple due to stiffness matrix reduces to 2 elements.

However, for anisotropic material solving Hooke's Law becomes difficult. The 6x6-matrix equation must be solved. In addition, the stress and strain components are directionally different from each other.

When compared to isotropic materials, the deformation characteristics will not be determined very easily. Because, all of the 21 constants must be known of somehow obtained. It can be theoretically or experimentally.

Our topic is about carbon fiber, which is an orthotropic material. The elastic constants are directionally independent from each other. These constants generally obtained experimentally. For carbon fiber, the elastic constants differ from texture to texture.

However, there are relationships about fiber angle and material thickness. Since the unidirectional lamina constants are known, the angled constants can be determined by using transformation matrices (This will be introduced in the following chapters).

2.5. The Stiffness Matrix of an Orthotropic Material with Engineering Constants

2.5.1. Fundamental definitions

The elasticity modulus in direction 1, E_1, is defined as

$$E_1 = \frac{\sigma_1}{\varepsilon_1} \qquad (\mathbf{2.16})$$

Similarly, the elasticity moduli in directions 2 and 3 can be written as follows,

$$E_2 = \frac{\sigma_2}{\varepsilon_2} = \frac{1}{S_{22}} \tag{2.17}$$

$$E_3 = \frac{\sigma_3}{\varepsilon_3} = \frac{1}{S_{33}} \tag{2.18}$$

Moreover, the Poisson's ratios, ν_{12} and ν_{21} are defined as

$$\nu_{12} = -\frac{\varepsilon_2}{\varepsilon_1} \quad and \quad \nu_{21} = -\frac{\varepsilon_1}{\varepsilon_2} \tag{2.19}$$

Similarly, the other Poisson's Ratios can be written as,

$$\nu_{13} = -\frac{\varepsilon_3}{\varepsilon_1} \quad and \quad \nu_{31} = -\frac{\varepsilon_1}{\varepsilon_3} \tag{2.20}$$

$$\nu_{23} = -\frac{\varepsilon_3}{\varepsilon_2} \quad and \quad \nu_{32} = -\frac{\varepsilon_2}{\varepsilon_3} \tag{2.21}$$

The shear modulus in plane 2-3 is defined as,

$$G_{23} = G_{32} = \frac{\tau_{23}}{\gamma_{23}} \tag{2.22}$$

Similarly, the shear moduli in plane 3-1 and 1-2 can be written as follows,

$$G_{31} = G_{13} = \frac{\tau_{31}}{\gamma_{31}} \tag{2.23}$$

$$G_{12} = G_{21} = \frac{\tau_{12}}{\gamma_{12}} \tag{2.24}$$

2.5.2. Representation of the stiffness matrix of an orthotropic material with engineering constants

As mentioned above a unidirectional lamina with fiber laying on a rectangular array shows orthotropic behavior. Moreover, the stiffness matrix of an isotropic material in engineering constants was represented in previous sections.

Since our topic about carbon fiber composite, the stiffness matrix had to be written in engineering constants. Unless the matrix is written in engineering constants, the

stiffness matrix cannot be used because the engineering constants are known so they can be used properly.

To do that, first of all, a rectangle orthotropic part is taken apart from a part and exerted different loading conditions. See following figure for the loading conditions.

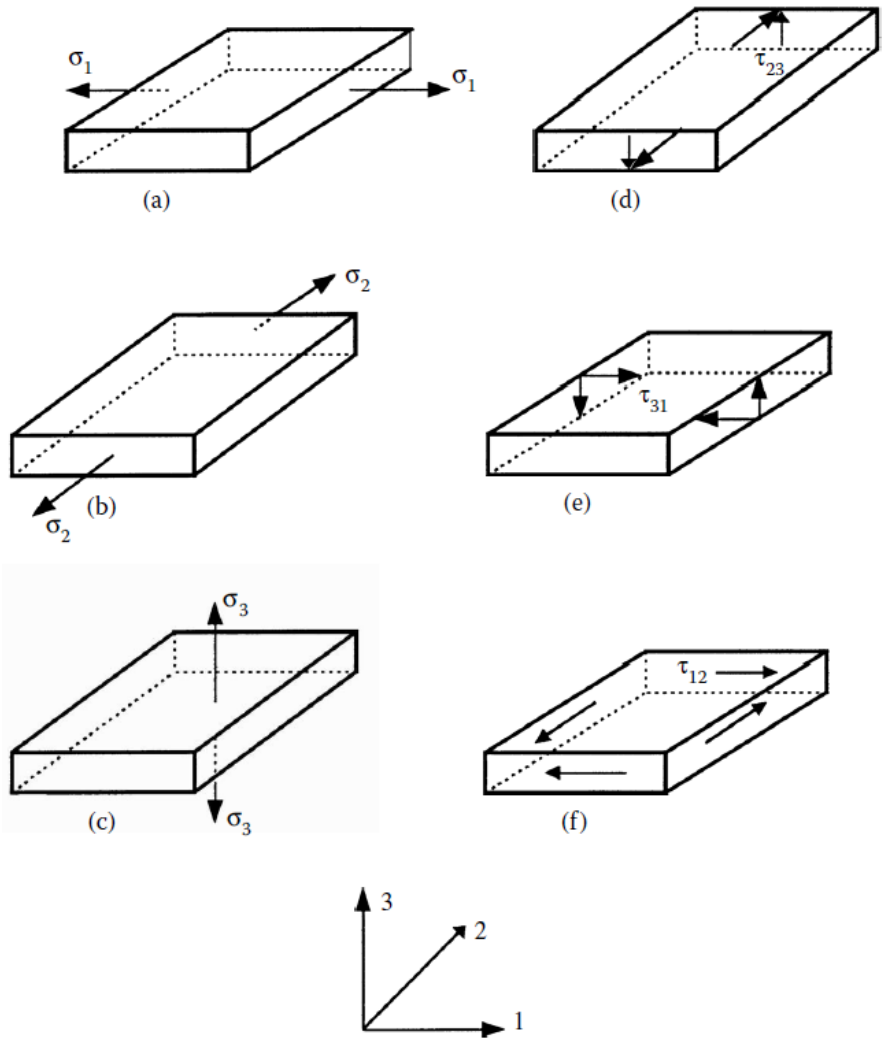

Figure 2.17 : Loading conditions of an orthotropic material.

As shown in the;

- *Figure 2.17a* $\sigma_1 \neq 0$ whereas $\sigma_2 = \sigma_3 = \tau_{23} = \tau_{31} = \tau_{12} = 0$.
- *Figure 2.17b* $\sigma_2 \neq 0$ whereas $\sigma_1 = \sigma_3 = \tau_{23} = \tau_{31} = \tau_{12} = 0$.
- *Figure 2.17c* $\sigma_3 \neq 0$ whereas $\sigma_1 = \sigma_2 = \tau_{23} = \tau_{31} = \tau_{12} = 0$.
- *Figure 2.17d* $\tau_{23} \neq 0$ whereas $\sigma_1 = \sigma_2 = \sigma_3 = \tau_{31} = \tau_{12} = 0$.
- *Figure 2.17e* $\tau_{31} \neq 0$ whereas $\sigma_1 = \sigma_2 = \sigma_3 = \tau_{23} = \tau_{12} = 0$.
- *Figure 2.17f* $\tau_{12} \neq 0$ whereas $\sigma_1 = \sigma_2 = \sigma_3 = \tau_{23} = \tau_{31} = 0$.

Remark of the generalized Hooke's Law with compliance matrix for an orthotropic material as follows;

$$[\varepsilon] = [S][\sigma] \quad \overset{OR}{\rightarrow} \quad \begin{bmatrix} \varepsilon_1 \\ \varepsilon_2 \\ \varepsilon_3 \\ \gamma_{23} \\ \gamma_{31} \\ \gamma_{12} \end{bmatrix} = \begin{bmatrix} S_{11} & S_{12} & S_{13} & 0 & 0 & 0 \\ S_{12} & S_{22} & S_{23} & 0 & 0 & 0 \\ S_{13} & S_{23} & S_{33} & 0 & 0 & 0 \\ 0 & 0 & 0 & S_{44} & 0 & 0 \\ 0 & 0 & 0 & 0 & S_{55} & 0 \\ 0 & 0 & 0 & 0 & 0 & S_{66} \end{bmatrix} \begin{bmatrix} \sigma_1 \\ \sigma_2 \\ \sigma_3 \\ \tau_{23} \\ \tau_{31} \\ \tau_{12} \end{bmatrix} \qquad (\mathbf{2.25})$$

2.5.2.1. The case in the *figure 2.17a*

As in the case of *Figure 2.17a* the strains from the Hooke's Law will be,

$$\begin{aligned} \varepsilon_1 &= S_{11}\sigma_1 \\ \varepsilon_2 &= S_{12}\sigma_1 \\ \varepsilon_3 &= S_{13}\sigma_1 \\ \gamma_{23} &= 0 \\ \gamma_{31} &= 0 \\ \gamma_{12} &= 0 \end{aligned} \qquad (\mathbf{2.26})$$

From the above relationship the followings can be written,

$$S_{11} = \frac{\varepsilon_1}{\sigma_1} \qquad (\mathbf{2.27})$$

In the section 2.5.1 the elasticity modulus in direction 1 is defined. As a result, the following relation can be written.

$$E_1 = \frac{\sigma_1}{\varepsilon_1} = \frac{1}{S_{11}} \quad \overset{yields}{\longrightarrow} \quad S_{11} = \frac{1}{E_1} \qquad (\mathbf{2.28})$$

If the following equations are proportioned, we get,

$$\begin{matrix} \varepsilon_1 = S_{11}\sigma_1 \\ \varepsilon_2 = S_{12}\sigma_1 \end{matrix} \quad \overset{yields}{\longrightarrow} \quad \frac{S_{11}}{S_{12}} = \frac{\varepsilon_1}{\varepsilon_2} \qquad (\mathbf{2.29})$$

$$\begin{matrix} \varepsilon_1 = S_{11}\sigma_1 \\ \varepsilon_3 = S_{13}\sigma_1 \end{matrix} \quad \overset{yields}{\longrightarrow} \quad \frac{S_{11}}{S_{13}} = \frac{\varepsilon_1}{\varepsilon_3} \qquad (\mathbf{2.30})$$

From the section 1.5.1 the Poisson ratios are defined as follows and by using the above relationship we get,

$$\nu_{12} = -\frac{\varepsilon_2}{\varepsilon_1} \quad \xrightarrow{yields} \quad \nu_{12} = -\frac{S_{12}}{S_{11}} \tag{2.31}$$

$$\nu_{13} = -\frac{\varepsilon_3}{\varepsilon_1} \quad \xrightarrow{yields} \quad \nu_{13} = -\frac{S_{13}}{S_{11}} \tag{2.32}$$

2.5.2.2. The case in the *figure 2.17b*

As in the case of *Figure 2.17b* the strains from the Hooke's Law will be,

$$\begin{aligned} \varepsilon_1 &= S_{12}\sigma_2 \\ \varepsilon_2 &= S_{22}\sigma_2 \\ \varepsilon_3 &= S_{23}\sigma_2 \\ \gamma_{23} &= 0 \\ \gamma_{31} &= 0 \\ \gamma_{12} &= 0 \end{aligned} \tag{2.33}$$

From the above relationship the followings can be written,

$$S_{22} = \frac{\varepsilon_2}{\sigma_2} \tag{2.34}$$

In the previous sections, the elasticity modulus in direction 2 is defined. As a result, the following relation can be written.

$$E_2 = \frac{\sigma_2}{\varepsilon_2} = \frac{1}{S_{22}} \quad \xrightarrow{yields} \quad S_{22} = \frac{1}{E_2} \tag{2.35}$$

If the following equations are proportioned, we get,

$$\begin{matrix} \varepsilon_2 = S_{22}\sigma_2 \\ \varepsilon_1 = S_{12}\sigma_2 \end{matrix} \quad \xrightarrow{yields} \quad \frac{S_{22}}{S_{12}} = \frac{\varepsilon_2}{\varepsilon_1} \tag{2.36}$$

$$\begin{matrix} \varepsilon_2 = S_{22}\sigma_2 \\ \varepsilon_3 = S_{23}\sigma_2 \end{matrix} \quad \xrightarrow{yields} \quad \frac{S_{22}}{S_{23}} = \frac{\varepsilon_2}{\varepsilon_3} \tag{2.37}$$

From the previous sections, the Poisson ratios are defined as follows and by using the above relationship we get,

$$\nu_{21} = -\frac{\varepsilon_1}{\varepsilon_2} \quad \xrightarrow{yields} \quad \nu_{21} = -\frac{S_{12}}{S_{22}} \tag{2.38}$$

$$\nu_{23} = -\frac{\varepsilon_3}{\varepsilon_2} \quad \xrightarrow{yields} \quad \nu_{23} = -\frac{S_{23}}{S_{22}} \tag{2.39}$$

2.5.2.3. The case in the *figure 2.17c*

As in the case of *Figure 2.17c* the strains from the Hooke's Law will be,

$$\begin{aligned} \varepsilon_1 &= S_{13}\sigma_3 \\ \varepsilon_2 &= S_{23}\sigma_3 \\ \varepsilon_3 &= S_{33}\sigma_3 \\ \gamma_{23} &= 0 \\ \gamma_{31} &= 0 \\ \gamma_{12} &= 0 \end{aligned} \tag{2.40}$$

From the above relationship the followings can be written,

$$S_{33} = \frac{\varepsilon_3}{\sigma_3} \tag{2.41}$$

In the previous sections, the elasticity modulus in direction 3 is defined. As a result, the following relation can be written.

$$E_3 = \frac{\sigma_3}{\varepsilon_3} = \frac{1}{S_{33}} \quad \xrightarrow{yields} \quad S_{33} = \frac{1}{E_3} \tag{2.42}$$

If the following equations are proportioned, we get,

$$\begin{matrix} \varepsilon_3 = S_{33}\sigma_3 \\ \varepsilon_1 = S_{13}\sigma_3 \end{matrix} \quad \xrightarrow{yields} \quad \frac{S_{33}}{S_{13}} = \frac{\varepsilon_3}{\varepsilon_1} \tag{2.43}$$

$$\begin{matrix} \varepsilon_3 = S_{33}\sigma_3 \\ \varepsilon_2 = S_{23}\sigma_3 \end{matrix} \quad \xrightarrow{yields} \quad \frac{S_{33}}{S_{23}} = \frac{\varepsilon_3}{\varepsilon_2} \tag{2.44}$$

From the previous sections, the Poisson ratios are defined as follows and by using the above relationship we get,

$$\nu_{31} = -\frac{\varepsilon_1}{\varepsilon_3} \quad \xrightarrow{yields} \quad \nu_{31} = -\frac{S_{13}}{S_{33}} \tag{2.45}$$

$$\nu_{32} = -\frac{\varepsilon_2}{\varepsilon_3} \quad \xrightarrow{yields} \quad \nu_{32} = -\frac{S_{23}}{S_{33}} \tag{2.46}$$

2.5.2.4. The case in the *figure 2.17d*

As in the case of *Figure 2.17d* the strains from the Hooke's Law will be,

$$\begin{gathered}\varepsilon_1 = 0 \\ \varepsilon_2 = 0 \\ \varepsilon_3 = 0 \\ \gamma_{23} = S_{44}\tau_{23} \\ \gamma_{31} = 0 \\ \gamma_{12} = 0\end{gathered} \tag{2.47}$$

From the above relationship the followings can be written,

$$S_{44} = \frac{\gamma_{23}}{\tau_{23}} \tag{2.48}$$

In the previous sections, the shear modulus in plane 2-3 is defined. As a result, the following relation can be written.

$$G_{23} = \frac{\tau_{23}}{\gamma_{23}} = \frac{1}{S_{44}} \quad \xrightarrow{yields} \quad S_{44} = \frac{1}{G_{23}} \tag{2.49}$$

2.5.2.5. The case in the *figure 2.17e*

As in the case of *Figure 2.17e* the strains from the Hooke's Law will be,

$$\begin{gathered}\varepsilon_1 = 0 \\ \varepsilon_2 = 0 \\ \varepsilon_3 = 0 \\ \gamma_{23} = 0 \\ \gamma_{31} = S_{55}\tau_{31} \\ \gamma_{12} = 0\end{gathered} \tag{2.50}$$

From the above relationship the followings can be written,

$$S_{55} = \frac{\gamma_{31}}{\tau_{31}} \tag{2.51}$$

In the previous sections, the shear modulus in plane 3-1 is defined. As a result, the following relation can be written.

$$G_{31} = \frac{\tau_{31}}{\gamma_{31}} = \frac{1}{S_{55}} \quad \xrightarrow{yields} \quad S_{55} = \frac{1}{G_{31}} \tag{2.52}$$

2.5.2.6. The case in the *figure 2.17f*

As in the case of *Figure 2.17f* the strains from the Hooke's Law will be,

$$\begin{gathered} \varepsilon_1 = 0 \\ \varepsilon_2 = 0 \\ \varepsilon_3 = 0 \\ \gamma_{23} = 0 \\ \gamma_{31} = 0 \\ \gamma_{12} = S_{66}\tau_{12} \end{gathered} \tag{2.53}$$

From the above relationship the followings can be written,

$$S_{66} = \frac{\gamma_{12}}{\tau_{12}} \tag{2.54}$$

In the previous sections, the shear modulus in plane 1-2 is defined. As a result, the following relation can be written.

$$G_{12} = \frac{\tau_{12}}{\gamma_{12}} = \frac{1}{S_{66}} \quad \xrightarrow{yields} \quad S_{66} = \frac{1}{G_{12}} \tag{2.55}$$

2.5.2.7. Summary of this section

From the sections above the compliance components (S_{ij}) are related with the engineering constants. Totally, three elasticity moduli E_1, E_2 and E_3; six Poisson ratios ν_{12}, ν_{13}, ν_{21}, ν_{23}, ν_{31} and ν_{32}; and three shear moduli G_{23}, G_{31} and G_{12} are related with the compliance components. To revise that, see the equations below.

$$S_{11} = \frac{1}{E_1} \quad S_{22} = \frac{1}{E_2} \quad S_{33} = \frac{1}{E_3} \tag{2.56}$$

$$\nu_{12} = -\frac{S_{12}}{S_{11}} \quad \nu_{13} = -\frac{S_{13}}{S_{11}} \quad \nu_{21} = -\frac{S_{12}}{S_{22}} \tag{2.57}$$

$$\nu_{23} = -\frac{S_{23}}{S_{22}} \quad \nu_{31} = -\frac{S_{13}}{S_{33}} \quad \nu_{32} = -\frac{S_{23}}{S_{33}} \tag{2.58}$$

$$S_{44} = \frac{1}{G_{23}} = \frac{1}{G_{32}} \quad S_{55} = \frac{1}{G_{31}} = \frac{1}{G_{13}} \quad S_{66} = \frac{1}{G_{12}} = \frac{1}{G_{21}} \qquad (\mathbf{2.59})$$

As it is seen, the S_{ii} values are clearly obtained. However, the S_{ij} values are still not known. From the above relation the ν_{ij} values and ν_{ji} values can be related to each other by using the relationship of the elasticity modulus. This relation is known as reciprocal Poisson's ratio. See the following relation.

Let us take the following relations.

$$\nu_{12} = -\frac{S_{12}}{S_{11}} \quad and \quad \nu_{21} = -\frac{S_{12}}{S_{22}} \qquad (\mathbf{2.60})$$

Here we can write the following relationship.

$$S_{11} = \frac{1}{E_1} \rightarrow \frac{1}{S_{11}} = E_1 \quad and \quad S_{22} = \frac{1}{E_2} \rightarrow \frac{1}{S_{22}} = E_2 \qquad (\mathbf{2.61})$$

So we get,

$$\nu_{12} = -S_{12}E_1 \quad and \quad \nu_{21} = -S_{12}E_2 \qquad (\mathbf{2.62})$$

Now S_{12} value can be written both in the two equations.

$$\begin{matrix} S_{12} = -\frac{\nu_{12}}{E_1} \\ S_{12} = -\frac{\nu_{21}}{E_2} \end{matrix} \xrightarrow{yields} \frac{\nu_{12}}{E_1} = \frac{\nu_{21}}{E_2} \qquad (\mathbf{2.63})$$

Similarly,

$$\frac{\nu_{13}}{E_1} = \frac{\nu_{31}}{E_3} \qquad (\mathbf{2.64})$$

$$\frac{\nu_{23}}{E_2} = \frac{\nu_{32}}{E_3} \qquad (\mathbf{2.65})$$

Now the following compliance components can be concluded.

$$S_{12} = -\frac{\nu_{12}}{E_1} = -\frac{\nu_{21}}{E_2} \qquad (\mathbf{2.66})$$

$$S_{13} = -\frac{\nu_{13}}{E_1} = -\frac{\nu_{31}}{E_3} \tag{2.67}$$

$$S_{23} = -\frac{\nu_{23}}{E_2} = -\frac{\nu_{32}}{E_3} \tag{2.68}$$

As it is seen S_{12}, S_{13} and S_{23} components, have two reciprocate. That is why ν_{ij} and ν_{ji} components are called reciprocated Poisson's ratios. Both values give same results but in the literature, the Poisson's ratios are obtained as ν_{12}, ν_{13}, ν_{23}. So the following compliance matrix will be generated by using the ν_{12}, ν_{13}, ν_{23} Poisson's ratios.

$$S = \begin{bmatrix} \frac{1}{E_1} & -\frac{\nu_{12}}{E_1} & -\frac{\nu_{13}}{E_1} & 0 & 0 & 0 \\ -\frac{\nu_{12}}{E_1} & \frac{1}{E_2} & -\frac{\nu_{23}}{E_2} & 0 & 0 & 0 \\ -\frac{\nu_{13}}{E_1} & -\frac{\nu_{23}}{E_2} & \frac{1}{E_3} & 0 & 0 & 0 \\ 0 & 0 & 0 & \frac{1}{G_{23}} & 0 & 0 \\ 0 & 0 & 0 & 0 & \frac{1}{G_{13}} & 0 \\ 0 & 0 & 0 & 0 & 0 & \frac{1}{G_{12}} \end{bmatrix} \tag{2.69}$$

The stiffness matrix C is the inverse of the compliance matrix S. The following matrix is the stiffness matrix for an orthotropic material. In this following stiffness matrix, both ν_{ij} and ν_{ji} values are used. Simply, by using, the reciprocating Poisson ratio relationship, the ν_{ji} values can be calculated easily.

$$C = \begin{bmatrix} \frac{1-\nu_{23}\nu_{32}}{E_2E_3\Delta} & \frac{\nu_{21}+\nu_{23}\nu_{31}}{E_2E_3\Delta} & \frac{\nu_{31}+\nu_{21}\nu_{23}}{E_2E_3\Delta} & 0 & 0 & 0 \\ \frac{\nu_{21}+\nu_{23}\nu_{31}}{E_2E_3\Delta} & \frac{1-\nu_{13}\nu_{31}}{E_1E_3\Delta} & \frac{\nu_{23}+\nu_{12}\nu_{31}}{E_1E_3\Delta} & 0 & 0 & 0 \\ \frac{\nu_{31}+\nu_{21}\nu_{23}}{E_2E_3\Delta} & \frac{\nu_{23}+\nu_{12}\nu_{31}}{E_1E_3\Delta} & \frac{1-\nu_{12}\nu_{21}}{E_1E_2\Delta} & 0 & 0 & 0 \\ 0 & 0 & 0 & G_{23} & 0 & 0 \\ 0 & 0 & 0 & 0 & G_{13} & 0 \\ 0 & 0 & 0 & 0 & 0 & G_{12} \end{bmatrix} \tag{2.70}$$

Where

$$\Delta = \frac{1-\nu_{12}\nu_{21}-\nu_{23}\nu_{32}-\nu_{13}\nu_{31}-2\nu_{21}\nu_{32}\nu_{12}}{E_1E_2E_3} \tag{2.71}$$

As it is seen, computing stiffness matrix C is much more difficult than by computing the compliance matrix S. Firstly, computing the compliance matrix S, then by taking inverse of it to find the stiffness matrix S, is much easier.

2.6. Hooke's Law for a Two-Dimensional Unidirectional Lamina

2.6.1. Plane stress assumption

A lamina is a very thin structure. Since it is very thin, the stress distribution along its thickness axis will be zero. If a plate is very thin, it can be considered, as there are no out-of-plane loads so it can be treated as under plane stress. Because of this, the 3rd dimensional (thickness related dimension) stress components will be zero. See the figure below for the plane stress assumption.

$$\sigma_3 = \tau_{23} = \tau_{31} = 0 \qquad (\mathbf{2.72})$$

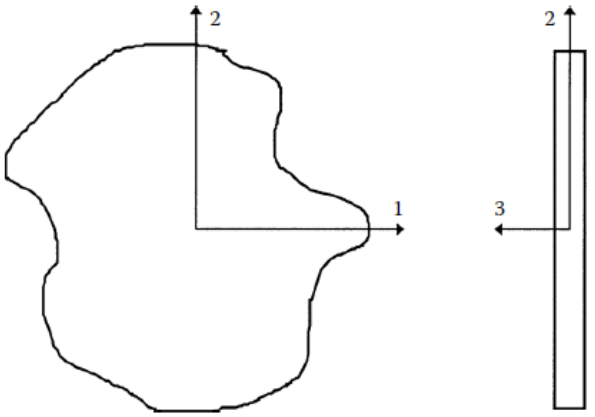

Figure 2.18 : Plane stress condition of a thin plate.

2.6.2. The hooke's law for two dimensions

A unidirectional lamina can be considered as an orthotropic material. Since there is no out-of-plane stresses occur in a lamina, the plane stress assumption can be applied for a lamina. As a result of this, that equation was written $\sigma_3 = \tau_3 = \tau_3 = 0$, then,

$$\varepsilon_3 = S_{13}\sigma_1 + S_{23}\sigma_2 \qquad (\mathbf{2.73})$$

$$\gamma_{23} = \gamma_{31} = 0 \qquad (\mathbf{2.74})$$

Here, the strain component ε_3 is not an independent variable; it is the function of the stress components of the 1 and 2 axes. As a result of this the stress strain relationship of an orthotropic material will be changes and the number of independent variables were reduced. The following equation shows the stress strain relationship of an orthotropic lamina. As mentioned before this equation is generated for plane stress assumption.

$$\begin{bmatrix} \varepsilon_1 \\ \varepsilon_2 \\ \gamma_{12} \end{bmatrix} = \begin{bmatrix} S_{11} & S_{12} & 0 \\ S_{12} & S_{22} & 0 \\ 0 & 0 & S_{66} \end{bmatrix} \begin{bmatrix} \sigma_1 \\ \sigma_2 \\ \tau_{12} \end{bmatrix} \qquad (\mathbf{2.75})$$

As it is seen, the number of independent variables is reduced from 9 to 4.

As known, the stiffness matrix is the inverse of the compliance matrix. Therefore, by inverting the above equation it gives the following.

$$\begin{bmatrix} \sigma_1 \\ \sigma_2 \\ \tau_{12} \end{bmatrix} = \begin{bmatrix} Q_{11} & Q_{12} & 0 \\ Q_{12} & Q_{22} & 0 \\ 0 & 0 & Q_{66} \end{bmatrix} \begin{bmatrix} \varepsilon_1 \\ \varepsilon_2 \\ \gamma_{12} \end{bmatrix} \qquad (\mathbf{2.76})$$

The Qij components are the reduced stiffness components. These can be related with the compliance components.

$$Q_{11} = \frac{S_{22}}{S_{11}S_{22} - {S_{12}}^2} \qquad (\mathbf{2.77})$$

$$Q_{12} = \frac{S_{12}}{S_{11}S_{22} - {S_{12}}^2} \qquad (\mathbf{2.78})$$

$$Q_{22} = \frac{S_{11}}{S_{11}S_{22} - {S_{12}}^2} \qquad (\mathbf{2.79})$$

$$Q_{66} = \frac{1}{S_{66}} \qquad (\mathbf{2.80})$$

As mentioned before, the stiffness and compliance constants can be written in terms of engineering constants. The following expressions are the compliance constants in terms of engineering constants.

$$S_{11} = \frac{1}{E_1} \quad S_{22} = \frac{1}{E_2} \quad S_{12} = -\frac{\nu_{12}}{E_1} \quad S_{66} = \frac{1}{G_{12}} \tag{2.81}$$

The reduced compliance matrix in terms of engineering constants can be seen blow.

$$S = \begin{bmatrix} \frac{1}{E_1} & -\frac{\nu_{12}}{E_1} & 0 \\ -\frac{\nu_{12}}{E_1} & \frac{1}{E_2} & 0 \\ 0 & 0 & \frac{1}{G_{12}} \end{bmatrix} \tag{2.82}$$

The stiffness matrix is the inverse of the compliance matrix. When the inversion operation complete, the following stiffness components will be obtained.

$$Q_{11} = \frac{E_1}{1 - \nu_{21}\nu_{12}} \tag{2.83}$$

$$Q_{12} = \frac{\nu_{12}\, E_2}{1 - \nu_{21}\nu_{12}} \tag{2.84}$$

$$Q_{22} = \frac{E_2}{1 - \nu_{21}\nu_{12}} \tag{2.85}$$

$$Q_{66} = G_{12} \tag{2.86}$$

The above expression can be represented in the matrix form as follows.

$$Q = \begin{bmatrix} \frac{E_1}{1 - \nu_{21}\nu_{12}} & \frac{\nu_{12}\, E_2}{1 - \nu_{21}\nu_{12}} & 0 \\ \frac{\nu_{12}\, E_2}{1 - \nu_{21}\nu_{12}} & \frac{E_2}{1 - \nu_{21}\nu_{12}} & 0 \\ 0 & 0 & G_{12} \end{bmatrix} \tag{2.87}$$

2.6.3. Hooke's law for two dimensional angle lamina

As known, the composite materials are made of fibers and matrices. Therefore, the fibers have better strength on their longitudinal axis and less strength on their transverse axis. For that reason, the laminas may stack in different angles when manufacturing laminates with compatible matrix. The following figure shows the coordinate axes for an angle lamina.

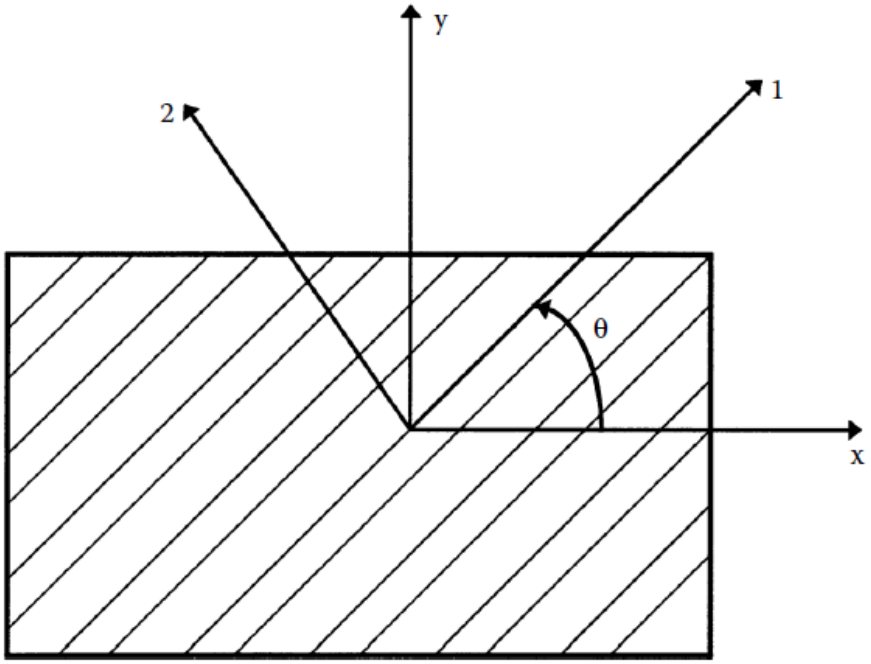

Figure 2.19 : Local and global axes for an angle lamina.

In the figure above, the 1 and 2 axes are called local axes or the material axes. The direction 1 is parallel to the fiber orientation and the direction 2 is perpendicular the fiber orientation. In some resources the axis that is parallel to the fiber orientation is represented as L and the axis that is perpendicular to the fiber orientation is represented as T. The axes x and y are the global axes which means that the axes of the whole part. The angle θ is the angle between these two coordinate systems. In the previous sections, the equations are obtained for the 1 and 2 axes. In this section the transformations of the coordinate systems from 1-2 to x-y will be performed.

The transformation between the local and global axes for the stresses as follows.

$$\begin{bmatrix} \sigma_x \\ \sigma_y \\ \tau_{xy} \end{bmatrix} = [T]^{-1} \begin{bmatrix} \sigma_1 \\ \sigma_2 \\ \tau_{12} \end{bmatrix} \qquad (\mathbf{2.88})$$

Here, $[T]$ is the transformation matrix

$$[T]^{-1} = \begin{bmatrix} c^2 & s^2 & -2sc \\ s^2 & c^2 & 2sc \\ sc & -sc & c^2 - s^2 \end{bmatrix} \qquad (\mathbf{2.89})$$

$$[T] = \begin{bmatrix} c^2 & s^2 & 2sc \\ s^2 & c^2 & -2sc \\ -sc & sc & c^2 - s^2 \end{bmatrix} \quad (\mathbf{2.90})$$

And,

$$c = Cos(\theta) \quad (\mathbf{2.91})$$

$$s = Sin(\theta) \quad (\mathbf{2.92})$$

The stress – strain equation (equation 2.76) can be rewritten by using the transformation relationship.

$$\begin{bmatrix} \sigma_x \\ \sigma_y \\ \tau_{xy} \end{bmatrix} = [T]^{-1}[Q] \begin{bmatrix} \varepsilon_1 \\ \varepsilon_2 \\ \gamma_{12} \end{bmatrix} \quad (\mathbf{2.93})$$

In addition, the strains for global and local axes can be written by using the transformation equations.

$$\begin{bmatrix} \varepsilon_1 \\ \varepsilon_2 \\ \gamma_{12}/2 \end{bmatrix} = [T] \begin{bmatrix} \varepsilon_x \\ \varepsilon_y \\ \gamma_{xy}/2 \end{bmatrix} \quad (\mathbf{2.94})$$

This equation can also be represented as,

$$\begin{bmatrix} \varepsilon_1 \\ \varepsilon_2 \\ \gamma_{12}/2 \end{bmatrix} = [R][T][R]^{-1} \begin{bmatrix} \varepsilon_x \\ \varepsilon_y \\ \gamma_{xy}/2 \end{bmatrix} \quad (\mathbf{2.95})$$

Where R is called Reuter matrix and represented as,

$$[R] = \begin{bmatrix} 1 & 0 & 0 \\ 0 & 1 & 0 \\ 0 & 0 & 2 \end{bmatrix} \quad (\mathbf{2.96})$$

If the equation 2.95, is written in the equation 2.93 the following equation is obtained.

$$\begin{bmatrix} \sigma_x \\ \sigma_y \\ \tau_{xy} \end{bmatrix} = [T]^{-1}[Q][R][T][R]^{-1} \begin{bmatrix} \varepsilon_x \\ \varepsilon_y \\ \gamma_{xy} \end{bmatrix} \quad (\mathbf{2.97})$$

Here the expression $[T]^{-1}[Q][R][T][R]^{-1}$ can be written as,

$$[T]^{-1}[Q][R][T][R]^{-1} = \begin{bmatrix} \overline{Q}_{11} & \overline{Q}_{12} & \overline{Q}_{16} \\ \overline{Q}_{12} & \overline{Q}_{22} & \overline{Q}_{26} \\ \overline{Q}_{16} & \overline{Q}_{26} & \overline{Q}_{66} \end{bmatrix} \quad (\mathbf{2.98})$$

If the equation 2.98 is rewritten,

$$\begin{bmatrix} \sigma_x \\ \sigma_y \\ \tau_{xy} \end{bmatrix} = \begin{bmatrix} \overline{Q}_{11} & \overline{Q}_{12} & \overline{Q}_{16} \\ \overline{Q}_{12} & \overline{Q}_{22} & \overline{Q}_{26} \\ \overline{Q}_{16} & \overline{Q}_{26} & \overline{Q}_{66} \end{bmatrix} \begin{bmatrix} \varepsilon_x \\ \varepsilon_y \\ \gamma_{xy} \end{bmatrix} \quad (\mathbf{2.99})$$

Here the $\overline{Q}_{ij}$ matrix is called as transformed reduced stiffness matrix. If the components of the $\overline{Q}_{ij}$ matrix written explicitly,

$$\overline{Q}_{11} = Q_{11}c^4 + Q_{22}s^4 + 2(Q_{12} + 2Q_{66})s^2c^2$$

$$\overline{Q}_{12} = (Q_{11} + Q_{22} - 4Q_{66})s^2c^2 + Q_{12}(c^4 + s^2)$$

$$\overline{Q}_{22} = Q_{11}s^4 + Q_{22}c^4 + 2(Q_{12} + 2Q_{66})s^2c^2 \quad (\mathbf{2.100})$$

$$\overline{Q}_{16} = (Q_{11} - Q_{12} - 2Q_{66})c^3s - (Q_{22} - Q_{12} - 2Q_{66})s^3c$$

$$\overline{Q}_{26} = (Q_{11} - Q_{12} - 2Q_{66})s^3c - (Q_{22} - Q_{12} - 2Q_{66})c^3s$$

$$\overline{Q}_{66} = (Q_{11} + Q_{22} - Q_{12} - 2Q_{66})s^2c^2 + Q_{66}(s^4 + c^4)$$

As it is seen, the components of transformed reduced stiffness matrix are a function of theta by sine and cosine functions from the result of the transformation matrix.

If the inverse of the equation 2.99 is taken, the following result is obtained.

$$\begin{bmatrix} \varepsilon_x \\ \varepsilon_y \\ \gamma_{xy} \end{bmatrix} = \begin{bmatrix} \overline{S}_{11} & \overline{S}_{12} & \overline{S}_{16} \\ \overline{S}_{12} & \overline{S}_{22} & \overline{S}_{26} \\ \overline{S}_{16} & \overline{S}_{26} & \overline{S}_{66} \end{bmatrix} \begin{bmatrix} \sigma_x \\ \sigma_y \\ \tau_{xy} \end{bmatrix} \quad (\mathbf{2.101})$$

Here the $\overline{S}_{ij}$ matrix is called the transformed reduced compliance matrix and it can be shown in explicit form as,

$$\overline{S}_{11} = S_{11}c^4 + S_{22}s^4 + (2Q_{12} + Q_{66})s^2c^2$$

$$\overline{S}_{12} = (S_{11} + S_{22} - S_{66})s^2c^2 + S_{12}(s^4 + c^4)$$

$$\overline{S}_{22} = S_{11}s^4 + S_{22}c^4 + (2S_{12} + S_{66})s^2c^2 \qquad (\mathbf{2.102})$$

$$\overline{S}_{16} = (2S_{11} - 2S_{12} - S_{66})c^3s - (2S_{22} - 2S_{12} - S_{66})s^3c$$

$$\overline{S}_{16} = (2S_{11} - 2S_{12} - S_{66})s^3c - (2S_{22} - 2S_{12} - S_{66})c^3s$$

$$\overline{S}_{66} = 2(2S_{11} + 2S_{22} - 4S_{12} - S_{66})s^2c^2 + S_{66}(s^4 + c^4)$$

As it is seen, the components of transformed reduced compliance matrix are a function of theta by sine and cosine functions from the result of the transformation matrix.

The equation 2.75 and 2.76 are generated for a unidirectional lamina that loaded in the material axis directions. For this loading condition, there is no coupling between the normal and shear stresses. That means, if a normal force only applied on a body that contains an angle lamina results only normal strains or vice versa.

However, for an angle lamina, coupling occurs between normal and shear stresses. That means, if a normal force only applied on a body that contains an angle lamina results both normal and shear strains.

The equations 2.99 and 2.101 are written for an angle lamina. In those equations, the stiffness and compliance components are transformed from local axes (material's axis) to the global axes (part's axis).

2.7. Introducing the A, B and D Matrices

The matrices A, B and D are related with the loading conditions of a shell and will be used in classical laminate theory. The matrix A is called as the extensional stiffness matrix of the composite shell. The matrix B is called as the bending – extension coupling matrix and the matrix D is called as the flexural or bending stiffness matrix of a shell. These matrices can be calculated as follows.

$$A_{ij} = \sum_{k=1}^{N} \left[\overline{Q_{ij}}\right]_k (h_k - h_{k-1}) \qquad (\mathbf{2.103})$$

$$B_{ij} = \frac{1}{2} \sum_{k=1}^{N} \left[\overline{Q_{ij}}\right]_k (h_k^2 - h_{k-1}^2) \qquad (\mathbf{2.104})$$

$$D_{ij} = \frac{1}{3} \sum_{k=1}^{N} \left[\overline{Q_{ij}}\right]_k (h_k^3 - h_{k-1}^3) \qquad (\mathbf{2.105})$$

Where;

$\left[\overline{Q_{ij}}\right]_k$ is the reduced stiffness matrix for an angle lamina.

h_k is the thickness related values for a lamina in the laminate.

N is the maximum layer number. (k = 1,2,3,…,N)

Note that, since the reduced stiffness matrix is 3x3, the A, B and D matrices will be written in the same manner.

3. FAILURE THEORIES IN ANGLE LAMINA

For the success in designs, the material must be used less and more effective. For that reason, the failure analysis must be performed carefully. In addition, the effect of stress resulted because of the load must be investigated for the fracture point of view.

To investigate the failure analysis of a laminate, the first thing to do is to investigate the failure analysis of a single lamina. From the strength of a single lamina, the strength of the laminate can be calculated. As mentioned before, the laminas strength analysis is performed at its own coordinate system that are, fiber direction and the direction that perpendicular to the fibers.

The mechanical properties of a unidirectional lamina are known. If the stresses with respect to the fiber axis and the axis perpendicular to the fibers, are calculated the failure analysis can be performed.

To do that the following steps can be applied.

- The critical buckling torque must be calculated. (See the section 5)
- By using this value, the stresses in each layer with respect to the part's coordinate system must be calculated. (See the section 5)
- After that by using transformation matrices, the calculated stress values must be converted to the lamina coordinate system. (Conversion from the global axes to the local axes)
- By using that stress values and the material properties the failure analysis can be performed.

For composite materials, the following failure theories can be applicable.

- Maximum stress failure theory
- Maximum strain failure theory
- Tsai – Hill failure theory
- Tsai – Wu failure theory

3.1. Maximum Stress Failure Theory

This theory is referenced from the Tresca (maximum shear stress) and Rankine (maximum normal stress) failure theory for isotropic materials and the solution principle is very similar to it. The stresses acting on a lamina are resolved into the normal and shear stresses in the local axes.

This theory says that, the lamina is failed if any of the normal and shear stresses in the local axes of a lamina is equal to or larger than the corresponding ultimate strengths of the unidirectional lamina.

As mentioned before, after the global stresses (the stresses occurred on the part's coordinate axes) are calculated, those stresses should be converted to the local stresses by using transformation matrices.

The lamina is considered to be failed if the following situation occurred.

$$-(\sigma_1^C)_{ult} < \sigma_1 < (\sigma_1^T)_{ult}$$

$$-(\sigma_2^C)_{ult} < \sigma_2 < (\sigma_2^T)_{ult} \qquad \textbf{(3.1)}$$

$$-(\tau_{12})_{ult} < \tau_{12} < (\tau_{12})_{ult}$$

Where,

$(\sigma_1^C)_{ult}$: Ultimate longitudinal compressive strength. (Fiber axis)

$(\sigma_1^T)_{ult}$: Ultimate longitudinal tensile strength. (Fiber axis)

$(\sigma_2^C)_{ult}$: Ultimate transverse compressive strength. (Perpendicular to the fiber axis)

$(\sigma_2^T)_{ult}$: Ultimate transverse tensile strength. (Perpendicular to the fiber axis)

$(\tau_{12})_{ult}$: Ultimate in – plane shear strength.

σ_1 : Stress occurred on longitudinal direction. (Fiber axis)

σ_2 : Stress occurred on longitudinal direction. (Fiber axis)

τ_{12} : In – plane shear stress.

3.2. Maximum Strain Theory

This theory is referenced from the Tresca (maximum shear stress) and St. Venant (maximum normal strain) failure theory for isotropic materials and the solution principle is very similar to it. The strains acting on a lamina are resolved into the strains in the local axes.

This theory says that, the lamina is failed if any of the normal and shear strains in the local axes of a lamina is equal to or larger than the corresponding ultimate strengths of the unidirectional lamina.

As mentioned before, after the global stresses (the stresses occurred on the part's coordinate axes) are calculated, those stresses should be converted to the local stresses by using transformation equations.

The lamina is considered to be failed if the following situation occurred.

$$-(\varepsilon_1^C)_{ult} < \varepsilon_1 < (\varepsilon_1^T)_{ult}$$

$$-(\varepsilon_2^C)_{ult} < \varepsilon_2 < (\varepsilon_2^T)_{ult} \quad \textbf{(3.2)}$$

$$-(\gamma_{12})_{ult} < \gamma_{12} < (\gamma_{12})_{ult}$$

Where,

$(\varepsilon_1^C)_{ult}$: Ultimate longitudinal compressive strain. (Fiber axis)

$(\varepsilon_1^T)_{ult}$: Ultimate longitudinal tensile strain. (Fiber axis)

$(\varepsilon_2^C)_{ult}$: Ultimate transverse compressive strain. (Perpendicular to the fiber axis)

$(\varepsilon_2^T)_{ult}$: Ultimate transverse tensile strain. (Perpendicular to the fiber axis)

$(\gamma_{12})_{ult}$: Ultimate in – plane shear strain.

ε_1 : Strain occurred on longitudinal direction. (Fiber axis)

ε_2 : Strain occurred on longitudinal direction. (Fiber axis)

γ_{12} : In – plane shear strain.

3.3. Tsai – Hill Failure Theory

This theory is similar to the Von – Mises's distortional energy yield criterion for isotropic materials. This theory is rearranged anisotropic materials. Distortion energy is a part of the total strain energy in a body.

The strain energy in a body consists of two parts; one is the dilation energy, which is caused by change in the volume, and the other is called the distortion energy, which is caused by the change in shape of the body.

This theory says that; the distortion energy caused by the stress occurred in the material, is greater than the failure distortion energy of the material.

Hill adopted the Von – Mises's distortion energy failure theory to the anisotropic materials then, Tsai rearranged it for unidirectional lamina.

The lamina has failed if the following inequality satisfies.

$$(G_2 + G_3){\sigma_1}^2 + (G_1 + G_3){\sigma_2}^2 + (G_1 + G_2){\sigma_3}^2 - 2G_3\sigma_1\sigma_2 - 2G_2\sigma_1\sigma_3 - 2G_1\sigma_2\sigma_3 + 2G_4\tau_{23}^2 + 2G_5\tau_{13}^2 + 2G_6\tau_{12}^2 < 1 \quad \textbf{(3.3)}$$

Where, G_1, G_2, G_3, G_4, G_5 and G_6, are related with the failure strengths of the material and they can be calculated as follows.

- Apply $\sigma_1 = (\sigma_1^T)_{ult}$ to a unidirectional lamina then the lamina will be failed. Therefore, the equation 3.3 reduces to the following.

$$(G_2 + G_3)(\sigma_1^T)_{ult}^2 = 1 \quad \textbf{(3.4)}$$

- Apply $\sigma_2 = (\sigma_2^T)_{ult}$ to a unidirectional lamina then the lamina will be failed. Therefore, the equation 3.3 reduces to the following.

$$(G_1 + G_3)(\sigma_2^T)_{ult}^2 = 1 \quad \textbf{(3.5)}$$

- Apply $\sigma_3 = (\sigma_2^T)_{ult}$ to a unidirectional lamina and assuming that the normal tensile failure strength is same in direction (2) and direction (3) then the lamina will be failed. Therefore, the equation 3.3 reduces to the following.

$$(G_1 + G_2)(\sigma_2^T)_{ult}^2 = 1 \quad \textbf{(3.6)}$$

- Apply $\tau_{12} = (\tau_{12})_{ult}$ to a unidirectional lamina then the lamina will be failed. Therefore, the equation 3.3 reduces to the following.

$$2G_6(\tau_{12})_{ult}^2 = 1 \quad \textbf{(3.7)}$$

Therefore, by using the equations from 3.4 to 3.7 the G_1, G_2, G_3, G_4, G_5 and G_6 constants can be calculated by the following.

$$G_1 = \frac{1}{2}\left(\frac{2}{[(\sigma_2^T)_{ult}]^2} - \frac{1}{[(\sigma_1^T)_{ult}]^2}\right)$$

$$G_2 = \frac{1}{2}\left(\frac{1}{[(\sigma_1^T)_{ult}]^2}\right)$$

$$G_3 = \frac{1}{2}\left(\frac{1}{[(\sigma_1^T)_{ult}]^2}\right) \qquad \textbf{(3.8)}$$

$$G_3 = \frac{1}{2}\left(\frac{1}{[(\tau_{12})_{ult}]^2}\right)$$

Since the unidirectional lamina shows plane – stress assumption (no stress distribution in the thickness axis) so, $\sigma_3 = \tau_{31} = \tau_{23} = 0$, then the equation 3.3 reduces to the following.

$$\left[\frac{\sigma_1}{(\sigma_1^T)_{ult}}\right]^2 - \left[\frac{\sigma_1\sigma_2}{(\sigma_1^T)_{ult}^2}\right] + \left[\frac{\sigma_2}{(\sigma_2^T)_{ult}}\right]^2 + \left[\frac{\tau_{12}}{(\tau_{12})_{ult}}\right]^2 < 1 \qquad \textbf{(3.8)}$$

From the global stresses the local stresses can be found, then by using the equation 3.8, it can be found out if the material is failed or not. If the equation 3.8 satisfies, the material is said to be not failed.

3.3.1. Modified Tsai – Hill failure theory

Generally, the transverse tensile strength of a unidirectional lamina is much less than the transverse compressive strength. In the equation 3.8 as it is seen the ultimate compressive strengths are nor written. Therefore, the effects of the compressive strengths are not taken into account.

The modified Tsai – Hill failure theory includes the compressive effects into the equation. In the following equation, both the ultimate tensile strength values and the ultimate compressive strength values are taken into account.

$$\left[\frac{\sigma_1}{X_1}\right]^2 - \left[\left(\frac{\sigma_1}{X_2}\right)\left(\frac{\sigma_2}{X_2}\right)\right] + \left[\frac{\sigma_2}{Y}\right]^2 + \left[\frac{\tau_{12}}{S}\right]^2 < 1 \qquad \textbf{(3.9)}$$

Where,

$$X_1 = \begin{cases} (\sigma_1^T)_{ult} \;\; if \;\; \sigma_1 > 0 \\ (\sigma_1^C)_{ult} \;\; if \;\; \sigma_1 < 0 \end{cases}$$

$$X_2 = \begin{cases} (\sigma_1^T)_{ult} \;\; if \;\; \sigma_2 > 0 \\ (\sigma_1^C)_{ult} \;\; if \;\; \sigma_2 < 0 \end{cases} \qquad \textbf{(3.10)}$$

$$Y = \begin{cases} (\sigma_2^T)_{ult} \;\; if \;\; \sigma_2 > 0 \\ (\sigma_2^C)_{ult} \;\; if \;\; \sigma_2 < 0 \end{cases}$$

$$S = (\tau_{12})_{ult}$$

As it is seen the X_1, X_2, Y and S values are chosen from the equation 3.10. If the calculated stress is negative, it means that it is a compressive stress. According to the result of the equation 3.10, the equation 3.9 can be rewritten.

For solving the failure part of the thesis topic, the modified Tsai – Hill failure theory will be used. This theory is much more realistic but less conservative.

3.4. Tsai – Wu Failure Theory

This failure theory is similar to the total strain energy failure theory of Beltrami. The total strain energy failure theory of Beltrami is valid for isotropic materials. Tsai – Wu applied this failure theory to a lamina in plane stress state.

A lamina is considered to be failed if the following situation occurs.

$$H_1\sigma_1 + H_2\sigma_2 + H_6\tau_{12} + H_{11}\sigma_1^2 + H_{22}\sigma_2^2 + H_{66}\tau_{12}^2 + 2H_{12}\sigma_1\sigma_2 < 1 \qquad \textbf{(3.11)}$$

The constants H_1, H_2, H_6, H_{11}, H_{22} and H_{66} can be found by using 5 strength components, which are $(\sigma_1^T)_{ult}$, $(\sigma_2^T)_{ult}$, $(\sigma_1^C)_{ult}$, $(\sigma_2^C)_{ult}$ and $(\tau_{12})_{ult}$ of a unidirectional lamina.

4. BUCKLING OF COMPOSITE SHELL STRUCTURES

4.1. Introduction to Shell Structures

A body is called a shell if thickness dimension is very small when compared to the other dimensions. A shell body is a thin walled body whose middle bod is curved in at least one direction. A cylindrical shell has only one direction in which the middle surface is curved whereas a spherical shell the curvature exists in both directions. The shell theory is more complicated when compared to the beam and plate theory. The reason is the curvature.

4.2. Analysis of Composite Material Circular Cylindrical Shell

4.2.1. General equations

The Figure 4.1 shows the simplest shell geometry, which is a circular cylindrical shell. The u, v and w shows the positive directions and positive directions of coordinates x and ξ. The remaining coordinate θ is the circumferential coordinate.

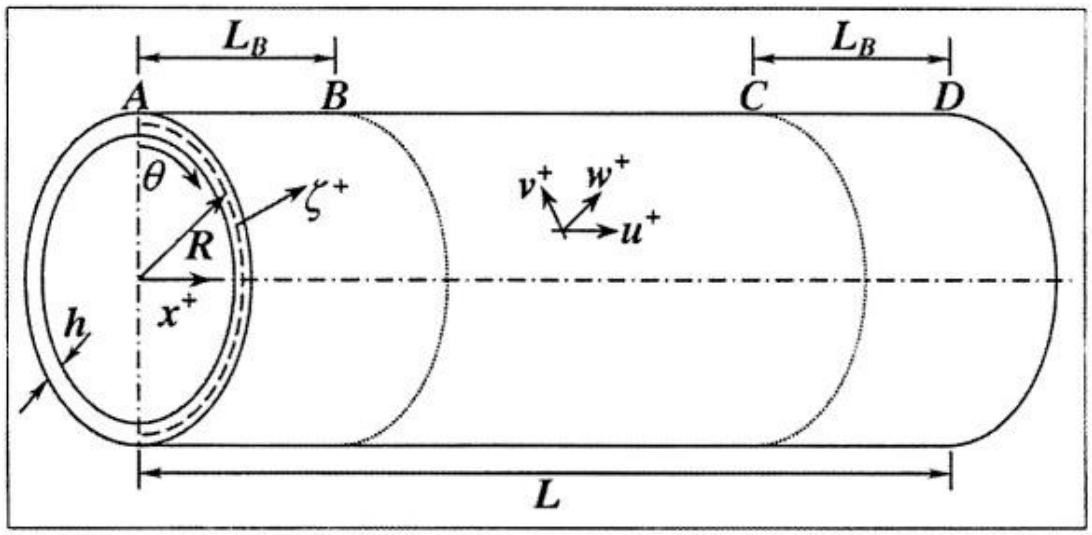

Figure 4.1 : A circular cylindrical shell geometry.

The assumptions that are made in the classical plate theory is also valid in the classical shell theory which is discussed here. Therefore, the following equations are valid.

$$\sigma_\xi = \varepsilon_\xi = \varepsilon_{x\xi} = \varepsilon_{\theta\xi} = 0$$

$$u(x,\theta,\xi) = u_0(x,\theta) + \xi\beta_x(x,\theta) \qquad \textbf{(4.1)}$$

$$v(x,\theta,\xi) = v_0(x,\theta) + \xi\beta_\theta(x,\theta)$$

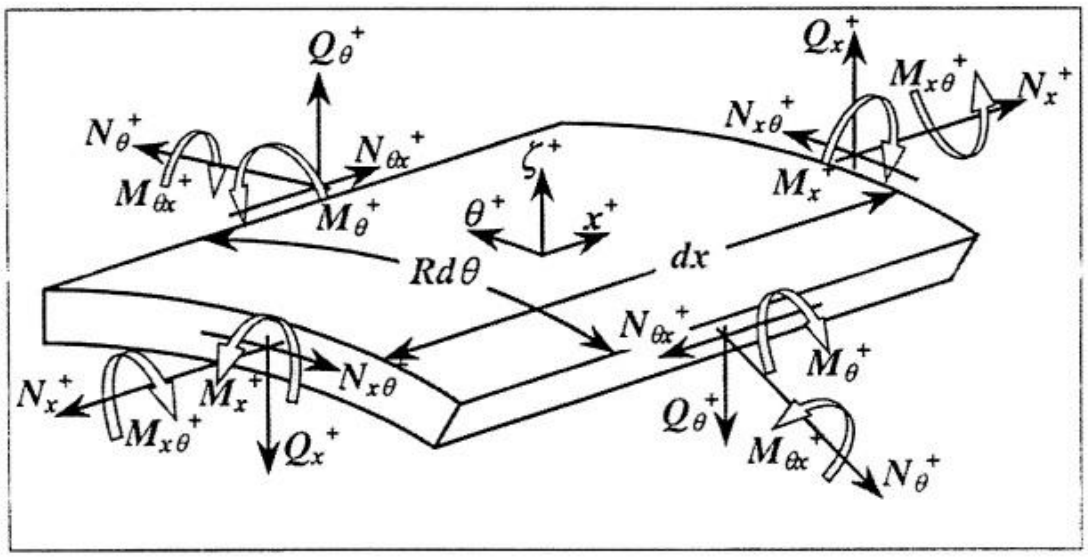

Figure 4.2 : Positive directions of an infinitesimal shell portion.

Since the shell structures are very thin structures, the thickness dimension is negligible when compared to the other dimensions. This assumption also makes composite equations less complicated.

$$\frac{h}{R} \ll 1 \qquad \textbf{(4.2)}$$

Where,

h: The thickness of the cylindrical shell

R: The mean radius of the cylindrical shell

The equation 4.2 tells that, a body is considered as a shell if the h/R ratio is much less than 1.

For an accurate shell composite analysis, it is true that the transverse shear deformation must be included because of the fact that the elasticity modulus in the fiber directions

is a fiber dependent property whereas the transverse shear modulus is a matrix-dominated property.

This results a simplification I the governing equations. Elasticity equations in a curvilinear coordinate system must be introduced firstly for deriving the governing differential equations for cylindrical shells. The equilibrium equations for cylindrical shells can be seen below.

$$\frac{\partial N_x}{\partial x} + \frac{1}{R}\frac{\partial N_{x\theta}}{\partial \theta} + q_x = 0 \quad \textbf{(4.3)}$$

$$\frac{\partial N_{x\theta}}{\partial x} + \frac{1}{R}\frac{\partial N_x}{\partial \theta} + \frac{Q_\theta}{R} + q_\theta = 0 \quad \textbf{(4.4)}$$

$$\frac{\partial Q_x}{\partial x} + \frac{1}{R}\frac{\partial Q_\theta}{\partial \theta} + \frac{1}{R}N_\theta + p(x,\theta) = 0 \quad \textbf{(4.5)}$$

$$\frac{\partial M_x}{\partial x} + \frac{1}{R}\frac{\partial M_{x\theta}}{\partial \theta} - (Q_x - m_x) = 0 \quad \textbf{(4.6)}$$

$$\frac{\partial M_{x\theta}}{\partial x} + \frac{1}{R}\frac{\partial M_\theta}{\partial \theta} - (Q_\theta - m_\theta) = 0 \quad \textbf{(4.7)}$$

Where,

$$q_x = \sigma_{\xi x}(h/2) - \sigma_{\xi x}(-h/2) = \tau_{1x} - \tau_{2x}$$

$$q_\theta = \sigma_{\xi\theta}(h/2) - \sigma_{\xi\theta}(-h/2) = \tau_{1\theta} - \tau_{2\theta}$$

$$m_x = \frac{h}{2}\left[\sigma_{\xi x}(h/2) + \sigma_{\xi x}(-h/2)\right] = \frac{h}{2}[\tau_{1x} + \tau_{2x}]$$

$$m_\theta = \frac{h}{2}\left[\sigma_{\xi\theta}(h/2) + \sigma_{\xi\theta}(-h/2)\right] = \frac{h}{2}[\tau_{1\theta} + \tau_{2\theta}]$$

These equilibrium equations are independent of the material system. The circumferential terms can also be written in terms of ds, the arc distance where $ds = Rd\theta$. The quantities q_x, q_θ, m_x and m_θ are functions of the surface shear stresses on the outer and inner surfaces of the composite shell wall, and $p(x,\theta)$ is the laterally distributed load per unit area, positive in the positive ξ direction.

For the case where the transverse shear deformation is ignored (classical theory) the relations between the rotations β_x and β_θ and the displacements are given by the following.

$$\beta_x + \frac{\partial w}{\partial x} = 0 \qquad \textbf{(4.8)}$$

$$\beta_\theta + \frac{1}{R}\frac{\partial w}{\partial \theta} - \frac{v_0}{R} = 0 \qquad \textbf{(4.9)}$$

The material properties enter through the constitutive equations. For simplicity, it is assumed that the lamination stacking sequence is mid-plane symmetric such that there is no bending - stretching coupling, i.e. [B] = 0, and that there are no other coupling terms, i.e. $(\,)_{16} = (\,)_{26} = 0$.

In addition, for the following derivation, the simplest case will be studied – that of a shell of one lamina only. Subsequently, generalizations are made to the configurations. In the current case, the stress-strain relations and the strain-displacement relations, utilizing the displacement assumptions of equation (4.1) are; for the case of one ply the derivations as follows.

$$\varepsilon_x = \frac{1}{E_x}[\sigma_x - v_{x\theta}\sigma_\theta] = \frac{\partial u_0}{\partial x} + \xi\left(\frac{\partial \beta_x}{\partial x}\right) \qquad \textbf{(4.10)}$$

$$\varepsilon_\theta = \frac{1}{E_x}[\sigma_\theta - v_{\theta x}\sigma_x] = \frac{1}{R}\left[\frac{\partial v_0}{\partial \theta} + w\right] + \frac{\xi}{R}\left(\frac{\partial \beta_\theta}{\partial \theta}\right) \qquad \textbf{(4.11)}$$

$$\varepsilon_{x\theta} = \frac{1}{2G_{x\theta}}\sigma_{x\theta} \qquad \textbf{(4.12)}$$

The in-plane stiffnesses and the flexural stiffnesses are given as follows.

$$K_x = \frac{E_x h}{(1 - v_{x\theta}v_{\theta x})}, \quad K_\theta = \frac{E_\theta h}{(1 - v_{x\theta}v_{\theta x})}$$
$$D_x = \frac{E_x h^3}{12(1 - v_{x\theta}v_{\theta x})}, \quad D_\theta = \frac{E_\theta h^3}{12(1 - v_{x\theta}v_{\theta x})} \qquad \textbf{(4.13)}$$

Remember that if the fibers are in the axial direction then $K_x = A_{11}$, $K_\theta = A_{22}$, $D_x = D_{11}$ and $D_\theta = D_{22}$. If the fibers are in the circumferential direction then the subscripts

(4.14)

are reversed. The orthotropic relationship holds here. This relationship can be seen below.

$$\frac{v_{x\theta}}{E_x} = \frac{v_{\theta x}}{E_\theta}$$

4.2.2. Axial symmetry

It can be assumed that the loads are axially symmetric for simplicity, which means that $\frac{\partial()}{\partial x} = 0$ in all equations.

If the equations 4.10 and 4.11 are multiplied by dξ and integrated from –h/2 to h/2, where the h is the shell thickness, the following result is obtained.

$$N_x - v_{x\theta} N_\theta = E_x h \frac{\partial u_0}{\partial x}$$

$$N_\theta - v_{\theta x} N_x = E_\theta h \frac{w}{R}$$

If the equations are rearranged for N_x and N_θ the following expressions are found.

$$N_x = K_x \left[\frac{\partial u_0}{\partial x} + v_{\theta x} \frac{w}{R} \right] \quad \textbf{(4.15)}$$

$$N_\theta = K_\theta \left[v_{x\theta} \frac{\partial u_0}{\partial x} + \frac{w}{R} \right] \quad \textbf{(4.16)}$$

Likewise, if the equations 4.10 and 4.11 are multiplied by ξdξ and integrated from –h/2 to h/2 the following result is obtained.

$$M_x - v_{x\theta} M_\theta = -\frac{E_x h^3}{12} \frac{\partial^2 w}{\partial x^2}$$

$$M_\theta - v_{\theta x} M_x = 0$$

If the equations are rearranged for M_x and M_θ the following expressions are found.

$$M_x = -D_x \frac{\partial^2 w}{\partial x^2} \quad \textbf{(4.17)}$$

$$M_\theta = v_{\theta x} M_x \quad \textbf{(4.18)}$$

For simplification, and further derivation, there are no surface shear stresses. Therefore, $q_x = q_\theta = m_x = m_\theta = 0$ can be written.

As a result, the above shell equations are simplified to the following.

$$\frac{dN_x}{dx} = 0 \tag{4.19}$$

$$\frac{dQ_x}{dx} - \frac{N_\theta}{R} + p(x) = 0 \tag{4.20}$$

$$\frac{dM_x}{dx} - Q_x = 0 \tag{4.21}$$

$$\beta_x + \frac{dw}{dx} = 0 \tag{4.22}$$

$$\beta_\theta = 0 \tag{4.23}$$

$$N_x = K_x\left[\varepsilon_{x_0} + v_{\theta x}\varepsilon_\theta\right] = K_x\left[\frac{du_0}{dx} + \frac{v_{\theta x}}{R}w\right] \tag{4.24}$$

$$N_\theta = K_\theta\left[\varepsilon_{\theta_0} + v_{x\theta}\varepsilon_{x_0}\right] = K_\theta\left[v_{x\theta}\frac{du_0}{dx} + \frac{w}{R}\right] \tag{4.25}$$

$$M_x = -D_x\frac{d^2w}{dx^2} \tag{4.26}$$

$$M_\theta = v_{\theta x}M_x \tag{4.27}$$

$$Q_x = -D_x\frac{d^3w}{dx^3} \tag{4.28}$$

From the equations 4.19 and 4.24,

$$\frac{d^2u_0}{dx^2} + \frac{v_{\theta x}}{R}\frac{dw}{dx} = 0 \tag{4.29}$$

From the equations 4.20, 4.25 and 4.28, it can be obtained.

$$-D_x\frac{d^4w}{dx^4} - \frac{K_\theta}{R}\left[v_{x\theta}\frac{du_0}{dx} + \frac{w}{R}\right] + p(x) = 0 \tag{4.30}$$

From equations, 4.29 and 4.30 the following governing equation is obtained.

$$\frac{d^4w}{dx^4} + \frac{K_\theta}{D_x R^2}(1 - v_{x\theta}v_{\theta x})w = \frac{1}{D_x}\left[p(x) - v_{\theta x}\frac{N_x}{R}\right] \qquad (\mathbf{4.31})$$

Now it can be defined that,

$$\varepsilon^4 = \frac{3(1 - v_{x\theta}v_{\theta x})}{h^2R^2}\frac{D_\theta}{D_x} \qquad (\mathbf{4.32})$$

the governing differential equation for the lateral deflection w, and in-plane displacements u_0 becomes the following.

$$\frac{d^4w}{dx^4} + 4\varepsilon^4 w = \frac{1}{D_x}\left[p(x) - \frac{v_{\theta x}}{R}N_x\right] \qquad (\mathbf{4.33})$$

$$\frac{d^2u_0}{dx^2} + \frac{v_{\theta x}}{R}\frac{dw}{dx} = 0 \qquad (\mathbf{4.34})$$

The form of (4.33) is desirable since it is uncoupled from the other governing equation (4.34). From (4.19), N_x is seen to be a constant as determined by the applied load, P, in the axial direction, which is $N_x = P/2\pi R$. In fact, it is seen from (4.33) that the presence of an axial in-plane force is that of an equivalent lateral pressure as far as the lateral displacement w is concerned.

Upon determining w and u_0 from Equations (4.33) and (4.34), the stress resultants and stress couples can be obtained from Equations (4.24) through (4.28). Stresses can then be determined from the following equations for a composite shell of one ply only.

$$\sigma_x = \frac{N_x}{h} + \frac{M_x\xi}{h^3/12} \qquad (\mathbf{4.35})$$

$$\sigma_\theta = \frac{N_\theta}{h} + \frac{M_\theta\xi}{h^3/12} \qquad (\mathbf{4.36})$$

$$\sigma_{xz} = \frac{3Q_x}{2h}\left[1 - \left(\frac{\xi}{h/2}\right)^2\right] \qquad (\mathbf{4.37})$$

The differential equation 4.33 is in the form of the differential equation of a beam lays on an elastic foundation. It can be replaced that D_x, with the flexural stiffness of a

beam, EI, and replacing $4\varepsilon^4 w$ by k, the beam foundation modulus. Thus, the physical intuition of all of the solutions for beams on an elastic foundation can be utilized.

The roots of the 4th degree differential equation 4.33 can be found by standard methods as, $\mp\varepsilon(1 \mp i)$. Here $i = \sqrt{-1}$. And the general solution of the differential equation will be as follows.

$$w(x) = Ae^{-\varepsilon x}\cos\varepsilon x + Be^{-\varepsilon x}\sin\varepsilon x + Ce^{\varepsilon x}\cos\varepsilon x + Ee^{\varepsilon x}\sin\varepsilon x + w_p(x) \qquad (\mathbf{4.38})$$

At the equation 4.38 the A, B, C and E are the integration constants and $w_p(x)$ is the particular integral.

The in-plane displacement $u_0(x)$ can be found by integrating the equation 4.24 and the result will be as follows.

$$u_0(x) = \frac{N_x x}{K_x} - \frac{v_{\theta x}}{R}\int w dx + F \qquad (\mathbf{4.39})$$

Where, N_x is constant and F is the integration constant.

It is seen, that for circular cylindrical shells subjected to axially symmetric loads there are six boundary conditions, three at each end. The natural boundary conditions are thus given by,

- Either u_x is known or $N_x = 0$.
- Either $\frac{dw}{dx}$ is known or $M_x = 0$.
- Either w is known or $Q_x = 0$.

The above situations describe the simply supported, clamped and free edge BCs.

4.3. Edge Load and Particular Solution

4.3.1. Circular cylindrical shell, semi – infinite in length subjected to a moment couple M_0 at x=0

Figure 4.3 shows that a circular cylindrical shell that is subjected to an edge moment and $p(x) = 0$ for $0 \leq x \leq \infty$.

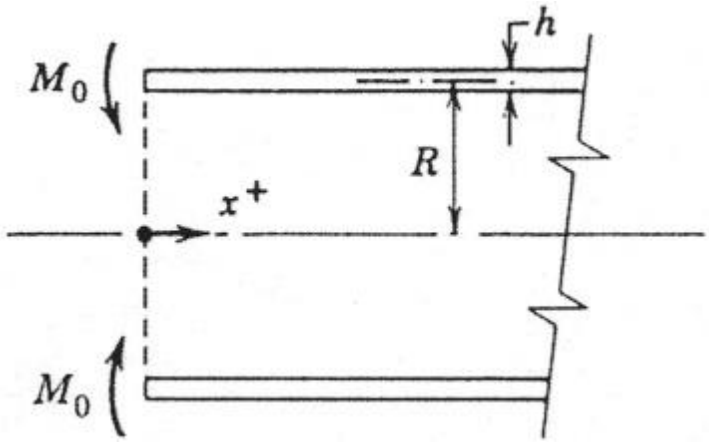

Figure 4.3 : A circular cylindrical shell subjected to an edge moment.

It can be seen that C=E=0 from the solution of the homogeneous part of the equation 4.38. The constants A and B can be found by using the equations 4.26 and 4.28.

$$M_x(0) = M_0 = -D_x \frac{d^2w(0)}{dx^2} \qquad (\mathbf{4.40})$$

$$Q_x(0) = 0 = -D_x \frac{d^3w(0)}{dx^3} \qquad (\mathbf{4.41})$$

By rearranging the equation 4.38 with the above relations, the following expression can be found.

$$w(x) = \frac{M_0}{2\varepsilon^2 D_x} e^{-\varepsilon x}(\sin \varepsilon x - \cos \varepsilon x) \qquad (\mathbf{4.42})$$

It can be seen from final deflection expression that the amount of deflection decreases exponentially with the edge moment multiplier when getting away from the shell edge.

4.3.2. Circular cylindrical shell, semi – infinite in length subjected to transverse shear force Q_0 at x=0

The following figure 4.4 shows that a circular cylindrical shell that is subjected to an transverse shear force and again $p(x) = 0$ for $0 \leq x \leq \infty$. Also the constants C=E=0.

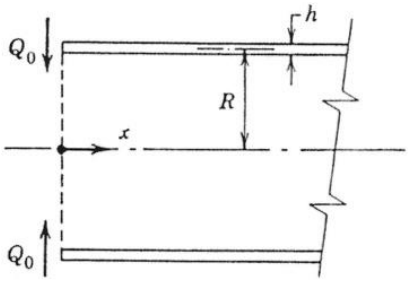

Figure 4.4 : A circular cylindrical shell subjected to transverse shear.

The constants A and B can be found by using the equations 4.26 and 4.28.

$$M_x(0) = 0 = -D_x \frac{d^2w(0)}{dx^2} \qquad (\mathbf{4.43})$$

$$Q_x(0) = Q_0 = -D_x \frac{d^3w(0)}{dx^3} \qquad (\mathbf{4.44})$$

By rearranging the equation 4.38 with the above relations, the following expression can be found.

$$w(x) = \frac{Q_0}{2\varepsilon^3 D_x} e^{-\varepsilon x}(\cos \varepsilon x) \qquad (\mathbf{4.45})$$

It can be seen from final deflection expression that the amount of deflection decreases exponentially with the transverse shear force multiplier when getting away from the shell edge.

4.3.3. Circular cylindrical shell, semi – infinite in length subjected to an edge moment and a transverse shear force at x=L

The following figure 4.5 shows the loading conditions on a circular cylindrical shell for $p(x) = 0$ for $-\infty \leq x \leq L$. The solution of the equation 4.38 shows that C=E=0.

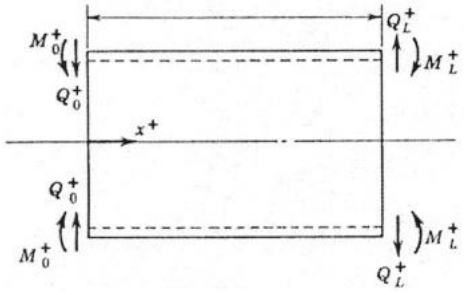

Figure 4.5 : Positive direction for edge loads on a cylindrical shell.

From the equations, 4.26 and 4.28 the following two expressions were obtained.

$$M_x(L) = -D_x \frac{d^2w(L)}{dx^2} = M_L \qquad (\mathbf{4.46})$$

$$Q_x(L) = -D_x \frac{d^3w(L)}{dx^3} = 0 \qquad (\mathbf{4.47})$$

By using these results, the equation 4.38 can be rewritten as the following.

$$w(x) = \frac{M_L}{2\varepsilon^2 D_x} e^{-\varepsilon(L-x)}(\sin\varepsilon(L-x) - \cos\varepsilon(L-x)) \qquad (\mathbf{4.48})$$

It can be seen from final deflection expression that the amount of deflection decreases exponentially with the edge moment multiplier when getting away from the shell edge.

At the shell edge $(x = L)$ if the shell edge load is taken into consideration the following results are obtained

$$M_x(L) = -D_x \frac{d^2w(L)}{dx^2} = 0 \qquad (\mathbf{4.49})$$

$$Q_x(L) = -D_x \frac{d^3w(L)}{dx^3} = Q_L \qquad (\mathbf{4.50})$$

By using the above expressions the deflection equation can be written as,

$$w(x) = \frac{Q_L}{2\varepsilon^3 D_x} e^{-\varepsilon(L-x)}(\cos\varepsilon(L-x)) \qquad (\mathbf{4.51})$$

Similarly, it can be seen from final deflection expression that the amount of deflection decreases exponentially with the transverse shear force multiplier when getting away from the shell edge.

4.3.4. Generalization

By looking the equation 4.38, it can be seen that the constants A and B decreases when the value of x increases, whereas the constants C and E increases when the value of x increases for a circular cylindrical shell subjected to axially symmetric in-plane and lateral loads. This can cause a big problem computationally and even at the best, in

solving for boundary value constants A, B, C and E will involve terms involving $e^{-\varepsilon x}$ ve$^{-\varepsilon(L-x)}$ ile $e^{+\varepsilon x}$ ve$^{+\varepsilon(L-x)}$ where the exponent can be quite large.

To solve this situation, the solutions 4.42, 4.45, 4.48 and 4.51 is imported to the general solution 4.38. Thus, the equation 4.54 will be more convenient to use.

4.3.5. Particular solution

As it is seen from the equation 4.33, if the derivative of the load is equal to zero the particular solution as follows.

$$w_p(x) = \frac{1}{4\varepsilon^4 D_x}\left[p(x) - \frac{v_{\theta x} N_x}{R}\right] \qquad (\mathbf{4.52})$$

This equation is a particular solution that can be used for the axially symmetrical loaded shells. The following expression can be used for laminated structures by writing $v_{\theta x} = A_{12}/A_{11}$.

$$w_p(x) = \frac{1}{4\varepsilon^4 D_x}\left[p(x) - \frac{A_{12}}{A_{11}}\frac{N_x}{R}\right] \qquad (\mathbf{4.53})$$

4.3.6. Best form of solution utilizing the bending boundary layer

$$\begin{aligned} w(x) = {} & \frac{M_0}{2\varepsilon^2 D_x} e^{-\varepsilon x}(\sin\varepsilon x - \cos\varepsilon x) - \frac{Q_0}{2\varepsilon^3 D_x} e^{-\varepsilon x}\cos\varepsilon x \\ & + \frac{M_L}{2\varepsilon^2 D_x} e^{-\varepsilon(L-x)}(\sin\varepsilon(L-x) - \cos\varepsilon(L-x)) \\ & + \frac{Q_L}{2\varepsilon^3 D_x} e^{-\varepsilon(L-x)}(\cos\varepsilon(L-x)) + w_p(x) \end{aligned} \qquad (\mathbf{4.54})$$

At the equation above instead of using the integration constants A, B, C and E the M_0, M_L, Q_0 ve Q_L constants are used.

The main advantage of that equation is that it can be seen at the homogenous part of the solution the trigonometric functions are used which means that the trigonometric function oscillate between +1 and -1, multiplied by an exponential term with negative exponent, hence an exponential decay. It can be assumed that any term is negligible when $e^{-\varepsilon x} \leq 0.006$ or $e^{-\varepsilon(L-x)} \leq 0.006$ that condition occurs whenever εx or

$\varepsilon(L-x)$ is greater then 5.15. If $v_{\theta x}v_{x\theta}$ is taken as 0.09 then, that condition is met exactly whenever the following expression yields.

$$x > 4\sqrt{Rh(D_x/D_\theta)^{1/2}}$$

$$L - x > 4\sqrt{Rh(D_x/D_\theta)^{1/2}} \qquad (\mathbf{4.55})$$

This is important because at a distance greater than $4\sqrt{Rh(D_x/D_\theta)^{1/2}}$ away from either end of the shell, the entire homogeneous solution of equation 4.54 essentially goes to zero, and can be neglected. In the case of continuous loads $p(x)$, the particular solution is one leading to membrane stresses and displacements. Because of this the region $0 \le x \le 4\sqrt{Rh(D_x/D_\theta)^{1/2}}$ and $0 \le L - x \le 4\sqrt{Rh(D_x/D_\theta)^{1/2}}$ is called the "bending boundary layer." It is seen that the length of the bending boundary layer is a function of the flexural stiffnesses D_x and D_θ.

Computationally, equation 4.54 is very useful. For a shell longer than the bending boundary layer, that is, $L \ge 4\sqrt{Rh(D_x/D_\theta)^{1/2}}$ in the region $0 \le x \le 4\sqrt{Rh(D_x/D_\theta)^{1/2}}$, the terms involving M_L and Q_L are neglected; in the region $0 \le L - x \le 4\sqrt{Rh(D_x/D_\theta)^{1/2}}$ the terms involving M_0 and Q_0 can be ignored; in the region $4\sqrt{Rh(D_x/D_\theta)^{1/2}} \le x \le L - 4\sqrt{Rh(D_x/D_\theta)^{1/2}}$, the terms involving M_L, Q_L, M_0 and Q_0can be ignored. In addition, when the shell is longer than the bending boundary layer and when $d^2p(x)/dx^2 = d^3p(x)/dx^3 = 0$ then, the following expressions can be written.

$$M_0 = M_x(0) \quad M_L = M_x(L)$$

$$Q_0 = Q_x(0) \quad Q_L = Q_x(L)$$

Although this situation is valid for one lamina, if all couplings are zero this can be applied for laminated structures.

4.2. General Solution for Cylindrical Shells under Axially Symmetrical Loads

The deflection expression for an axially symmetrical loaded and symmetrical in the middle surface, orthotropic shells is defined in the following equation.

$$w(x) = \frac{M_0}{2\varepsilon^2 D_{11}} e^{-\varepsilon x}(\sin \varepsilon x - \cos \varepsilon x) - \frac{Q_0}{2\varepsilon^3 D_{11}} e^{-\varepsilon x} \cos \varepsilon x$$
$$+ \frac{M_L}{2\varepsilon^2 D_{11}} e^{-\varepsilon(L-x)}(\sin\varepsilon(L-x) - \cos\varepsilon(L-x))$$
$$+ \frac{Q_L}{2\varepsilon^3 D_{11}} e^{-\varepsilon(L-x)}(\cos\varepsilon(L-x))$$
$$+ \frac{1}{4\varepsilon^4 D_{11}}\left[p(x) - \frac{A_{12}}{A_{11}}\frac{N_x}{R}\right] \qquad (\mathbf{4.56})$$

Where,

$$\varepsilon^4 = \frac{3(1 - v_{x\theta} v_{\theta x})}{h^2 R^2}\frac{D_{22}}{D_{11}} \qquad (\mathbf{4.57})$$

$$\frac{dw}{dx} = \frac{M_0}{\varepsilon D_{11}} e^{-\varepsilon x} \cos \varepsilon x + \frac{Q_0}{2\varepsilon^2 D_{11}} e^{-\varepsilon x}(\sin \varepsilon x + \cos \varepsilon x)$$
$$- \frac{M_L}{\varepsilon D_{11}} e^{-\varepsilon(L-x)} \cos\varepsilon(L-x)$$
$$+ \frac{Q_L}{2\varepsilon^2 D_{11}} e^{-\varepsilon(L-x)}(\sin \varepsilon(L-x) \cos\varepsilon(L-x))$$
$$+ \frac{1}{4\varepsilon^4 D_{11}}\frac{dp(x)}{dx} \qquad (\mathbf{4.58})$$

$$M_x = -D_{11}\frac{d^2 w}{dx^2}$$
$$= M_0 e^{-\varepsilon x}(\sin \varepsilon x + \cos \varepsilon x) - \frac{Q_0}{\varepsilon} e^{-\varepsilon x} \sin \varepsilon x$$
$$+ M_L e^{-\varepsilon(L-x)}(\sin\varepsilon(L-x) + \cos\varepsilon(L-x))$$
$$+ \frac{Q_L}{\varepsilon} e^{-\varepsilon(L-x)} \sin \varepsilon(L-x) - \frac{1}{4\varepsilon^4}\frac{d^2 p(x)}{dx^2} \qquad (\mathbf{4.59})$$

$$
\begin{aligned}
Q_x &= -D_{11}\frac{d^3w}{dx^3} \\
&= -2M_0\varepsilon e^{-\varepsilon x}\sin\varepsilon x + Q_0 e^{-\varepsilon x}(\cos\varepsilon x - \sin\varepsilon x) \\
&+ 2M_L\varepsilon e^{-\varepsilon(L-x)}\sin\varepsilon(L-x) \\
&+ Q_L e^{-\varepsilon(L-x)}[-\cos\varepsilon(L-x) + \sin\varepsilon(L-x)] \\
&- \frac{1}{4\varepsilon^4}\frac{d^3p(x)}{dx^3}
\end{aligned} \tag{4.60}
$$

$$
N_x = Constant \tag{4.61}
$$

The stress values for every lamina for axially symmetrical loads.

$$
\begin{Bmatrix}\sigma_x \\ \sigma_\theta\end{Bmatrix}_k = \begin{bmatrix}Q_{11} & Q_{12} \\ Q_{12} & Q_{22}\end{bmatrix}_k \begin{Bmatrix}\varepsilon_x^0 \\ \varepsilon_\theta^0\end{Bmatrix} + \begin{bmatrix}Q_{11} & Q_{12} \\ Q_{12} & Q_{22}\end{bmatrix}_k \begin{Bmatrix}\kappa_x \\ 0\end{Bmatrix}\xi \tag{4.62}
$$

Where,

$$
\varepsilon_x^0 = \frac{\partial u_0}{\partial x},\ \ \varepsilon_\theta^0 = \frac{w}{R} \quad and \quad \kappa_x = \frac{\partial^2 w}{\partial x^2}
$$

In a laminated cylindrical shell wherein $\frac{d^2p(x)}{dx^2} = 0$all interlaminar shear stresses also, go to zero outside of the bending boundary layer.

4.3. Mid-Plane Asymmetric Circular Cylindrical Shells

The composite shells that are asymmetric in mid-plane are commonly used in many applications. The exterior environment may differ markedly from the interior environment to which the shell is exposed the outer environment may have extremes of temperature and humidity, blast damage, etc. while the inner environment may have chemical, abrasive, esthetic or other considerations. In addition, stealth considerations may play a role in some shell structures.

4.3.1. Obtaining the differential equations

The equilibrium and the strain displacement equations of the shell with mid-plane asymmetry under axially symmetric loads are the same from the equation 4.19 to 4.28.

However, the constitutive equations for the mid-plane asymmetric composite, which is specially orthotropic so that the material axes 1-2-3 coincide with the $x-\theta-\varepsilon$ axes are found from Equation (2.66) to be the following.

$$N_x = A_{11}\varepsilon_{x_0} + A_{12}\varepsilon_{\theta_0} + B_{11}\kappa_x + B_{12}\kappa_\theta \qquad (\mathbf{4.63})$$

$$N_\theta = A_{12}\varepsilon_{x_0} + A_{22}\varepsilon_{\theta_0} + B_{12}\kappa_x + B_{22}\kappa_\theta \qquad (\mathbf{4.64})$$

$$M_x = B_{11}\varepsilon_{x_0} + B_{12}\varepsilon_{\theta_0} + D_{11}\kappa_x + D_{12}\kappa_\theta \qquad (\mathbf{4.65})$$

$$M_\theta = B_{12}\varepsilon_{x_0} + B_{22}\varepsilon_{\theta_0} + D_{12}\kappa_x + D_{22}\kappa_\theta \qquad (\mathbf{4.66})$$

By using the above equations with the equilibrium and strain – displacement equation the equation 4.34 will be the following.

$$A_{11}\frac{d^2u_0}{dx^2} + \frac{A_{12}}{R}\frac{dw}{dx} - B_{11}\frac{d^3w}{dx^3} = 0 \qquad (\mathbf{4.67})$$

With the same manner the equation 4.33 will be the following.

$$\left(\frac{A_{11}D_{11} - B_{11}^2}{A_{11}}\right)\frac{d^4w}{dx^4} + \frac{2}{R}\left(\frac{A_{12}B_{11}}{A_{11}} - B_{12}\right)\frac{d^2w}{dx^2} + \frac{1}{R^2}\left(\frac{A_{11}A_{22} - A_{12}^2}{A_{11}}\right)w = p(x) - \frac{A_{12}}{A_{11}}\frac{N_x}{R} \qquad (\mathbf{4.68})$$

Defining a reduced or effective flexural stiffness as:

$$D_e = \frac{A_{11}D_{11} - B_{11}^2}{A_{11}} \qquad (\mathbf{4.69})$$

In addition, the following expression can be defined.

$$4\varepsilon^4 \equiv \frac{1}{D_e R^2}\left(\frac{A_{11}A_{22} - A_{12}^2}{A_{11}}\right) \qquad (\mathbf{4.70})$$

As a result, the equation 4.68 will be the following.

$$\frac{d^4w}{dx^4} + \frac{2}{D_e R}\left(\frac{A_{12}B_{11}}{A_{11}} - B_{12}\right)\frac{d^2w}{dx^2} + 4\varepsilon^4 w = \frac{1}{D_e}\left[p(x) - \frac{A_{12}}{A_{11}}\frac{N_x}{R}\right] \qquad (\mathbf{4.71})$$

Here, except the D_e flexural stiffness, this equation is similar to the equation 4.33 that is the equation for cylindrical shell subjected to the axially symmetric load in the middle axis.

Remark of the mid plane asymmetry parameter as follows.

$$\emptyset \equiv \frac{B_{11}}{\sqrt{A_{11}D_{11}}} \tag{4.72}$$

By using the mid plane asymmetry expression the equation 4.71 rewritten.

$$\frac{d^4w}{dx^4} + C\emptyset\frac{d^2w}{dx^2} + 4\varepsilon^4 w = \frac{1}{D_e}\left[p(x) - \frac{A_{12}}{A_{11}}\frac{N_x}{R}\right] \tag{4.73}$$

Where,

$$C \equiv \frac{2}{D_e R}\sqrt{\frac{D_{11}}{A_{11}}}\frac{(A_{12}B_{11} - A_{11}B_{12})}{B_{11}} \tag{4.74}$$

Thus, equations 4.67 and 4.73 are the two governing differential equations to solve for the circular cylindrical shell of a mid-plane asymmetric composite subjected to axially symmetric lateral and axial loads.

4.3.2. Perturbation solution

Since $|\emptyset| < \mp 1$ is valid, the lateral deflection expression at the equation 4.73 can be written as a perturbation series as follows.

$$w(x) = \sum_{n=0}^{\infty} w_n(x)\emptyset^n \tag{4.75}$$

If this expression is written to the equation 4.73, the following equation is obtained.

$$\frac{d^4w_0(x)}{dx^4} + \emptyset\frac{d^4w_1(x)}{dx^4} + \cdots + \emptyset^n\frac{d^4w_n(x)}{dx^4}$$
$$+ C\emptyset\left[\frac{d^2w_0(x)}{dx^2} + \emptyset\frac{d^2w_1(x)}{dx^2} + \cdots + \emptyset^n\frac{d^2w_n(x)}{dx^2}\right]$$
$$+ 4\varepsilon^4w_0(x) + 4\varepsilon^4\emptyset w_1(x) + \cdots + 4\varepsilon^4\emptyset^n w_n(x)$$
$$= \frac{1}{D_e}\left[p(x) - \frac{A_{12}}{A_{11}}\frac{N_x}{R}\right] \qquad (\mathbf{4.76})$$

This can now be separated into a series of differential equations by collecting on powers $\emptyset$ of where $\emptyset^0 = 1$.

$$n = 0 \Rightarrow \frac{d^4w_0(x)}{dx^4} + 4\varepsilon^4w_0(x) = \frac{1}{D_e}\left[p(x) - \frac{A_{12}}{A_{11}}\frac{N_x}{R}\right]$$

$$n = 1 \Rightarrow \frac{d^4w_1(x)}{dx^4}\emptyset^1 + C\frac{d^2w_0(x)}{dx^2}\emptyset^1 + 4\varepsilon^4w_1(x)\emptyset^1 = 0$$

$$n = n \Rightarrow \frac{d^4w_n(x)}{dx^4}\emptyset^n + C\frac{d^2w_{n-1}(x)}{dx^2}\emptyset^n + 4\varepsilon^4w_n(x)\emptyset^n = 0 \qquad (\mathbf{4.77})$$

If the problems are solved successively from n = 0, it is first seen that the differential equation for n = 0 is the customary axially- and mid-plane symmetric cylindrical shell equation. There are many solutions available for this problem. For n≥1 it is seen that the term involving the second derivative is actually known as it involves the w-solution for n-1. Thus, these terms can be moved to the right-hand side and the equations 4.77 can be written as the following.

$$n = 0 \Rightarrow \frac{d^4w_0(x)}{dx^4} + 4\varepsilon^4w_0(x) = \frac{1}{D_e}\left[p(x) - \frac{A_{12}}{A_{11}}\frac{N_x}{R}\right]$$

$$n = 1 \Rightarrow \frac{d^4w_1(x)}{dx^4}\emptyset^1 + 4\varepsilon^4w_1(x)\emptyset^1 = -C\frac{d^2w_0(x)}{dx^2}\emptyset^1 \qquad (\mathbf{4.78})$$

$$n > 1 \Rightarrow \frac{d^4w_n(x)}{dx^4}\emptyset^n + 4\varepsilon^4w_n(x)\emptyset^n = -C\frac{d^2w_{n-1}(x)}{dx^2}\emptyset^n$$

The forcing function of the n=0 is the actual applied load to the shell. For $n \geq 1$, the forcing function involves derivatives of the (n-1) equation solution and is therefore a known quantity.

By using this solution technique, the equation 4.71 can be rearranged for the axially symmetrical and mid-plane symmetrical cylindrical shells.

4.3.3. Edge load solutions and the bending boundary layer for a mid – plane asymmetric shell

It has been shown that for the mid-plane asymmetric shell the boundary layer exists and has the same length as it is for the usual mid-plane symmetric shell as given by equation 4.55.

As in the case of beams and plates, when loads applied to circular cylindrical shells are compressive, are in beam type bending, involve an external pressure or are torsional about the longitudinal axis, buckling can occur. Such buckling can result in shell failure, and if the buckling stress is lower than the allowable stress from a strength point of view, then that value is the limit to the useful load carrying capability of the shell.

4.4. Buckling of Shell Structures

The analytical solution of buckling of columns and plates are easier when compared with the shells. In addition, the experimental studies are close to the analytical solution for columns and plates. However, making a good convergence between analytical solution and experimental analysis is difficult for shells.

The shell structures are sensitive the initial imperfections. The wall thickness differences in the whole geometry or the ovality of the shell affects the buckling load very much. Since the theory evaluates the shell completely perfect, the theoretical solution gives much higher value of load when compared the experimental analysis. As a stability theory, the imperfections in the material or the load axis may cause a 0.1 times of the theoretical solution. Also the theoretical solution makes some assumptions for that reason, if one want to converge the experimental analysis, some empirical equations may be used and some coefficients can be found.

If this situation is considered, to compensate this difference, the analytical solution has to be multiplied with a coefficient called a failure coefficient to converge the real, experimental analysis. That practical analytical solution is firstly introduced by NASA.

4.5. Buckling of Cylindrical Composite Shells

Buckling can occur in various loading conditions. They can be axial compression, hydrostatic pressure, lateral pressure, torsion or bending. The general loading condition of the cylindrical composite shell is shown in the figure below.

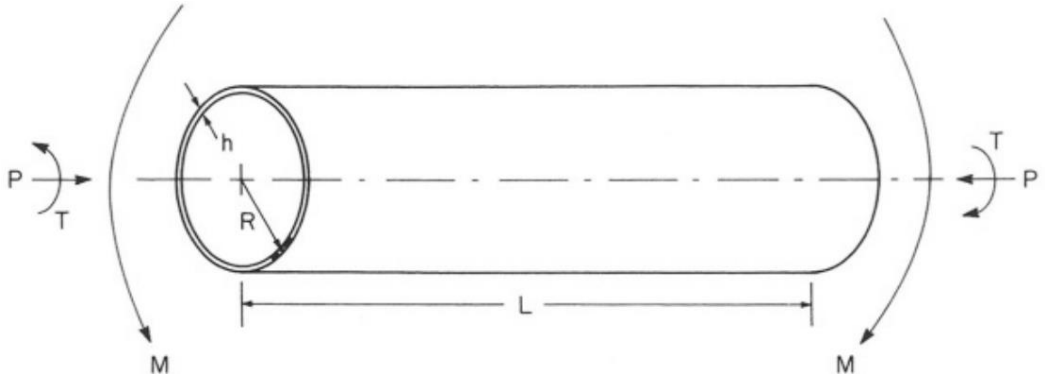

Figure 4.6 : A circular cylindrical shell subjected to several of loads.

In this thesis the buckling situation of cylindrical composite shells are investigated under torsional loads.

In this chapter, the shell equations and the composite equations are combined. In addition, the stress and strain values will be calculated. After that a failure analysis will be run to see whether or not the shell is buckled or yielded.

4.6. Buckling of Circular Cylindrical Shells under Torsional Loads

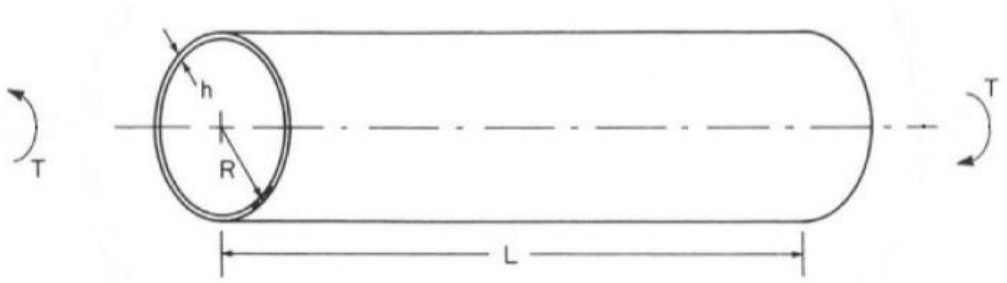

Figure 4.7 : A circular cylindrical shell subjected to a torsional load.

As it is seen in the Figure 4.5 the composite cylindrical shell is subjected to a torsional load.

The shell has a length L, mean radius R, total thickness of h and the shell is subjected to a torque of T.

The equations solve the critical buckling torque that causes buckling directly. Furthermore, that torque must be converted to a value of $N_{x\theta}$.

$$N_{x\theta} = \frac{T_{cr}}{2\pi R^2} \tag{4.79}$$

To solve the buckling problem firstly some assumptions must be made to simplify the solution. These assumptions are listed as follows.

- Special anisotropy $[that\ is\ (\quad)_{16} = (\quad)_{26}]$
- Prebuckled deformations are not taken into account
- Ends of the cylindrical shell are supported by rings rigid in their planes, but offer no resistance to rotation or bending out of their plane.

The critical buckling torque can be calculated from the following equation.

$$T_{cr} = 21.75(D_{22})^{5/8}\left(\frac{A_{11}A_{22} - A_{12}^2}{A_{22}}\right)^{3/8}\frac{R^{5/4}}{L^{1/2}} \tag{4.80}$$

There is a restriction for that equation. It can be seen in the following equation.

$$\left(\frac{D_{22}}{D_{11}}\right)^{5/6}\left(\frac{A_{11}A_{22} - A_{12}^2}{12\,A_{22}\,D_{11}}\right)^{1/2}\frac{L^2}{R} \geq 500 \tag{4.81}$$

Where,

A_{ij} is the extensional stiffness matrix (see the equation 4.82)

B_{ij} is the bending – extension coupling matrix (see the equation 4.83)

D_{ij} is the flexural or bending stiffness (see the equation 4.84), The details are introduces in the section 2.7.

L is the cylinder length

R is the cylinder mean radius

$$A_{ij} = \sum_{k=1}^{N}\left[\overline{Q_{ij}}\right]_k(h_k - h_{k-1}) \tag{4.82}$$

$$B_{ij} = \frac{1}{2} \sum_{k=1}^{N} \left[\overline{Q_{ij}}\right]_k (h_k^2 - h_{k-1}^2) \qquad (\mathbf{4.83})$$

$$D_{ij} = \frac{1}{3} \sum_{k=1}^{N} \left[\overline{Q_{ij}}\right]_k (h_k^3 - h_{k-1}^3) \qquad (\mathbf{4.84})$$

Where;

$\left[\overline{Q_{ij}}\right]_k$ is the reduced stiffness matrix for an angle lamina.

h_k is the thickness related values for a lamina in the laminate.

N is the maximum layer number. (k = 1,2,3,…,N)

By using the equation 4.80 the critical torque can be calculated. Since the critical torque and the $N_{x\theta}$ value known, the strains can be calculated by using the following matrix equation.

$$\begin{bmatrix} N_x \\ N_\theta \\ N_{x\theta} \\ \cdots \\ M_x \\ M_\theta \\ M_{x\theta} \end{bmatrix} = \begin{bmatrix} A_{11} & A_{12} & A_{16} & \vdots & B_{11} & B_{12} & B_{16} \\ A_{12} & A_{22} & A_{26} & \vdots & B_{12} & B_{22} & B_{26} \\ A_{16} & A_{26} & A_{66} & \vdots & B_{16} & B_{26} & B_{66} \\ \cdots & \cdots & \cdots & \vdots & \cdots & \cdots & \cdots \\ B_{11} & B_{12} & B_{16} & \vdots & D_{11} & D_{12} & D_{16} \\ B_{12} & B_{22} & B_{26} & \vdots & D_{12} & D_{22} & D_{26} \\ B_{16} & B_{26} & B_{66} & \vdots & D_{16} & D_{26} & D_{66} \end{bmatrix} \begin{bmatrix} \varepsilon_X^0 \\ \varepsilon_\theta^0 \\ 2\varepsilon_{X\theta}^0 \\ \cdots \\ \kappa_X \\ \kappa_\theta \\ 2\kappa_{X\theta} \end{bmatrix} \qquad (\mathbf{4.85})$$

Here, the N_x is related with the compressional loads, N_θ is related with the hydrostatic pressure and $N_{x\theta}$ is related with the torque and lateral forces. The M values are moment values.

In this condition the only force is the torque so the only $N_{x\theta}$ is defferent than zero the other values are equal to zero.

$$N_x = N_\theta = M_x = M_\theta = M_{x\theta} = 0 \qquad N_{x\theta} = N_{x\theta_{cr}} \qquad (\mathbf{4.86})$$

After the strains are calculated the stresses can now be calculated by using the following equation.

$$\begin{bmatrix} \sigma_x \\ \sigma_\theta \\ \sigma_{x\theta} \end{bmatrix}_k = \left[\overline{Q}\right]_k \begin{bmatrix} \varepsilon_x^0 \\ \varepsilon_\theta^0 \\ 2\varepsilon_{x\theta}^0 \end{bmatrix} + z\left[\overline{Q}\right]_k \begin{bmatrix} \kappa_x \\ \kappa_\theta \\ 2\kappa_{x\theta} \end{bmatrix} \qquad (\mathbf{4.87})$$

Here, the Q matrix is the reduced stiffness matrix of an angle lamina. z is the shell thickness. k is the layer number. Since the strains are calculated, the stresses for each layer with respect to the part coordinate axis can be calculated from the above expression.

To use the mechanical properties of the material, the coordinate transformation must be performed. The following transformation matrices can be used.

$$[T] = \begin{bmatrix} (\cos\theta)^2 & (\sin\theta)^2 & 2\sin\theta\cos\theta \\ (\sin\theta)^2 & (\cos\theta)^2 & -2\sin\theta\cos\theta \\ \sin\theta\cos\theta & -\sin\theta\cos\theta & (\cos\theta)^2 - (\sin\theta)^2 \end{bmatrix} \quad (\mathbf{4.88})$$

As a result, the following relation can be written,

$$\begin{bmatrix} \sigma_1 \\ \sigma_2 \\ \tau_{12} \end{bmatrix}_k = [T] \begin{bmatrix} \sigma_x \\ \sigma_\theta \\ \sigma_{x\theta} \end{bmatrix}_k \quad (\mathbf{4.89})$$

4.6.1. Summary of this section

In this section, the formulation to calculate the buckling force is introduced. Now, the solution procedure will be listed to be understood well.

- First of all, the material properties must be known to be insert directly to the equations 4.82 to 4.84.
- The A, B and D values are known now.
- By using those values, the buckling torque can be calculated by using the equation 4.80.
- However, there is a restriction for the equation 4.80 so that restriction must be controlled by using the equation 4.81.
- If the equation 4.81 yields, the calculated buckling torque will be true.
- After that, the strains can be calculated by using the equation 4.85. In this equation, the $N_{x\theta}$ will be different than zero and the other values will be zero if the only load is torque on the cylindrical shell. $N_{x\theta}$ can be calculated by using the equation 4.79
- Then, the stresses can be calculated by using the equation 4.87.

- These calculated stress values are respect to the part coordinate system. To compare if the shell is yielded or not those stress values must be converted to the lamina coordinate system.
- This conversion operation can be performed by using the transformation matrix, equation 4.88.
- The new lamina coordinate system stresses can be calculated by the equation 4.89.

As, a result the critical buckling torque T_{cr}, the $N_{x\theta_{cr}}$ value, strains, stresses with respect to the cylindrical shell coordinate system, stresses with respect to the lamina coordinate system are calculated. Now a failure analysis can be performed to see whether the shell is yielded or not. For the failure analysis, see the section 3.3.

5. THE ANALYTICAL SOLUTION AND ANGLE OPTIMIZATION

The layer angle optimization is a very crucial method for this problem. The optimization method chooses the best layer angle configuration in the all possible solutions. For this purpose, the mathematical modelling of this physical problem is performed and the best value is calculated by using computer programming tools.

There are many factors that affect the strength of the composites. The individual layer thicknesses, fiber and matrix material, fiber angles, length of the shell, mean radius of the shell can be a good example for those factors. The layer angle change affects the strength of the composite shell very much.

In this study, the effect of fiber angle change, to the cylindrical composite shells are investigated. The material buckling strength properties with different conditions were calculated by using a code that complied in the MATLAB.

Those material properties, are used in the buckling formulation in the literature and the buckling problem is solved. Also the failure analysis is performed to see the shell is yielded or buckled. For the buckling point of view, the shell must not yield so the buckling strength becomes much more important strength parameter. In the end, the best shell is calculated from the buckling point of view.

5.1. Matlab

MATLAB is a programming language and a numerical calculation software. It has been developed by Mathworks and commonly used by control engineering, linear algebra, numerical analysis, speech recognition, image processing and matrix calculations. In MATLAB, one can write subroutines in matrix form with control loops or logical tests.

In addition, MATLAB can be used as a graphic tool. Also it can be used for control simulations.

5.2. The Analytical Solution Procedure by Using MATLAB

All of the equations are known now, so now for the solution of the matrix equations MATLAB can be used. Solution procedure can be seen as follows. The other part of the solution is layer angle optimization, so the layer angles are changeable. The best angle configuration will be obtained by maximizing the buckling load.

The MATLAB code can be found in the appendix A and B.

- The program initiations, definitions. (# of layers, precision of the program, etc.)
- Material properties (Can be user input or it can be written in the program)
- Compliance matrix is written in terms of material properties (engineering constants).
- Stiffness matrix is calculated, by taking the inverse of the compliance matrix.
- The angle matrix is generated by evaluating the user inputs.
- The stiffness and the compliance matrices are modified with respect to the fiber angles.
- The plane stress assumption is used by deleting the 3rd 4th and 5th rows and columns.
- The layer thickness related values are calculated. (the h values.)
- The A, B and D matrices are calculated by using the modified stiffness matrices and the thickness related values.
- The dimensional properties are requested as a user input (the part length and the mean radius).
- For further calculations, the mass of the part is calculated.
- The critical torsional buckling load related value is calculated. $N_{x\theta_{cr}}$
- The critical torsional buckling load (buckling torque) is calculated by multiplying the circumference. (T_{cr})
- The strains are calculated by using the $N_{x\theta} = N_{x\theta_{cr}}$ equality.
- The stresses are calculated due to calculated strains.

- The Tsai – Hill failure theory is applied to see if the part is yield or not under the calculated buckling loads.
- The angle configuration that makes the buckling load maximum is obtained to see the best angle configuration.
- The critical torque, best angle configuration, stresses and the failure coefficients are printed on the screen.

5.2.1. Explanation of 4-D arrays and angle configurations

The key point to solve the problem in MATLAB is to use multiple dimensional arrays because the number of variables is 4. For that reason, at least 4-D arrays must be used.

The stiffness matrix for a layer with specified angle is 2-D.

Since all of the stiffness matrices are related with the layer number and the angle configuration, the dimension of the stiffness matrices will be 4-D.

The following illustration shows that situation.

Let's have 2 angle configurations and 2 layers;

$$[Q] = \begin{bmatrix} \begin{bmatrix} Q_{1111} & Q_{1211} & 0 \\ Q_{1211} & Q_{2211} & 0 \\ 0 & 0 & Q_{6611} \end{bmatrix} & \begin{bmatrix} Q_{1112} & Q_{1212} & 0 \\ Q_{1212} & Q_{2212} & 0 \\ 0 & 0 & Q_{6612} \end{bmatrix} \\ \begin{bmatrix} Q_{1121} & Q_{1221} & 0 \\ Q_{1221} & Q_{2221} & 0 \\ 0 & 0 & Q_{6621} \end{bmatrix} & \begin{bmatrix} Q_{1122} & Q_{1222} & 0 \\ Q_{1222} & Q_{2222} & 0 \\ 0 & 0 & Q_{6622} \end{bmatrix} \end{bmatrix} \qquad (\mathbf{5.1})$$

The sub matrices are the stiffness matrix of specified layer with specified angle configuration. The row number of the big matrix is the layer number and the column number of the big matrix is angle configurations.

The array manipulation of the program is written above. All of the inverse calculations and the matrix calculations and loops are performed in 4-D arrays.

The values must be stored in an array because at the end of the program the maximum angle configuration must be found. For that reason, all of probabilities must be stored for further maximization calculations.

5.2.2. A Matlab solution example

The following example shows how the MATLAB program runs. This is the results that directly taken from the MATLAB command window.

First, the program requests the user inputs such as the #of layers, the layer thicknesses the length of the cylinder and the diameter of the cylinder.

Then it will calculate the buckling load, optimum angles, stresses and the failure coefficient.

```
Command Window
  Enter the number of layers
  3
  Write the thickness of layer number 1 in  milimeters [mm]
  1
  Write the thickness of layer number 2 in  milimeters [mm]
  1
  Write the thickness of layer number 3 in  milimeters [mm]
  1
  Enter the Length of the cylinder in milimeters [mm]
  1100
  Enter the Diameter of the cylinder in milimeters [mm]
  1100
```

Figure 5.1 : The MATLAB command window inputs.

From those user inputs, the results are generated as follows. MATLAB computes the followings,

- Calculates the critical buckling torque.
- Calculates optimum angles.
- Calculates stress values with respect to the part coordinate system.
- Calculates stresses with respect to the lamina coordinate system.
- Calculates failure coefficients.
- Calculates the h/R and R/D ratios.
- Plots the buckling load vs angle graph for each layer.
- Plots also layer angle convergence graph.

```
Command Window
              RESULTS

Maximum buckling torque is 4.219987e+05
Nxtheta_cr = 2.220271e+05

Optimum angles are;
90.000000
0.000000
90.000000

The stress values with respect to the part and ply axes that occur
under the maximum buckling load as follows;

Stress values with respect to the part axes at the layer number 1 are
sigma_x       = -0.000000
sigma_theta   = -0.000000
sigma_x_theta = 37.004509

Stress values with respect to the part axes at the layer number 2 are
sigma_x       = 0.000000
sigma_theta   = -0.000000
sigma_x_theta = 37.004509

Stress values with respect to the part axes at the layer number 3 are
sigma_x       = -0.000000
sigma_theta   = -0.000000
sigma_x_theta = 37.004509
```

Figure 5.2 : The MATLAB command window outputs

```
Stress values with respect to the ply axes at the layer number 1 are
sigma_1  = -0.000000
sigma_2  = -0.000000
sigma_3  = -37.004509

Stress values with respect to the ply axes at the layer number 2 are
sigma_1  = 0.000000
sigma_2  = -0.000000
sigma_3  = 37.004509

Stress values with respect to the ply axes at the layer number 3 are
sigma_1  = -0.000000
sigma_2  = -0.000000
sigma_3  = -37.004509

Failure coefficient in each layer as follows
f1 = 0.296136
f2 = 0.296136
f3 = 0.296136


h/R ratio = 0.005455
R/L ratio = 0.500000
fx >>
```

Figure 5.3 : The MATLAB command window outputs continuation

As it is seen, the example part is shell with very lower h/R ratio and the fracture occurs because of buckling not because of yield.

The critical buckling load T_{cr} is displayed. The $N_{x\theta cr}$ value is used for stress analysis inside the program.

The optimum fiber angles are also displayed which gives the maximum buckling load.

The following figure is directly taken from MATLAB result. That graph shows the layer angle change in one layer by taking the other layer angles constant. In addition, it shows the most important layer angle. As it is seen, the change in the layer 2 affects the buckling load more than the change in layer 1 and 3 when compared.

In addition, the blue line which is the graph of first layer angle is not seen. The reason is the characteristics of layer 3 and 1 are the same. Since all of the layer thicknesses are the same, the layer 1 and 3 graphs are overlapping.

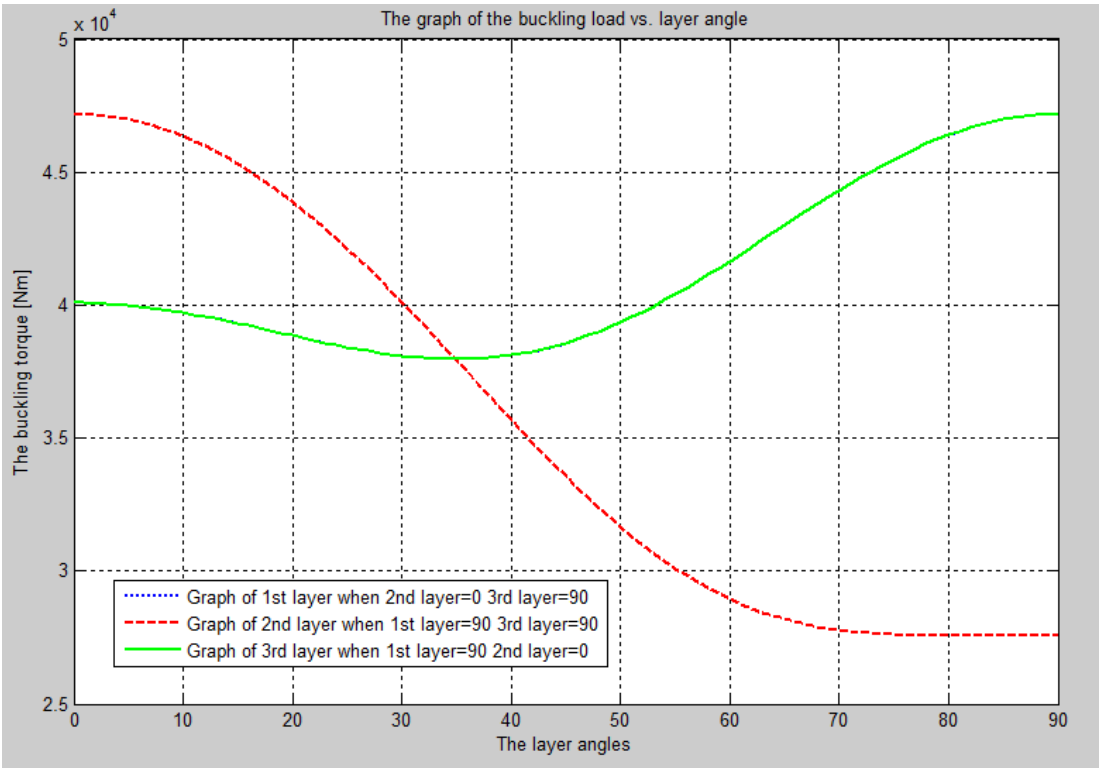

Figure 5.4 : The graph of buckling load vs. layer angle.

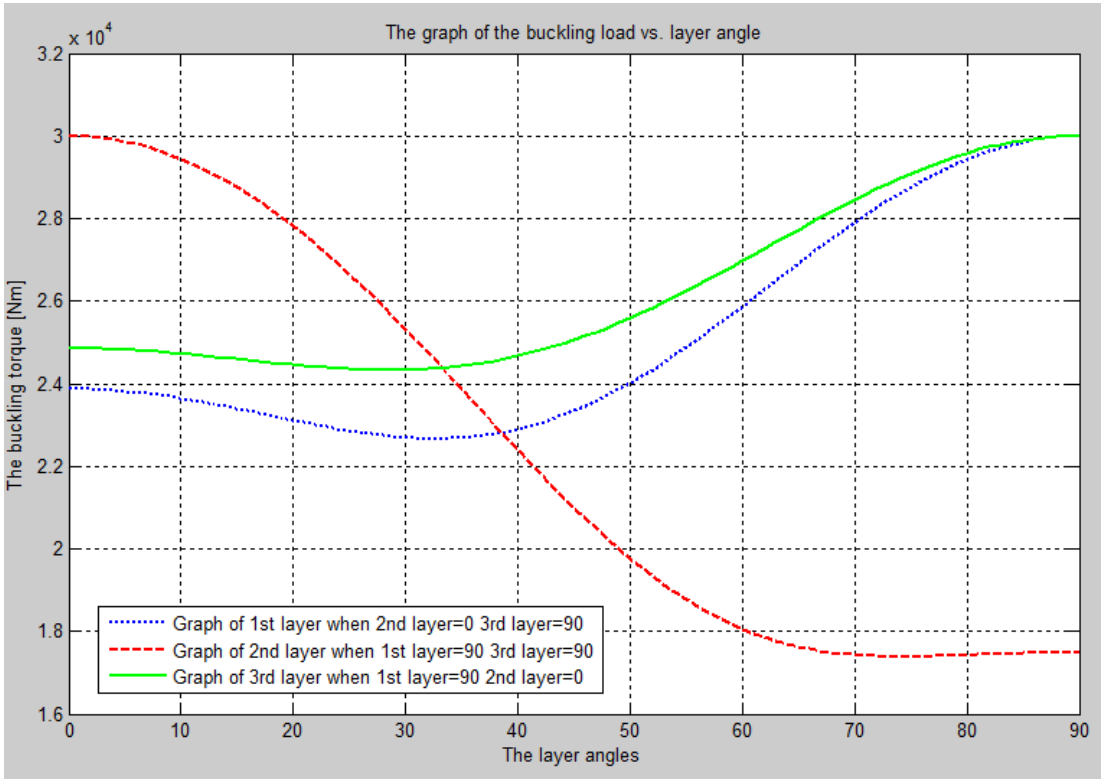

Figure 5.5 : The graph of buckling load vs. layer angle with different thicknesses.

The graph above shows again the layer angle change individually versus the critical buckling load, but this time the 3rd layer thickness is different than the 1st layer thickness.

As a result, if the layer angle increases, the change in buckling load decreases for 1st and 3rd layers.

For the angles, around 45° the change in load for 1st layer and the 3rd layer increases which means that when using the layer angles in these regions, the buckling load becomes much more sensitive.

5.3. Optimization

The fiber angles are optimized for the maximum buckling load for the defined geometrical values. As mentioned at the section 5.2.2, according to the user inputs the program calculated the optimum fiber angles that gives the maximum buckling load for the defined geometrical properties. The further calculations is for optimizing the layer angles.

The optimization procedure as follows.

- The user enters the number of layers.
- The precision of the program can be written in the code. The default precision value is 1°. This means that the program generates the angle matrix with 1° angle increments from 0° to 90°.
- According to the layer number and precision of the program, the code generates an angle matrix that contains all angle configurations.
- After that, the program solves the critical buckling value for all angle configurations.
- At the end of the solution, the program gives the maximum buckling load and the angle configuration that gives the maximum buckling load.
- As a result, the optimum fiber angles will be the angle configuration that gives the maximum buckling load.

Let's take 2 layers with 45° precision as an example.

$$\theta = \begin{bmatrix} 0 & 0 & 0 & 45 & 45 & 45 & 90 & 90 & 90 \\ 0 & 45 & 90 & 0 & 45 & 90 & 0 & 45 & 90 \end{bmatrix}$$

The row number gives the layer number and the column number gives all possible angle configurations. Main important thing here is $\begin{bmatrix} 0 \\ 90 \end{bmatrix}$ and $\begin{bmatrix} 90 \\ 0 \end{bmatrix}$ are different from each other because the layer thicknesses can be different which makes the reduced and modified stiffness matrix differ from each other.

The all of the possible angle configurations can be seen from the expression below.

$$Column\ number\ of\ the\ \theta\ matrix = Possible\ angle\ configurations = \left(\frac{90+p}{p}\right)^n$$

Where;

p: is the precision of the program. The angle increment. This value must be divisible with 90° without remainder such as 1°, 2°, 3°, 5°, 15°, 30°, 60° etc.

n: is the number of layers.

6. NUMERICAL STUDY

Finite element methods are used for solving the engineering problems that is to be solved analytically harder or impossible. Finite element methods does not solve the problem directly. They give a good approximation if all the data written correctly. Firstly the physical problem is modelled in the finite element program and the geometry is divided into many parts called meshes which has node points at the boundary layers.

The finite element methods can be used many eras such as, solid mechanics, fluid mechanics, acoustics, heat transfer, and electromagnetism. This method is widely used to compare the experimental results with the model environment for the problems that are hard to solve analytically. In addition, imperfections can be defined in those programs to simulate the real environment better.

In this study, the cylindrical composite shell structure that is obtained from the optimization study is used to compare the analytical solution and the numerical solution. The numerical study is performed in the ABAQUS program.

6.1. ABAQUS Finite Element Analysis Program

ABAQUS finite element analysis program is used in automotive and aerospace industries. In addition, the program has a large modelling capacity. Thanks to that, this program can be used for academic studies. The program can solve linear and nonlinear problems. The program can also be used in multi-physical studies suck as, structural analysis, acoustics or piezoelectric.

6.2. Definition of the Problem

In this study, the finite element model will be created for the layer angles that has been calculated from the optimization study. In the end, a torsional load is applied to the model and the buckling load is obtained. Finally, the finite element results and the analytical solution results are compared.

6.3. Finite Element Method Steps

6.3.1. Modelling of the thin walled cylindrical structure

As an example for the analysis, the diameter of the cylinder was chosen as 1100mm and the length was chosen as 1100mm.

Modelling of the 3D thin walled cylindrical shell structure was shown in the following figures.

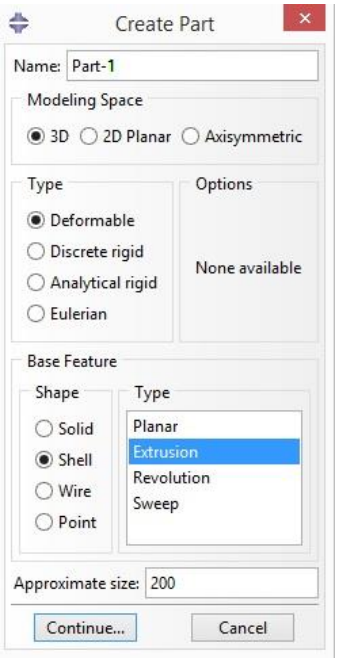

Figure 6.1 : Abaqus part modelling interface.

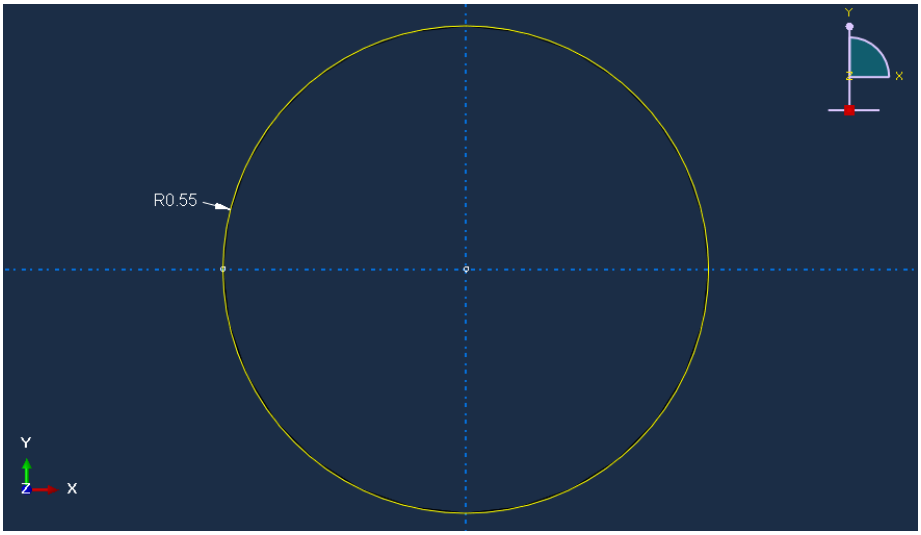

Figure 6.2 : Abaqus sketch environment.

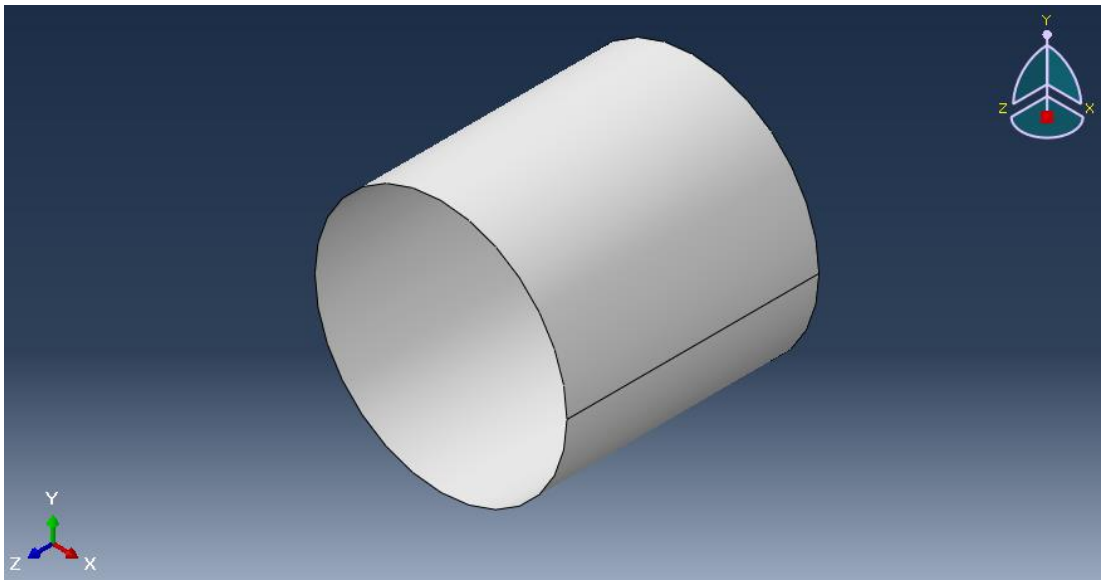

Figure 6.3 : 3D modelled cylindrical shell in Abaqus.

6.3.2. Modelling of the CFRP material

In this step, the material properties are written to the part. The material was chosen as CFRP. The following table shows the material properties.

Table 6.1 : Properties of the CFRP material.

E_1(GPa)	E_2(GPa)	ν_{12}	G_{12}(GPa)	G_{13}(GPa)	G_{23}(GPa)
136.9	9.86	0.293	5.654	5.654	2.689

The material properties are written to the Abaqus program by using the composite layup interface.

The number of composite layers are 3 and the thicknesses of each layer is defined as 1mm. The layer angles are taken from the optimization study as 90° – 0° – 90°. The following figure shows the Abaqus material property interface.

As mentioned before, the CFRP material is an orthotropic material which has 9 independent material coefficients but a lamina doesn't show a stress change on its thickness directions so the number of independent variables reduces to 5 ($G_{12} = G_{13}$).

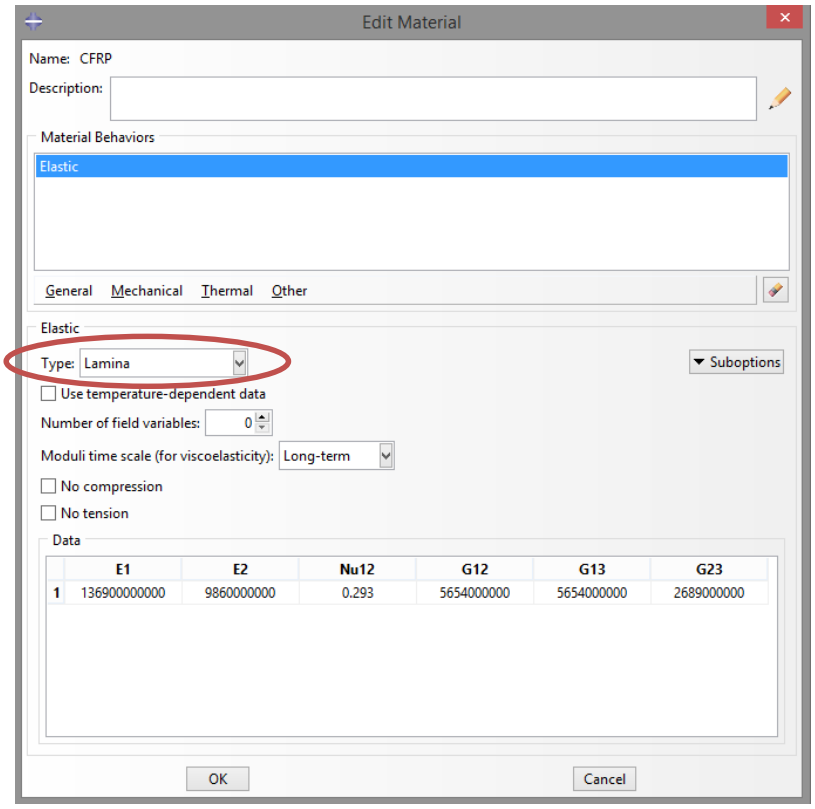

Figure 6.4 : Material properties of the CFRP material.

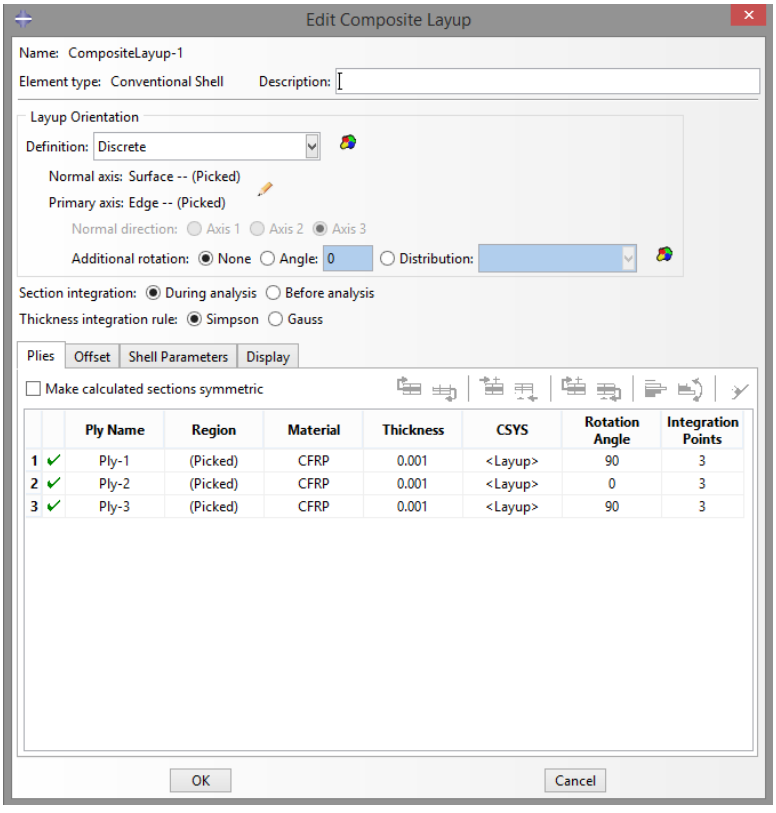

Figure 6.5 : Number of layers, layer angles and layer thicknesses.

6.3.3. Defining the boundary conditions and loads

In this step, the boundary conditions and the loading conditions are given to the cylindrical shell. The following figures shows the loading and boundary conditions of the cylinder.

For the torsional buckling state, a torsional moment is applied in the –z direction to the cylinder. The top of the cylinder is coupled with the edge of the cylinder to move together.

The other edge of the cylinder is considered to be fixed (encastre).

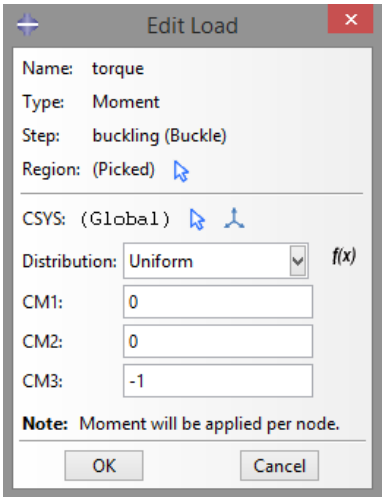

Figure 6.6 : Loading conditions of the shell.

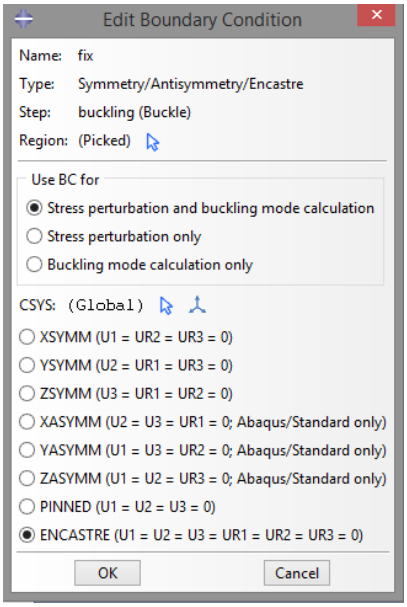

Figure 6.7 : Boundary conditions of the shell.

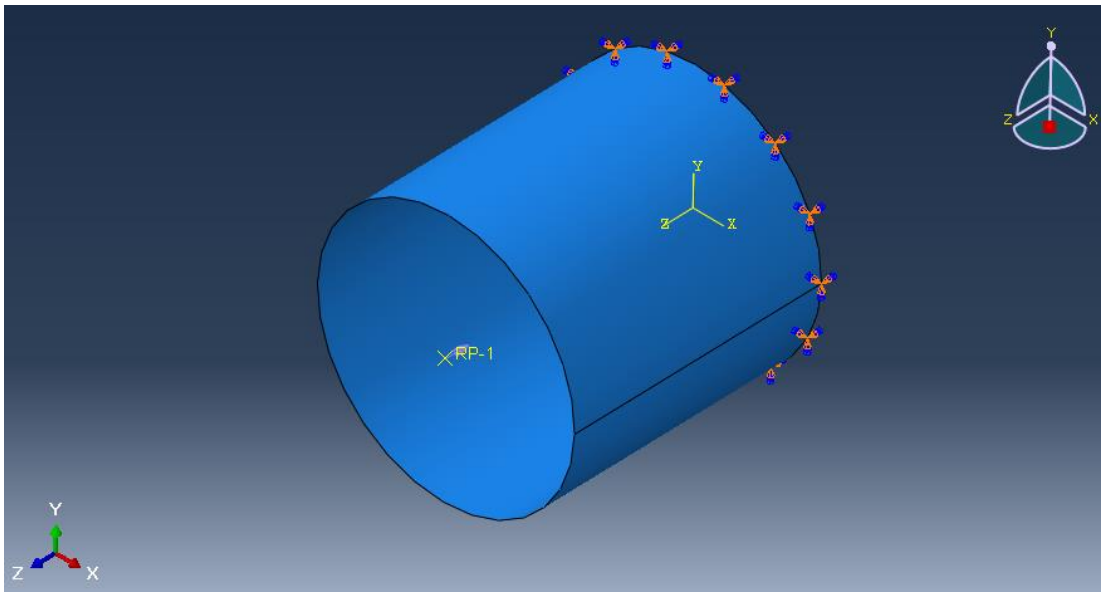

Figure 6.8 : Loading and boundary conditions are shown on the model.

6.3.4. Generating the meshed model

In this step, the cylindrical composite shell is meshed for small finite elements.

The rectangular (Quad) mesh type is used for the finite element analysis. The element size was chosen as 0.01.

The meshing step is shown in the following figure.

In addition, the meshed geometry is also shown in the following figure.

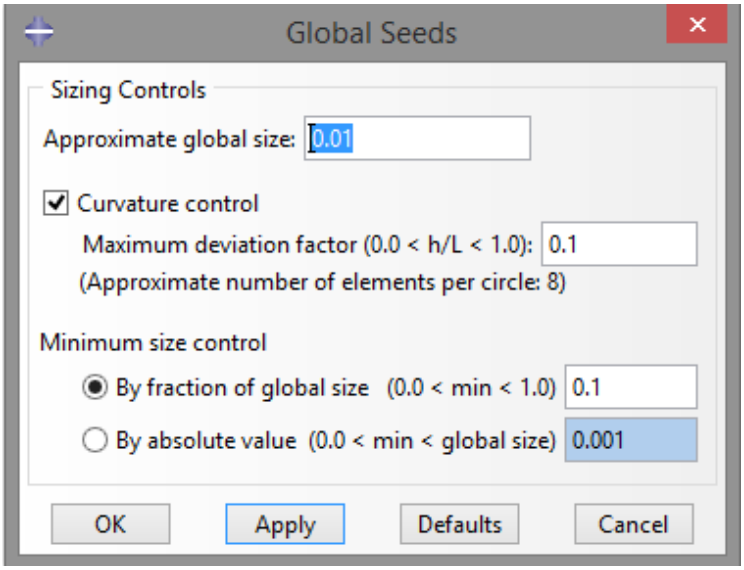

Figure 6.9 : Mesh size.

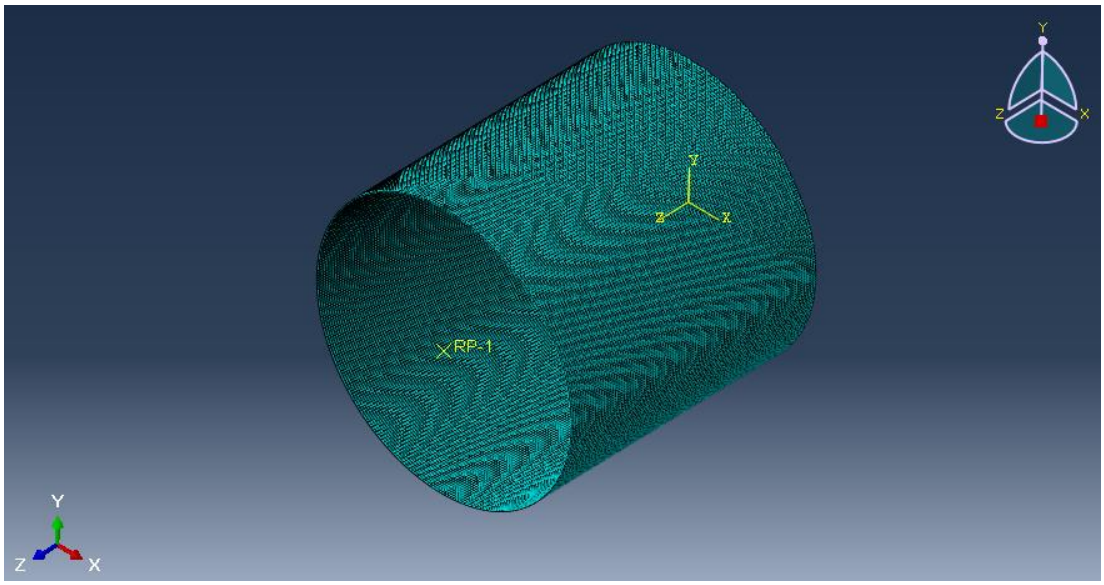

Figure 6.10 : Meshed model.

6.3.5. Finite element results

In the finite element result, the first eigenvalue was obtained as $\lambda = 2.37813x10^5$. Since this is an eigenvalue problem, the crtical load will be obtained by the following equation.

$$N_{x\theta_{cr}} = \lambda \; x \; N_{x\theta_0} \qquad (\mathbf{6.1})$$

Sine the initial load ($N_{x\theta_0}$) is 1, the calculated eigenvalue gives directly the critical load parameter.

In the finite element program, 5 eigenvalues are calculated. Those eigenvalues are shown in the following table. The minus sign show the negative direction.

Table 6.2 : Calculated eigenvalues.

λ_1	λ_2	λ_3	λ_4	λ_5
$2.37813x10^5$	$-2.37813x10^5$	$2.37813x10^5$	$-2.37813x10^5$	$2.40499x10^5$

The following figure shows the results from the first eigenvalue.

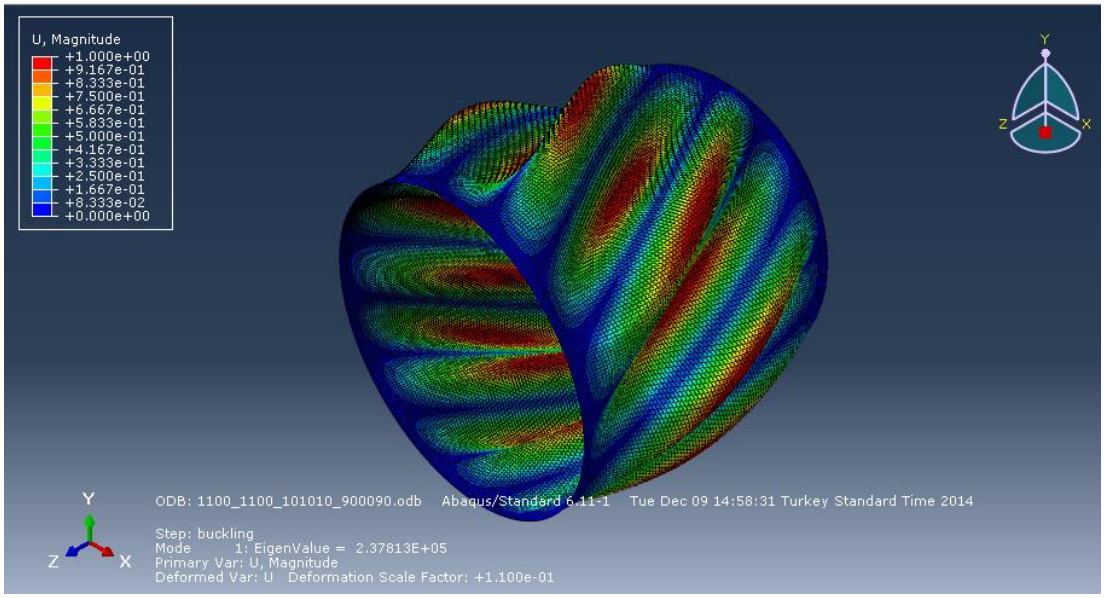

Figure 6.11 : The deformed representation of the first eigenvalue.

6.3.6. The effect of the mesh size to the solution

The mesh size is a very important parameter for FEM analysis. When the element size gets smaller, the results converges to the actual result. For this analysis, the mesh size effect was investigated by comparing the error from the analytical solution.

For the first eigenvalue, the mesh size effect was shown in the following table.

In the MATLAB analytical solution the load parameter was calculated as 2.220271×10^5.

When the mesh size getting smaller the finite element solution converges to the MATLAB analytical solution.

For the analysis, the geometrical values were kept constant, only the mesh size was changed.

In addition, another graph was drawn. The mesh density vs. error graph shows the error convergences to zero by decreasing the mesh size.

It has been seen that, after reaching 0.015 the result does not change very much.

Table 6.3 : Effect of the mesh size to the result.

Number of Layers	Length [m]	Diameter [m]	Thickness of Each Layer [m]	Layer Angles [°]	Mesh Size [m]	Node Density on the Circumference	Abaqus Result	Matlab Result	Error [%]
3	1.1	1.1	0.001	90 00 90	0.500	6.91	**6.80E+07**	**2.22E+05**	**99.67**
3	1.1	1.1	0.001	90 00 90	0.300	11.52	**2.85E+06**	**2.22E+05**	**92.20**
3	1.1	1.1	0.001	90 00 90	0.200	17.28	**9.17E+05**	**2.22E+05**	**75.80**
3	1.1	1.1	0.001	90 00 90	0.100	34.56	**3.76E+05**	**2.22E+05**	**40.89**
3	1.1	1.1	0.001	90 00 90	0.070	49.37	**2.97E+05**	**2.22E+05**	**25.36**
3	1.1	1.1	0.001	90 00 90	0.050	69.12	**2.68E+05**	**2.22E+05**	**17.08**
3	1.1	1.1	0.001	90 00 90	0.030	115.19	**2.47E+05**	**2.22E+05**	**10.24**
3	1.1	1.1	0.001	90 00 90	0.015	230.38	**2.39E+05**	**2.22E+05**	**7.22**
3	1.1	1.1	0.001	90 00 90	0.010	345.58	**2.38E+05**	**2.22E+05**	**6.64**
3	1.1	1.1	0.001	90 00 90	0.005	691.15	**2.37E+05**	**2.22E+05**	**6.29**

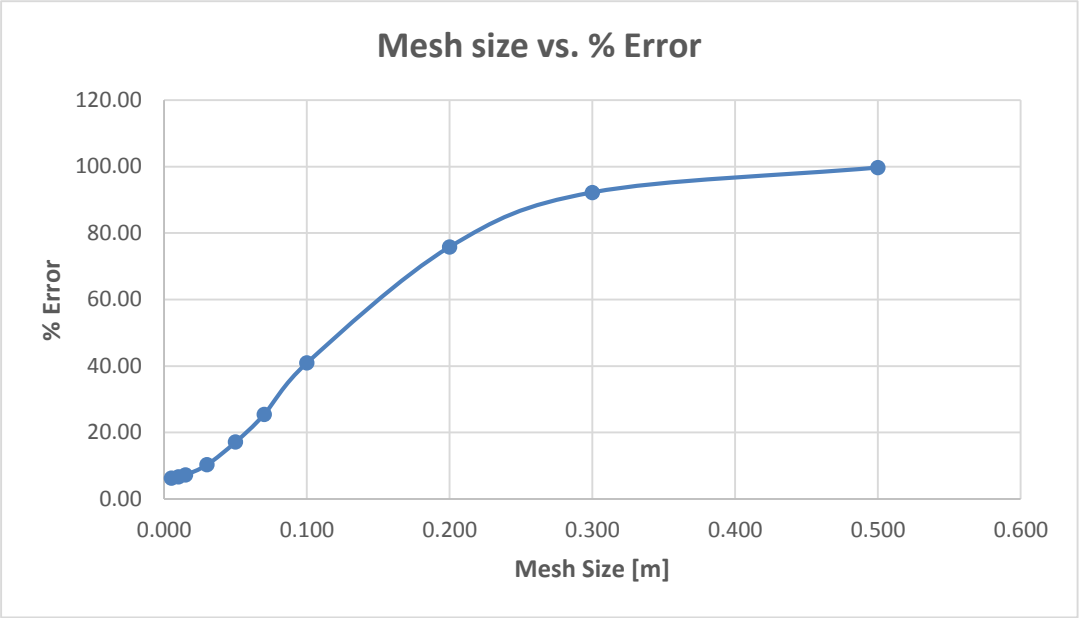

Figure 6.12 : The deformed representation of the first eigenvalue.

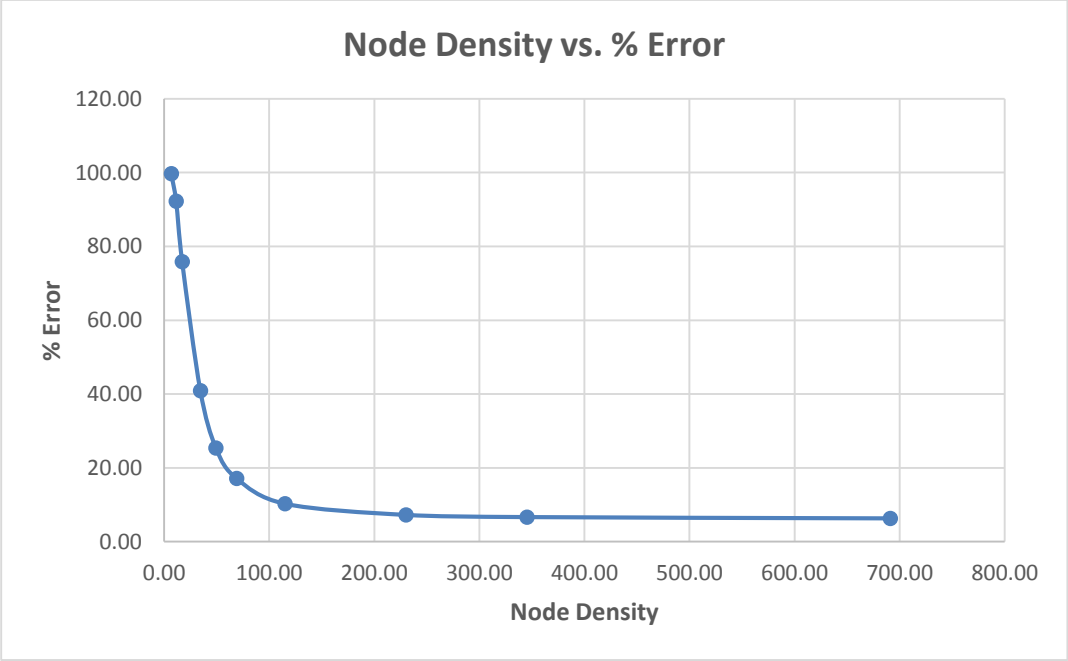

Figure 6.13 : The deformed representation of the first eigenvalue.

7. RESULTS

In this section, the analytical solution (MATLAB solution) and numerical solution (ABAQUS solution) will be evaluated.

First of all, the analytical solutions will be evaluated for different conditions such as, length change and thickness change.

After that, the numerical solution will be evaluated for different conditions such as, length change and thickness change.

In the end the analytical solution and the numerical solution will be shown in the same graph to see the convergence to each other.

In addition, the shell boundary will be shown. As mentioned before, the shell structures are thin walled structures and the thickness to radius ratio must be very small. This transition region will be shown. In some conditions, the analytical solution may act different in the shell transition region.

Finally, the buckling analysis will be run for different materials to prove that CFRP is much stronger than other types of commercial materials.

The materials that will be compared with the CFRP are a type of steel and GFRP. As known the GFRP material is also a composite material like CFRP but the GFRP material is less stiff and less strong when it is compared with the CFRP material. In the next sections, the comparison will be performed for shell point of view.

As mentioned the CFRP material will be compared with a type of steel. This comparison will be performed for two points of view. First is the same geometrical properties and the second is same mass.

As known the steel material is a ductile material. As a result steel is tough when it is compared with the CFRP material. However this thesis is about buckling and since the buckling occurs in elastic region, the ductility property is not important. Mass is another very important thing for designs so the steel vs CFRP comparison is performed also for the same mass.

7.1. Results from the Analytical Solution

7.1.1. The effect of cylinder length to the buckling load parameter

In this section, the effect of cylinder length, between 100mm – 1500mm, to the load parameter will be investigated for same diameter, layer thickness and number of layers. The results that are obtained from the analytical solution. As a result, of this investigation, when the length increases the load parameter decreases. In addition, the selected geometry does not show shell characteristic below 400mm length. After that by using excel, an interpolation is performed. The function can be seen on the graph.

Table 7.1 : Effect of the length to the analytical solution.

Number of Layers	Length [m]	Diameter [m]	Thickness of Each Layer [m]	Layer Angles [°]	$N_{x\theta cr}$ [N/m]
3	0.1	1.1	0.001	90 0 90	**7.36E+05**
3	0.3	1.1	0.001	90 0 90	**4.25E+05**
3	0.5	1.1	0.001	90 0 90	**3.29E+05**
3	0.7	1.1	0.001	90 0 90	**2.78E+05**
3	0.9	1.1	0.001	90 0 90	**2.45E+05**
3	1.1	1.1	0.001	90 0 90	**2.22E+05**
3	1.3	1.1	0.001	90 0 90	**2.04E+05**
3	1.5	1.1	0.001	90 0 90	**1.90E+05**

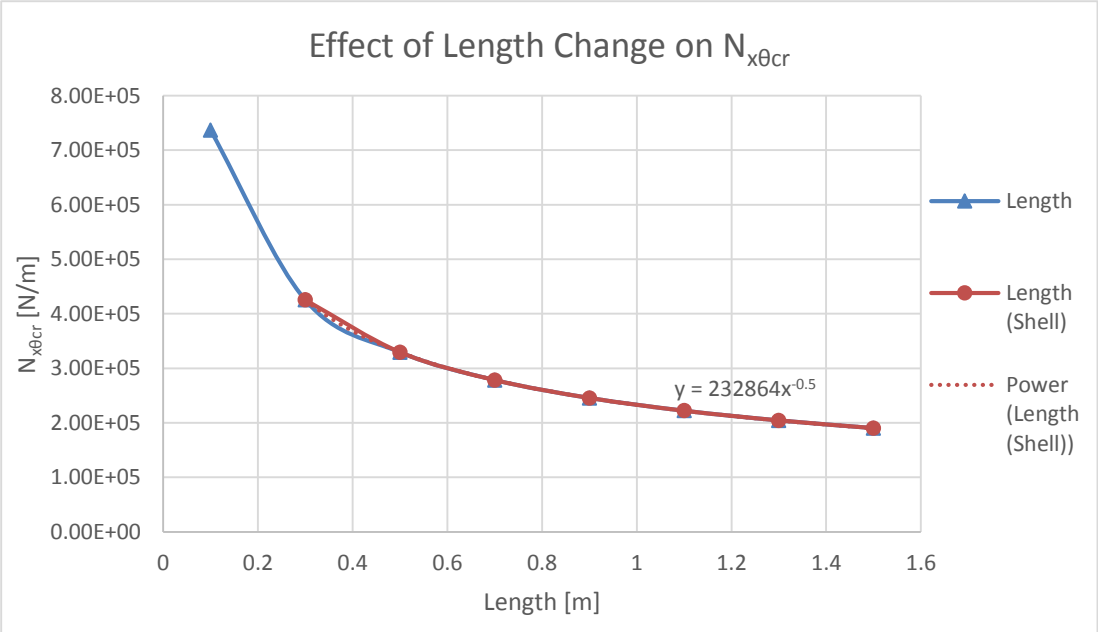

Figure 7.1 : Effect of the length to the analytical solution.

7.1.2. The effect of layer thickness to the buckling load parameter

In this section, the effect of layer thickness, between 0.1mm – 5mm, to the load parameter will be investigated for same diameter, length and number of layers. The result that is obtained from the analytical solution can be seen in the following table and following figure.

As a result, when the thickness increases the load parameter increases radically. In addition, the selected geometry moves away from the shell characteristics after 4mm thickness of each layer. After that by using excel, an interpolation is performed to find the function of the thickness parameter. The function can be seen on the graph.

Table 7.2 : Effect of the layer thickness to the analytical solution.

Number of Layers	Length [m]	Diameter [m]	Thickness of Each Layer [m]	Layer Angles [°]	$N_{x\theta cr}$ [N/m]
3	1.1	1.1	0.0001	90 0 90	**1.25E+03**
3	1.1	1.1	0.0005	90 0 90	**4.67E+04**
3	1.1	1.1	0.0010	90 0 90	**2.22E+05**
3	1.1	1.1	0.0015	90 0 90	**5.53E+05**
3	1.1	1.1	0.0020	90 0 90	**1.06E+06**
3	1.1	1.1	0.0030	90 0 90	**2.63E+06**
3	1.1	1.1	0.0040	90 0 90	**5.02E+06**
3	1.1	1.1	0.0050	90 0 90	**8.30E+06**

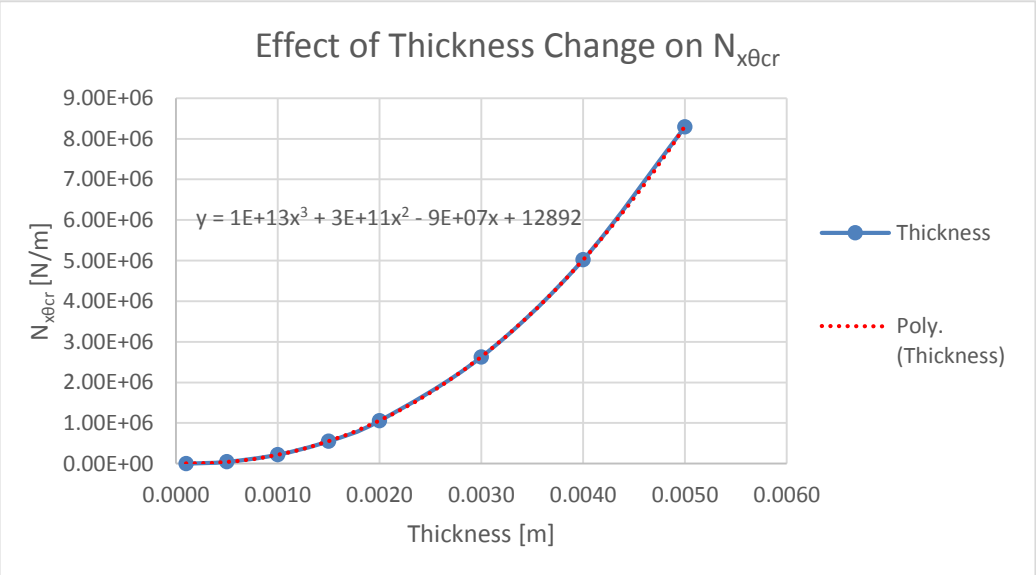

Figure 7.2 : Effect of the layer thickness to the analytical solution.

7.2. Results from the Numerical Solution

7.2.1. The effect of cylinder length to the buckling load parameter

In this section, the effect of cylinder length, between 100mm – 1500mm, to the load parameter will be investigated for same diameter, thickness, and number of layers. The results that are obtained from the numerical solution can be seen in the following table and following figure.

As a result, of this investigation, when the length increases the load parameter decreases. In addition, the selected geometry does not show shell characteristic below 400mm length. After that by using excel, an interpolation is performed to find the function of the length parameter. The function can be seen on the graph.

Table 7.3 : Effect of the length to the numerical solution.

Number of Layers	Length [m]	Diameter [m]	Thickness of Each Layer [m]	Layer Angles [°]	$N_{x\theta}$ [N/m]
3	0.1	1.1	0.001	90 0 90	**1.06E+06**
3	0.3	1.1	0.001	90 0 90	**3.36E+05**
3	0.5	1.1	0.001	90 0 90	**2.82E+05**
3	0.7	1.1	0.001	90 0 90	**2.62E+05**
3	0.9	1.1	0.001	90 0 90	**2.49E+05**
3	1.1	1.1	0.001	90 0 90	**2.29E+05**
3	1.3	1.1	0.001	90 0 90	**2.32E+05**
3	1.5	1.1	0.001	90 0 90	**2.25E+05**

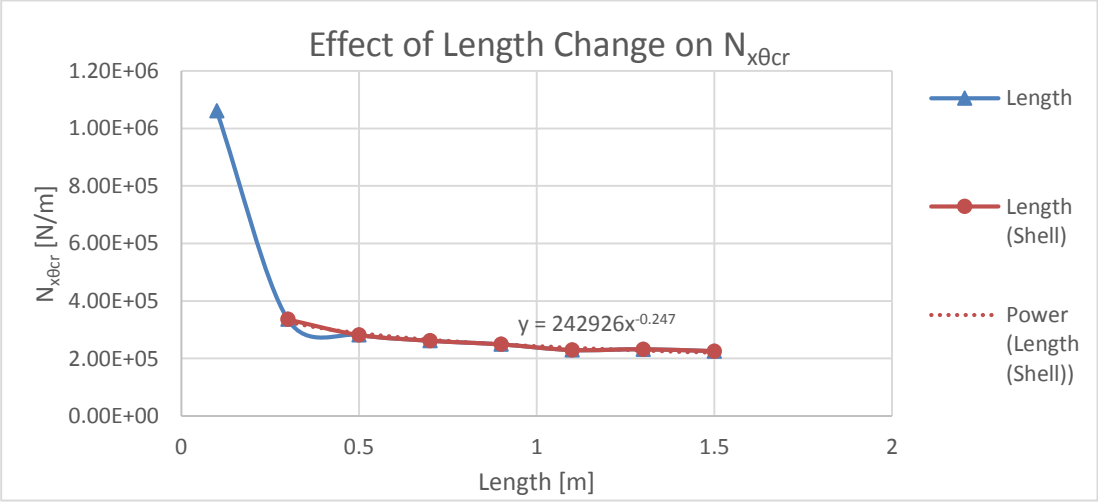

Figure 7.3 : Effect of the length to the numerical solution.

7.2.2. The effect of layer thickness to the buckling load parameter

In this section, the effect of layer thickness, between 0.1mm – 5mm, to the load parameter will be investigated for same diameter, length, and number of layers. The results that are obtained from the numerical solution can be seen in the following table and following figure.

As a result, when the thickness increases the load parameter increases radically. In addition, the selected geometry moves away from the shell characteristics after 4mm thickness of each layer. After that by using excel, an interpolation is performed to find the function of the thickness parameter. The function can be seen on the graph.

Table 7.4 : Effect of the layer thickness to the numerical solution.

Number of Layers	Length [m]	Diameter [m]	Thickness of Each Layer [m]	Layer Angles [°]	$N_{x\theta cr}$ [N/m]
3	1.1	1.1	0.0001	90 0 90	**1.91E+03**
3	1.1	1.1	0.0005	90 0 90	**5.66E+04**
3	1.1	1.1	0.0010	90 0 90	**2.39E+05**
3	1.1	1.1	0.0015	90 0 90	**5.54E+05**
3	1.1	1.1	0.0020	90 0 90	**1.01E+06**
3	1.1	1.1	0.0030	90 0 90	**2.33E+06**
3	1.1	1.1	0.0040	90 0 90	**4.19E+06**
3	1.1	1.1	0.0050	90 0 90	**6.65E+06**

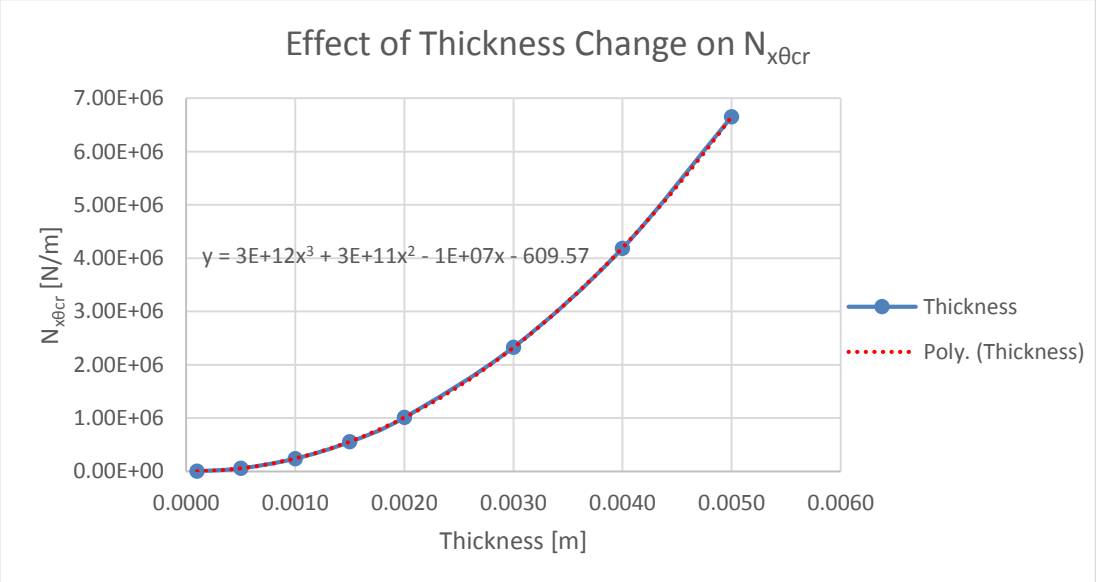

Figure 7.4 : Effect of the layer thickness to the numerical solution.

7.3. Comparison of the Numerical and Analytical Solutions

7.3.1. The comparison of cylinder length change

The solutions for length change both analytically and numerically were introduced in the previous sections. In this section, both analytical and numerical graphs were put on together and see the difference between analytical and numerical solutions.

The following figure shows both MATLAB analytical solution and ABAQUS numerical solution.

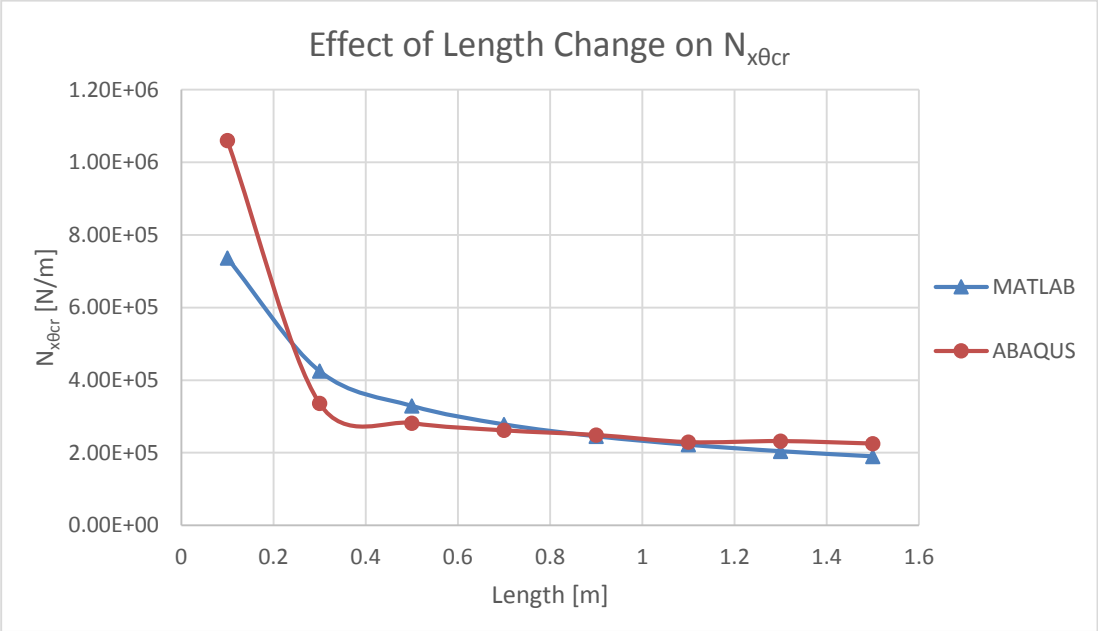

Figure 7.5 : Effect of the cylinder length to the analytical and numerical solutions.

As it is seen from the graph, both analytical solution and numerical solution converge each other in the shell region.

As mentioned before, the selected geometry does not show shell characteristics below 400mm length. In addition, it can be seen that MATLAB analytical solution and ABAQUS finite element analysis acts differently out of the shell region, but in the shell region, the solutions converge to each other.

Out of the shell region, the numerical solution is much higher than the analytical solution. Since the shell theory is not valid in that section so that result cannot be evaluated.

7.3.2. The comparison of layer thickness change

The solutions for layer thickness change both analytically and numerically were introduced in the previous sections. In this section, both analytical and numerical graphs were put on together and see the difference between analytical and numerical solutions.

The following figure shows both MATLAB analytical solution and ABAQUS numerical solution.

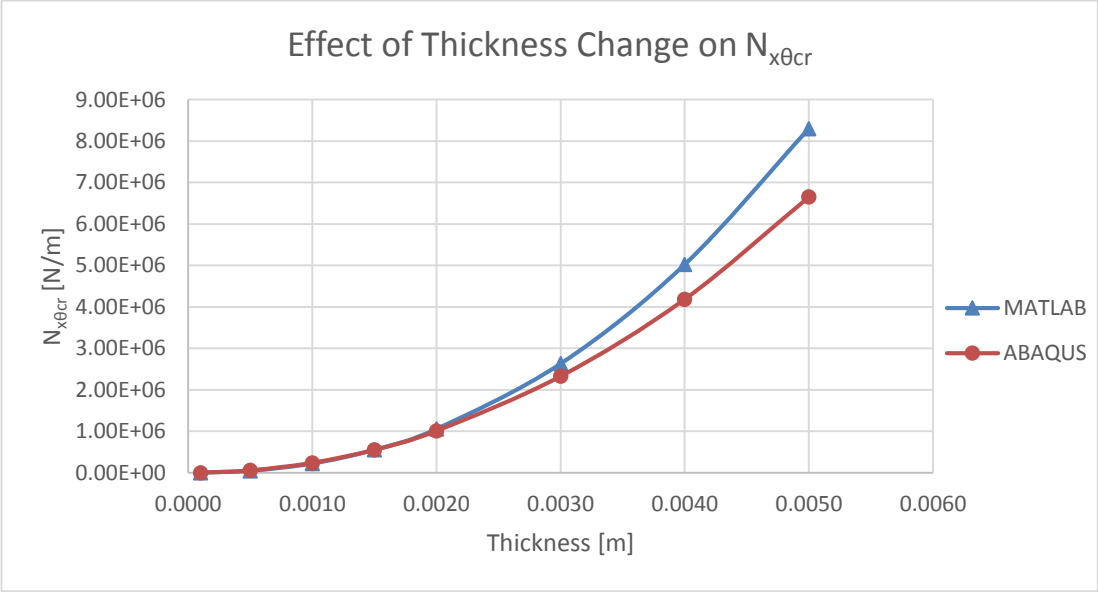

Figure 7.6 : Effect of the layer thickness to the analytical and numerical solutions.

As it is seen from the graph, both analytical solution and numerical solution diverge from each other out of the shell region.

As mentioned before, the selected geometry does not show shell characteristics after 4mm layer thickness.

In addition, it can be seen that MATLAB analytical solution and ABAQUS finite element analysis acts differently out of the shell region, but in the shell region, the solutions converge to each other.

Out of the shell region, the analytical solution is much higher than the numerical solution. Since the shell theory is not valid in that section so that result cannot be evaluated.

7.4. The Effect of Layer Angle Change

As mentioned before, the crucial thing in this thesis is the layer angle optimization. It has been said that the calculated layer angles in MATLAB are the optimum layer angles that resists the maximum buckling torque in the same geometrical properties.

To prove that, the following layer angle convergence plot was drawn. Moreover, in the section 5, analytical solution and optimization, the layer angle change for each layer individually is described.

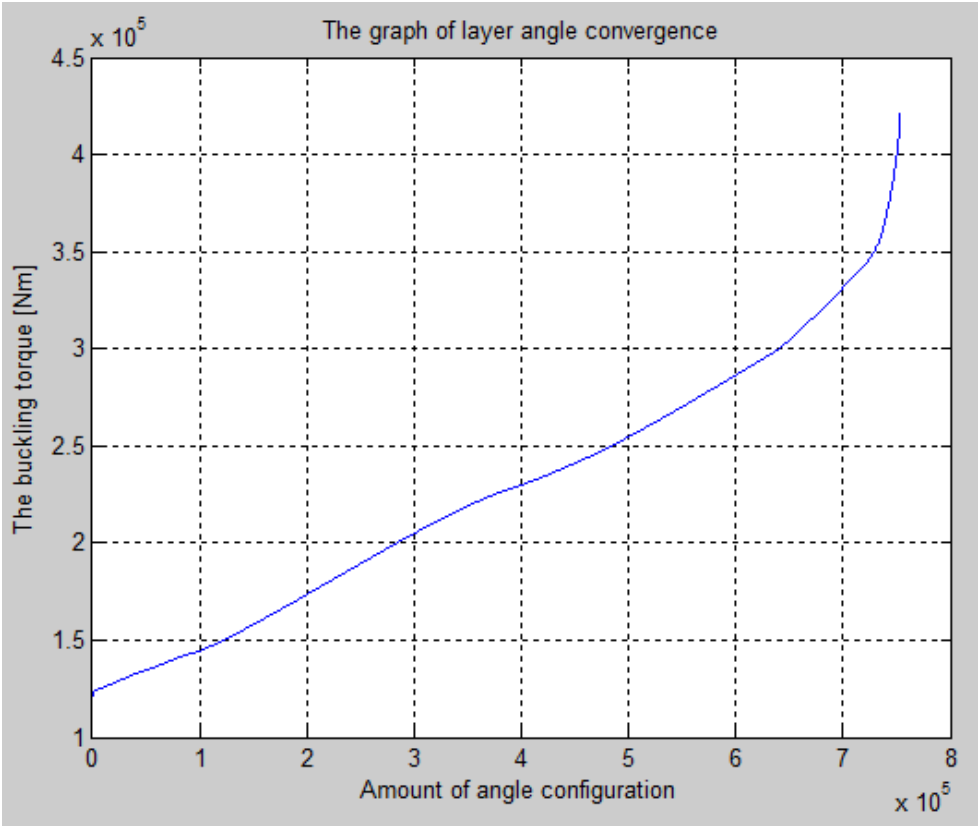

Figure 7.7 : Layer angle convergence

The graph shows that the layer angle convergence to the maximum buckling torque. The x-axis is the amount of layer angle configurations that is solved in the MATLAB program. The y-axis is the buckling torque. As x goes right the angle of the 1st and 3rd layers are goes to 90° and the 2nd layer angle goes to 0°. This is also be seen in the figure 5.1 and 5.2 in the section 5, analytical solution and optimization.

Moreover, by using finite element method the different layer angles are also be solved to see that the calculated layers are optimum or not.

The following table shows the randomly chosen angles that are solved in ABAQUS.

Table 7.5 : Effect of the layer angle.

#	Number of Layers	Length [m]	Diameter [m]	Thickness of Each Layer [m]	Layer Angles [°]	$N_{x\theta cr}$ [N/m]
1	3	1.1	1.1	0.001	0 0 0	**8.24E+04**
2	3	1.1	1.1	0.001	0 45 0	**9.47E+04**
3	3	1.1	1.1	0.001	0 90 0	**9.57E+04**
4	3	1.1	1.1	0.001	45 45 45	**1.13E+05**
5	3	1.1	1.1	0.001	30 60 90	**1.14E+05**
6	3	1.1	1.1	0.001	90 90 90	**1.88E+05**
7	3	1.1	1.1	0.001	90 0 90	**2.39E+05**

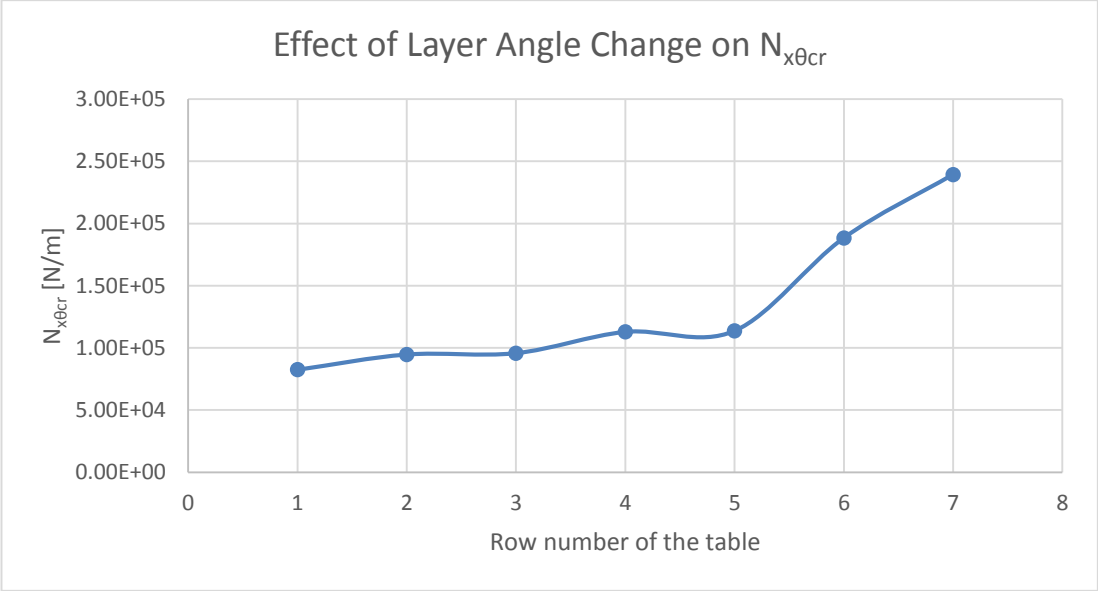

Figure 7.8 : Effect of layer angle

As it is seen from the numerical analysis that are performed in ABAQUS, the best angle configuration is 90° – 0° – 90°. Moreover, it can be seen that when the layer angle decreases the buckling load parameter also decreases. It has been also proven that the most critical layers are 1st and 3rd because when the angle of that layers change, the buckling load parameter increase which means that the selected geometry is much stronger when compared with the other configurations.

7.5. Comparison of CFRP with Different Materials

In this section, the strength and weight advantage of carbon fiber reinforced plastic (CFRP) will be shown. As known, CFRP materials are stronger when compared with other materials and has a great weight advantage.

7.5.1. Comparison of CFRP with GFRP

In this section, the CFRP material is compared with the glass fiber reinforced plastic (GFRP). The comparison procedure is performed with same length, diameter, layer thickness and number of layers. The following table shows the material properties of the GFRP and CFRP material.

Table 7.6 : Properties of the CFRP and GFRP material.

	E_1(GPa)	E_2(GPa)	ν_{12}	G_{12}(GPa)	G_{13}(GPa)	G_{23}(GPa)
CFRP	136.9	9.86	0.293	5.654	5.654	2.689
GFRP	45	12	0.2	5.5	5.5	5.5

As it can be seen from the following table, the GFRP material is weaker when it is compared with the CFRP material. GFRP is also heavier than CFRP.

Table 7.7 : Buckling load parameter comparison of CFRP and GFRP.

Material	**Number of Layers**	**Length [m]**	**Diameter [m]**	**Thickness of Each Layer [m]**	**Layer Angles [°]**	**Nxθcr Abaqus Solution [N/m]**
CFRP	3	1.1	1.1	0.001	90 0 90	**2.39E+05**
GFRP	3	1.1	1.1	0.001	90 0 90	**1.21E+04**

7.5.2. Comparison of CFRP with a type of steel

When comparing CFRP with steel the weight parameter will be a very important parameter. In this section, the investigation will be performed with same geometrical properties, which means that different weight. Moreover, the investigation will be performed with same weight, which means that different total thickness.

The following table shows the mechanical properties of CFRP and a kind of steel. The steel type is not very important because the young modulus does not much change from one kind to other kinds.

Table 7.8 : Properties of the CFRP and steel.

	E_1 [Gpa]	E_2 [Gpa]	ν_{12}	G_{12} [Gpa]	G_{13} [Gpa]	G_{23} [Gpa]
CFRP	136.900	9.860	0.293	5.654	5.654	2.689
	E [Gpa]		**ν**	**G [Gpa]**		
Steel	210.000		0.300	75.000		

The following table shows the buckling load parameter of the CFRP material and steel material with the same dimensional properties. As it is seen, the steel material is stronger than CFRP material, but in weight point of view, the steel material is 5 times heavier than CFRP material. However when the material masses are same the CFRP material is much stronger when compared with steel.

Table 7.9 : Buckling load comparison of the CFRP and steel with same dimensions.

Material	Length [m]	Diameter [m]	Total Thickness [mm]	Mesh Size [m]	Density [kg/m^3]	Mass [kg]	$N_{x\theta cr}$ Abaqus Solution [N/m]
CFRP	1.1	1.1	3.000	0.015	1590	18.132	**2.39E+05**
Steel	1.1	1.1	3.000	0.015	7800	88.951	**1.01E+06**

Table 7.10 : Buckling load comparison of the CFRP and steel with same mass.

Material	Length [m]	Diameter [m]	Total Thickness [mm]	Mesh Size [m]	Density [kg/m^3]	Mass [kg]	$N_{x\theta cr}$ Abaqus Solution [N/m]
CFRP	1.1	1.1	3.000	0.015	1590	18.132	**2.39E+05**
Steel	1.1	1.1	0.611	0.015	7800	88.951	**2.89E+04**

8. CONCLUSION AND SUGGESTIONS

In conclusion, the study makes sense on the torsional buckling behavior of the composite shells.

In literature, many researchers focused on buckling in experimental point of view, such as, Bisagiani and Cordisco (2003), researched the buckling and post-buckling behavior of the carbon fiber composite cylindrical structures under compression and torsional loads individually and together experimentally. They saw the effect of the layer stacking and the fiber angles.

Some other researchers focused on torsional buckling behavior of composite shells in finite element method such as, Gal, Levy, Abramovich and Pavsner (2006), investigated that the finite element model that they were developed. They resulted that the method that they developed gives good results with the experiments and the results in the literature.

However, nobody has focused on the torsional buckling behavior of shells both analytically and finite element method with optimizing the layer angles by using computer programming.

This optimization algorithm is crucial because of the MATLAB code solves the buckling problem for all angle configurations. For that reason, there is a big programming load because of using 4D arrays. In the end, the MATLAB program gives the best layer angle configuration depending the number of layers, diameter of shell, length of shell and each layer thickness. It can also give the optimum layer angles for different layer thicknesses. In addition, the program checks whether the shell was yielded or buckled by using failure theories and also gives the critical buckling torque.

Finally, by using the optimum layer angles, a finite element model has been generated in ABAQUS to prove the analytical solution. To do that the geometrical properties were specified from the analytical solution. For the finite element model, the best mesh dimension was specified and a 6.29% error was obtained between the MATLAB and ABAQUS solution.

More after the effect length, diameter and the layer thickness was investigated both analytically and numerically. The behavior of both analytical solution and numerical solution in the shell transition region was also investigated. In the perfectly shell region, it has been seen that, the both analytical and numerical solutions are not much far away from each other.

In the end, the analytical solution and the numerical solution was compared for varying thickness, length and diameter.

As a result, the written subroutine can be used for optimizing the layer angles for the defined geometrical properties.

In addition, an article was written about this thesis and it was approved and published by WASET (World Academy of Science Engineering and Technology) in the Vol:8 No:11 2014. Also, that paper was presented in the conference that was organized by WASET in İstanbul in November, 29th 2014.

As suggestions, the experimental study can be performed to that study to move that study one step forward. By using experimental study, the parameters from real life can be seen and the effect of imperfections due to real life can be seen and evaluated. By using those imperfections, the finite element model can be re generated and the real solutions can be estimated.

REFERENCES

Bisagni, C. and Cordisco P. (2003). An experimental investigation into the buckling and postbuckling of CFRP shells under combined axial and torsional loading, Composite Structures, 60, 391-402.

Meyer-Piening, H.-R., Farshad, M., Geier B., Zimmermann, R. (2001). Buckling loads of CFRP composite cylinders under combined axial and torsion loading – experiments and computations, Composite Structures, 53, 427-435.

Bisagni, C. (2000). Numerical analysis and experimental correlation of composite shell buckling and post-buckling, Composites Part B: engineering, 31, 655-667.

Smerdov, A. A. (2000). A computational study in optimum formulations of optimization problems on laminated cylindrical shells for buckling I. Shells under axial compression, Composites Science and Technology, 60, 2057-2066.

Smerdov, A. A. (2000). A computational study in optimum formulations of optimization problems on laminated cylindrical shells for buckling I. Shells under external pressure, Composites Science and Technology, 60, 2067-2076.

Moon, C.-J., Kim I.-H., Choi B.-H., Kweon J.-H., Choi J.-H. (2010). Buckling of filament-wound composite cylinders subjected to hydrostatic pressure for underwater vehicle applications, Composites Structures, 92, 2241-2251.

Lopatin, A. V. ve Morozov E. V. (2012). Buckling of a composite cantilever circular shell subjected to uniform external lateral pressure, Composite Structures, 94, 553-562.

Kim, S.-E. ve Kim C.-S. (2002). Buckling strength of the cylindrical shell and tank subjected to axially compressive loads, Thin-Walled Structures, 40, 329-353.

Gal, A., Levy, R., Abramovich, H., Pavsner, P. (2006). Buckling analysis of composite panels, Composite Structures, 73, 179-185.

Chen, Z., Yang L., Cao, G., Guo, W. (2012). Buckling of the axially compressed cylindrical shells with arbitrary axisymmetric thickness variation, Thin-Walled Structures, 60, 38-45.

Kirkpatrick, S. W. ve Holmes B. S. (1989). Axial buckling of a thin cylindrical shell: experiments and calculations, Computational Experiments, ASME Publications, 176, 329-353.

Goldfeld, Y., Arbocz J., Rothwell, A. (2005). Design and optimization of laminated conical shells for buckling, Thin-Walled Structures, 43, 107-133.

Tafreshi, A. (2004). Efficient modelling of delamination buckling in composite cylindrical shells under axial compression, Composite Structures, 64, 511-520.

Bert, C. W., Kim, C.-D. (1995). Analysis of buckling of hollow laminated composite drive shafts, Composites Science and Technology, 53, 343-351.

Shokrieh, M. M., Hasani, A., Lessard, L. B. (2004). Shear buckling of a composite drive shaft under torsion, Composite Structures, 64, 63-69.

Lennon, R. F. ve Das, P. K (2000). Torsional buckling behavior of stiffened cylinders under combined loading, Thin-Walled Structures, 38, 229-245.

Al-Hassani, S. T. S., Darvizeh, M., Haftchenari H. (1997). An analytical study of buckling of composite tubes with various boundary conditions, Composite Structures, 39, 157-164.

Bisagni, C. ve Cordisco P. (2006). Post-buckling and collapse experiments of stiffened composite cylindrical shells subjected to axial loading and torque, Composite Structures, 73, 138-149.

Messager, T., Pyrz M., Gineste, B., Chauchot, P. (2002). Optimal laminations of thin underwater composite cylindrical vessels, Composite Structures, 58, 529-537.

Tafreshi, A. (2006). Delamination buckling and postbuckling in composite cylindrical shells under combined axial compression and external pressure, Composite Structures, 72, 401-418.

Kaw, A. K. (2006). Mechanics of Composite Materials, Second edition, Taylor & Francis Group.

Berthelot, J.-M. (1999). Composite Materials Mechanical Behavior and Structural Analysis, Springer-Verlag Berlin Heidelberg GmbH.

NASA (1965). Buckling of Thin-walled Circular Cylinders, Nasa Space Vehicle Design Criteria, National Aeronautics and Space Administration.

Ural, T. (2009). Silindirik kompozit kabların burkulma analizi (Ph.D. Thesis), Atatürk University, Erzurum.

Vinson, J. R. ve Sierakowski R. L. (2004). The Behavior of Structures Composed of Composite Materials, Second Edition, Kluwer Academic Publishers.

Kollar, L. P. ve Springer G. S. (2003). Mechanics of Composite Structures, Cambridge University Press.

Tanov, R. ve Tabiei A. Static and Dynamic Buckling of Laminated Composite Shells, University of Cincinnati.

Pekbey, Y. (2005) Buckling of economical composite bars (Ph.D. Thesis), Dokuz Eylül University, İzmir.

Url-1 <*http://tr.wikipedia.org/wiki/MATLAB*>, date retrieved: 04.12.2014.

Url-2 <*http://en.wikibooks.org/wiki/MATLAB_Programming*>, date retrieved: 04.12.2014.

Url-3 <*http://en.wikipedia.org/wiki/Abaqus*>, date retrieved: 04.12.2014.

Url-4 <*http://tr.wikipedia.org/wiki/Sonlu_elemanlar_yöntemi*>, date retrieved: 04.12.2014.

APPENDICES

APPENDIX A: Main MATLAB code
APPENDIX B: Angle Generation Function

APPENDIX A

```
clear all
clc

%% Definitions

layer=input('Enter the number of layers\n');
angle_increment=1; % The value of angle increment ex; for the angle
of 30 degrees increment, the angles will be 0 30 60 90.
                   % This determines the resolution of the theta
matrix
angle=(90+angle_increment)/angle_increment;
row=layer; % Determines the number of rows of theta matrix
col=angle^layer; % Determines the number of columns of the theta
matrix
                 % All of the variables defined as "col" in the
zeros function or loops for matrices, are related with the number of
columns of the theta matrix.


%% Material properties
% Uncomment what you need

% E1=input('Enter E1\n');
% E2=input('Enter E2\n');
% E3=input('Enter E3\n');
% nu12=input('Enter nu12\n');
% nu13=input('Enter nu13\n');
% nu23=input('Enter nu23\n');
% G23=input('Enter G23\n');
% G13=input('Enter G13\n');
% G12=input('Enter G12\n');

%Properties of CF from the journal (experimental)
E1=136.9e9; %[Pa]
E2=9.86e9; %[Pa]
E3=9.86e9; %[Pa]
nu12=0.293;
nu13=0.293;
nu21=(E2*nu12)/E1;
nu23=0.45;
G12=5.654e9; %[Pa]
G13=5.654e9; %[Pa]
G23=2.689e9; %[Pa]

% %Mechanical properties CFRP
sig_1_T_ult=1500e6; %[Pa]
sig_1_C_ult=1500e6; %[Pa]
sig_2_T_ult=40e6;   %[Pa]
sig_2_C_ult=246e6;  %[Pa]
tau_1_2_ult=68e6;   %[Pa]

%% Compliance matrix (S) with the engineering constants

C=zeros(6,6,layer,col);
S=zeros(6,6,layer,col);
```

```
S(1,1,:,:)=1/E1;
S(1,2,:,:)=-nu12/E1;
S(1,3,:,:)=-nu13/E1;
S(2,2,:,:)=1/E2;
S(2,3,:,:)=-nu23/E2;
S(3,3,:,:)=1/E3;
S(4,4,:,:)=1/G23;
S(5,5,:,:)=1/G13;
S(6,6,:,:)=1/G12;

%Symmetry
S(2,1,:,:)=S(1,2,:,:);
S(3,1,:,:)=S(1,3,:,:);
S(4,1,:,:)=S(1,4,:,:);
S(5,1,:,:)=S(1,5,:,:);
S(6,1,:,:)=S(1,6,:,:);
S(3,2,:,:)=S(2,3,:,:);
S(4,2,:,:)=S(2,4,:,:);
S(5,2,:,:)=S(2,5,:,:);
S(6,2,:,:)=S(2,6,:,:);
S(4,3,:,:)=S(3,4,:,:);
S(5,3,:,:)=S(3,5,:,:);
S(6,3,:,:)=S(3,6,:,:);
S(5,4,:,:)=S(4,5,:,:);
S(6,4,:,:)=S(4,6,:,:);
S(6,5,:,:)=S(5,6,:,:);

%% Stiffness matrix (C) with engineering constants

for p=1:layer
    for j=1:col
        C(:,:,p,j)=inv(S(:,:,p,j));
    end
end

%Symmetry
C(2,1,:,:)=C(1,2,:,:);
C(3,1,:,:)=C(1,3,:,:);
C(4,1,:,:)=C(1,4,:,:);
C(5,1,:,:)=C(1,5,:,:);
C(6,1,:,:)=C(1,6,:,:);
C(3,2,:,:)=C(2,3,:,:);
C(4,2,:,:)=C(2,4,:,:);
C(5,2,:,:)=C(2,5,:,:);
C(6,2,:,:)=C(2,6,:,:);
C(4,3,:,:)=C(3,4,:,:);
C(5,3,:,:)=C(3,5,:,:);
C(6,3,:,:)=C(3,6,:,:);
C(5,4,:,:)=C(4,5,:,:);
C(6,4,:,:)=C(4,6,:,:);
C(6,5,:,:)=C(5,6,:,:);

%% Angle arrangement

theta=zeros(row,col);

% See angle_generation function
for i=1:row
    theta(i+1,:)=angle_generation(layer,angle,i);
```

```
end

c1=0;
dummy_angle=zeros(1,col);
for i=1:col
    dummy_angle(i)=c1;
    c1=c1+1;
    c1=mod(c1,angle);
end
theta(1,:)=dummy_angle;
theta(row+1,:)=[];

theta=theta.*angle_increment;

% Degrees to radians conversion
for p=1:layer
    theta(p,:)=(pi*theta(p,:))/180;
end

%% Calculation of transformation matrices and stiffness and
compliance matrices with respect to fiber angles

sz_theta=size(theta);

T_sig=zeros(6,6,sz_theta(1,1), sz_theta(1,2));
T_eps=zeros(6,6,sz_theta(1,1), sz_theta(1,2));
S_prime=zeros(6,6,sz_theta(1,1), sz_theta(1,2));
C_prime=zeros(6,6,sz_theta(1,1), sz_theta(1,2));

for p=1:layer
    for angle=1:sz_theta(1,2)
        %Transformation matrix for sigma (Berthelot page:103)
        T_sig(:,:,p,angle)=[  (cos(theta(p,angle)))^2
(sin(theta(p,angle)))^2 0 0 0
2*sin(theta(p,angle))*cos(theta(p,angle)); (sin(theta(p,angle)))^2
(cos(theta(p,angle)))^2 0 0 0 -
2*sin(theta(p,angle))*cos(theta(p,angle)); 0 0 1 0 0 0; 0 0 0
cos(theta(p,angle)) -sin(theta(p,angle)) 0; 0 0 0
sin(theta(p,angle)) cos(theta(p,angle)) 0; -
sin(theta(p,angle))*cos(theta(p,angle))
sin(theta(p,angle))*cos(theta(p,angle)) 0 0 0
((cos(theta(p,angle)))^2)-((sin(theta(p,angle)))^2)];

        %Transformation matrix for epsilon (Berthelot page:117)
        T_eps(:,:,p,angle)=[  (cos(theta(p,angle)))^2
(sin(theta(p,angle)))^2 0 0 0
sin(theta(p,angle))*cos(theta(p,angle)); (sin(theta(p,angle)))^2
(cos(theta(p,angle)))^2 0 0 0 -
sin(theta(p,angle))*cos(theta(p,angle)); 0 0 1 0 0 0; 0 0 0
cos(theta(p,angle)) -sin(theta(p,angle)) 0; 0 0 0
sin(theta(p,angle)) cos(theta(p,angle)) 0; -
2*sin(theta(p,angle))*cos(theta(p,angle))
2*sin(theta(p,angle))*cos(theta(p,angle)) 0 0 0
((cos(theta(p,angle)))^2)-((sin(theta(p,angle)))^2)];


S_prime(:,:,p,angle)=(T_eps(:,:,p,angle)\S(:,:,p,angle))*T_sig(:,:,p
,angle);
```

```
C_prime(:,:,p,angle)=(T_sig(:,:,p,angle)\C(:,:,p,angle))*T_eps(:,:,p
,angle);
    end
end

%% Deleting the first three rows and columns for plane stress
assumption

S_prime(3,:,:,:)=[];
S_prime(3,:,:,:)=[];
S_prime(3,:,:,:)=[];
S_prime(:,3,:,:)=[];
S_prime(:,3,:,:)=[];
S_prime(:,3,:,:)=[];
C_prime(3,:,:,:)=[];
C_prime(3,:,:,:)=[];
C_prime(3,:,:,:)=[];
C_prime(:,3,:,:)=[];
C_prime(:,3,:,:)=[];
C_prime(:,3,:,:)=[];
Q_prime=C_prime;
S_prime;

%% Calculation of h values (related with layer thicknesses)

t=zeros(1,layer);
for i=1:layer
    t(i)=input(['Write the thickness of layer number ' num2str(i) '
in  milimeters [mm]\n']);
end

% mm to m conversion
for i=1:layer
    t(i)=t(i)/1000;
end

T=sum(t);

dummy_t=cumsum(t);
sz_t=size(t);
dummy_t(sz_t(1,2)+1)=0;
sz_dummy_t=size(dummy_t);

counter=sz_dummy_t(1,2);
for i=1:sz_t(1,2)
    dummy_t(counter)=dummy_t(counter-1);
    counter=counter-1;
end
dummy_t(1)=0;


h=zeros(1,sz_dummy_t(1,2));
for i=1:sz_dummy_t(1,2)
    h(i)=-((T/2)-(dummy_t(i)));
end

%% Calculating the A, B and D matrices
```

```
sz_Q_prime=size(Q_prime);

A=zeros(sz_Q_prime(1,1),sz_Q_prime(1,2),sz_Q_prime(1,4));
A_sum=zeros(sz_Q_prime(1,1),sz_Q_prime(1,2),sz_Q_prime(1,3),sz_Q_pri
me(1,4));
for p=1:layer
    A_sum(:,:,p,:)=Q_prime(:,:,p,:)*(h(p+1)-h(p));
    A=sum(A_sum,3);
end
A=reshape(A,3,3,col);
A;

B=zeros(sz_Q_prime(1,1),sz_Q_prime(1,2),sz_Q_prime(1,4));
B_sum=zeros(sz_Q_prime(1,1),sz_Q_prime(1,2),sz_Q_prime(1,3),sz_Q_pri
me(1,4));
for p=1:layer
    B_sum(:,:,p,:)=Q_prime(:,:,p,:)*(((h(p+1))^2)-(h(p)^2));
    B=sum(B_sum,3);
end
B=reshape(B,3,3,col);
B=B/2;

D=zeros(sz_Q_prime(1,1),sz_Q_prime(1,2),sz_Q_prime(1,4));
D_sum=zeros(sz_Q_prime(1,1),sz_Q_prime(1,2),sz_Q_prime(1,3),sz_Q_pri
me(1,4));
for p=1:layer
    D_sum(:,:,p,:)=Q_prime(:,:,p,:)*(((h(p+1))^3)-(h(p)^3));
    D=sum(D_sum,3);
end
D=reshape(D,3,3,col);
D=D/3;

%% Defining the dimensional and buckling mode parameters (L,
Diameter, m, n)

L=input('Enter the Length of the cylinder in milimeters [mm]\n');
L=L/1000;
Diameter=input('Enter the Diameter of the cylinder in milimeters
[mm]\n');
R=Diameter/2;
R=R/1000;

%% mass calculation

rho_carbon=1800; %[kg/m3]
rho_epoxy=1200; %[kg/m3]
carbon_percent=0.65;
epoxy_percent=1-carbon_percent;
rho=rho_carbon*carbon_percent+rho_epoxy*epoxy_percent; %[kg/m3]

volume=2*pi*R*T*L;
mass=volume*rho;

%% Calculation of critical buckling load under torsion

%control due to torsion page 250 at shell book eq 5.124
control=zeros(1,col);
for i=1:col
```

```
    control(i)=((D(2,2,i)/D(1,1,i))^(5/6))*(((A(1,1,i)*A(2,2,i)-
(A(1,2,i)^2))/(12*A(2,2,i)*D(1,1,i)))^(1/2))*((L^2)/R);
end


Tcr=zeros(1,col);
Nxtheta_cr=zeros(1,col);
for i=1:col
     if control(i)>=500
        Tcr(i)=21.75*(D(2,2,i)^(5/8))*(((A(1,1,i)*A(2,2,i)-
(A(1,2,i)^2))/A(2,2,i))^(3/8))*((R^(5/4))/(L^(1/2)));
        Nxtheta_cr(i)=(Tcr(i))/(2*pi*(R^2));
     else
        Tcr(i)=-1;
        Nxtheta_cr(i)=-1;
     end
end


%% h/R ratio calculation (thickness/radius)
h_R_ratio=T/R;

%% R/L ratio calculation
R_L_ratio=R/L;

%% Stresses and Strains

stiff=[A,B;B,D];
Nx=zeros(1,col);
Ntheta=zeros(1,col);
Nxtheta=Nxtheta_cr;
Mx=zeros(1,col);
Mtheta=zeros(1,col);
Mxtheta=zeros(1,col);

eps=zeros(6,col);
Force_vector=[Nx;Ntheta;Nxtheta;Mx;Mtheta;Mxtheta];
for i=1:col
    eps(:,i)=stiff(:,:,i)\Force_vector(:,i);
end

ex=eps(1,:);
etheta=eps(2,:);
extheta=eps(3,:)/2;
kx=eps(4,:);
ktheta=eps(5,:);
kxtheta=eps(6,:)/2;

eps_0=[ex;etheta;extheta];
eps_k=[kx;ktheta;kxtheta];

sig=zeros(3,layer,col);
for i=1:layer
    for j=1:col

sig(:,i,j)=Q_prime(:,:,i,j)*eps_0(:,j)+T*Q_prime(:,:,i,j)*eps_k(:,j)
;
    end
end
```

```
Transform=zeros(3,3,layer,col);
for i=1:layer
    for j=1:col
        Transform(:,:,i,j)=[(cos(theta(i,j)))^2 (sin(theta(i,j)))^2
2*sin(theta(i,j))*cos(theta(i,j)); (sin(theta(i,j)))^2
(cos(theta(i,j)))^2 -2*sin(theta(i,j))*cos(theta(i,j)); -
sin(theta(i,j))*cos(theta(i,j)) sin(theta(i,j))*cos(theta(i,j))
(cos(theta(i,j)))^2-(sin(theta(i,j)))^2];
    end
end

sig_transform=zeros(3,layer,col);
for i=1:layer
    for j=1:col
        sig_transform(:,i,j)=Transform(:,:,i,j)*sig(:,i,j);
    end
end

sig_MPa=sig*10^-6; %in MPa
sig_transform_MPa=sig_transform*10^-6;

%% Failure theories

X1=zeros(layer,col);
X2=zeros(layer,col);
Y=zeros(layer,col);
S=zeros(layer,col);

for i=1:layer
    for j=1:col
        if sig_transform(1,i,j) > 0
            X1(i,j)=sig_1_T_ult;
        elseif sig_transform(1,i,j) < 0
            X1(i,j)=sig_1_C_ult;
        end

        if sig_transform(2,i,j) > 0
            X2(i,j)=sig_1_T_ult;
        elseif sig_transform(2,i,j) < 0
            X2(i,j)=sig_1_C_ult;
        end

        if sig_transform(2,i,j) > 0
            Y(i,j)=sig_2_T_ult;
        elseif sig_transform(2,i,j) < 0
            Y(i,j)=sig_2_C_ult;
        end

        S(i,j)=tau_1_2_ult;
    end
end

failure=zeros(layer,col);
for i=1:layer
    for j=1:col
        failure(i,j)=((sig_transform(1,i,j)/X1(i,j))^2) -
((sig_transform(1,i,j)*sig_transform(2,i,j))/(X2(i,j)*X2(i,j))) +
```

```
((sig_transform(2,i,j)/Y(i,j))^2) +
((sig_transform(3,i,j)/S(i,j))^2);
    end
end

%% Assigning the nonzero Nxcr and P values
Nxtheta_cr_non_zero=Nxtheta_cr;
Tcr_non_zero=Tcr;

%% Finding failed components and making the loads 0
[f_row,f_column]=find(failure>=1);

for i=1:length(f_column)
    Nxtheta_cr(f_column(i))=0;
end

for i=1:length(f_column)
    Tcr(f_column(i))=0;
end
%% Calculating the maximum load

max_torque=max(Tcr);
indice=find(Tcr==max_torque);


%% Degrees to radians conversion

% Just for theta matrix control
for p=1:layer
    theta(p,:)=(180*theta(p,:))/pi;
end

% rounding the theta matrix because of unit conversion errors
theta=round(theta);

%% Calculating the optimum angle configuration

optimum_angles=theta(:,indice);

%% Printing thevalues (Maximum buckling load, most suitable angles,
h/R ratio and R/L ratio)

fprintf('\n\n\t\t\tRESULTS')
fprintf('\n\nMaximum buckling load is %e\n',max_torque)
fprintf('\nOptimum angles are;\n')
fprintf('%f\n',optimum_angles)
fprintf('\nThe stress values with respect to the part and ply axes
that occur under the maximum buckling load as follows;\n')
for i=1:layer
    fprintf(['\nStress values with respect to the part axes at the
layer number '  num2str(i) ' are\n'])
    fprintf('sigma_x       = %f\n',sig_MPa(1,i,indice))
    fprintf('sigma_theta   = %f\n',sig_MPa(2,i,indice))
    fprintf('sigma_x_theta = %f\n',sig_MPa(3,i,indice))
end
fprintf('\n\n')
for i=1:layer
    fprintf(['\nStress values with respect to the ply axes at the
layer number '  num2str(i) ' are\n'])
```

```
    fprintf('sigma_1  = %f\n',sig_transform_MPa(1,i,indice))
    fprintf('sigma_2  = %f\n',sig_transform_MPa(2,i,indice))
    fprintf('sigma_3  = %f\n',sig_transform_MPa(3,i,indice))
end

fprintf('\nFailure coefficient in each layer as follows\n')
for i=1:layer
    fprintf(['f'  num2str(i) ' = %f\n'],failure(i,indice))
end

fprintf('\n\nh/R ratio = %f\n',h_R_ratio)
fprintf('R/L ratio = %f\n',R_L_ratio)

%% Graphs

max_load_non_zero=max(Tcr_non_zero);
indice_non_zero=find(Tcr_non_zero==max_load_non_zero);
optimum_angles_non_zero=theta(:,indice_non_zero);


% plot of the only one angle (interploated)
plot_angle_indices1=find(theta(layer,:)==optimum_angles_non_zero(lay
er,1) & theta(layer-1,:)==optimum_angles_non_zero(layer-1,1));
plot_angles1=theta(1,plot_angle_indices1);
Tcr_non_zero_graph1=zeros(1,length(plot_angle_indices1));
for i=1:length(plot_angle_indices1)
    Tcr_non_zero_graph1(i)=Tcr_non_zero(plot_angle_indices1(i));
end
% plot(plot_angles,Tcr_non_zero_graph)

% plot of the only one angle (interploated)
plot_angle_indices2=find(theta(layer,:)==optimum_angles_non_zero(lay
er,1) & theta(layer-2,:)==optimum_angles_non_zero(layer-2,1));
plot_angles2=theta(2,plot_angle_indices2);
Tcr_non_zero_graph2=zeros(1,length(plot_angle_indices2));
for i=1:length(plot_angle_indices2)
    Tcr_non_zero_graph2(i)=Tcr_non_zero(plot_angle_indices2(i));
end
% plot(plot_angles,Tcr_non_zero_graph)


% plot of the only one angle (interploated)
plot_angle_indices3=find(theta(layer-
1,:)==optimum_angles_non_zero(layer-1,1) & theta(layer-
2,:)==optimum_angles_non_zero(layer-2,1));
plot_angles3=theta(3,plot_angle_indices3);
Tcr_non_zero_graph3=zeros(1,length(plot_angle_indices3));
for i=1:length(plot_angle_indices3)
    Tcr_non_zero_graph3(i)=Tcr_non_zero(plot_angle_indices3(i));
end
% plot(plot_angles,Tcr_non_zero_graph)




figure
plot(plot_angles1,Tcr_non_zero_graph1,'b:','LineWidth',2')
hold on
plot(plot_angles2,Tcr_non_zero_graph2,'r--','LineWidth',2')
```

```
hold on
plot(plot_angles3,Tcr_non_zero_graph3,'g-','LineWidth',2')
hold on
legend(['Graph of 1st layer when 2nd layer='
num2str(optimum_angles_non_zero(2)) ' 3rd layer='
num2str(optimum_angles_non_zero(3))] , ['Graph of 2nd layer when 1st
layer=' num2str(optimum_angles_non_zero(1)) ' 3rd layer='
num2str(optimum_angles_non_zero(3))] , ['Graph of 3rd layer when 1st
layer=' num2str(optimum_angles_non_zero(1)) ' 2nd layer='
num2str(optimum_angles_non_zero(2))])
hold on
xlabel('The layer angles')
ylabel('The buckling load [N]')
title('The graph of the buckling load vs. layer angle')
grid
hold on
%grid minor
```

APPENDIX B

```
function A=angle_generation(layer,angle,req)

col=angle^layer;
c1=0;

A=zeros(1,col);
for i=1:col
    A(i)=c1;
    p=i;
    p=mod(p,angle^req);
    if p==0
        c1=c1+1;
    end
    c1=mod(c1,angle);
end
```

CURRICULUM VITAE

Name Surname	**:**	Güneş Aydın
Address	**:**	Şile – İstanbul
E-mail	**:**	gunesaydin7@gmail.com

Personal Information

Nationality	**:**	Turkish Republic
Date of Birth	**:**	22.06.1989
Driving License	**:**	B (2007)

Education Information

B.Sc.:	FMV Işık University – Turkey
09.2007 - 06.2011	Faculty of Engineering, Mechanical Engineering
B.Sc.:	FMV Işık University – Turkey
09.2009 - 06.2011	Faculty of Engineering, Electronics Engineering (Minor)

Professional Experience

FMV Işık University
Student Assistant
September 2009 - June 2011

Repkon Machine and Tool Industry and Trade Inc.
Mechanical Design Engineer
October 2011 – January 2014

Repkon Machine and Tool Industry and Trade Inc.
Mechanical and Fluid System Design Engineer
January 2014 – June 2014

Repkon Machine and Tool Industry and Trade Inc.
Fluid Systems and Process Development Department Responsible
June 2014 – Cont.

Seminars, Courses and Certificates

- "İletişim Becerileri" eğitimi – Eğitim Akademi – 21-22 Ekim 2011
- "AutoCAD Mechanical 2012 Temel Eğitimi" – Altar Teknoloji – 24.02.2012
- "SolidWorks" eğitimi – Yenasoft – 17-21 Aralık 2012
- "3DVIA Composer" eğitimi – Yenasoft – 26 Ocak 2013
- "İş sağlığı ve güvenliği işe giriş eğitimi" – Ahmed Ferit Özceylan (Eğitmen – C sınıfı İSG uzmanı) – 13.-3.2014
- "Skidcar ileri sürüş teknikleri eğitimi" – Autodrom – 09.03.2013
- "ISO 9001:2008 İç Denetçi" eğitimi – Kalitek – 10.05.2014
- "Ölçme tekniği ve kontrol bilgisi" eğitimi – İMES eğitim – 11.08.2014
- "Certificate of Presentation" WASET ICMEME 2014: XII International Conference on Mechanical, Electronics and Mechatronics Engineering – 29.11.2014

Capabilities

- English as a foreign language (Advanced)
- MATLAB programming.
- ABAQUS CAE knowledge.
- SolidWorks knowledge.
- Autodesk Inventor knowledge.
- Microsoft office knowledge.
- The mechanical team leader of FMV Işık University, solarcar team between 2010 and 2014.

Publisions

Güneş Aydın, Razi Kalantari Osgouei, Murat Emre Öztürk, Ahmad Partovi Meran, Ekrem Tüfekçi "Buckling Analysis of Composite Shells under Compression and Torsional Loads: Numerical and Analytical Study" WASET ICMEME:XII International Conference on Mechanical, Electronics and Mechatronics Engineering, 28-29 November 2014, Istanbul, Turkey.

Presentations

Güneş Aydın, Razi Kalantari Osgouei, Murat Emre Öztürk, Ahmad Partovi Meran, Ekrem Tüfekçi "Buckling Analysis of Composite Shells under Compression and Torsional Loads: Numerical and Analytical Study" WASET ICMEME:XII International Conference on Mechanical, Electronics and Mechatronics Engineering, 29 November 2014, Istanbul, Turkey.